Available online at www.sciencedirect.com
ScienceDirect
Tectonophysics 451 (2008) 97–122
TECTONOPHYSICS
www.elsevier.com/locate/tecto

Detrital zircon provenance of Neoproterozoic to Cenozoic deposits in Iran: Implications for chronostratigraphy and collisional tectonics

B.K. Horton [a,b,*], J. Hassanzadeh [a,c], D.F. Stockli [d], G.J. Axen [a,e], R.J. Gillis [a,f], B. Guest [a,g], A. Amini [c], M.D. Fakhari [a], S.M. Zamanzadeh [c], M. Grove [a]

[a] Department of Earth and Space Sciences, University of California, Los Angeles, CA 90095-1567, USA
[b] Institute for Geophysics and Department of Geological Sciences, Jackson School of Geosciences, University of Texas, Austin, TX 78712-0254, USA
[c] School of Geology, University College of Science, University of Tehran, P.O. Box 14155-6455, Tehran, Iran
[d] Department of Geology, University of Kansas, Lawrence, KS 66045, USA
[e] Department of Earth and Environmental Science, New Mexico Institute of Mining and Technology, Socorro, NM 87801, USA
[f] Alaska Division of Geological and Geophysical Surveys, Fairbanks, AK 99709, USA
[g] Department of Earth and Environmental Sciences, Ludwig Maximilians University, Munich 80333, Germany

Received 15 October 2007; accepted 6 November 2007
Available online 23 December 2007

Abstract

Ion-microprobe U–Pb analyses of 589 detrital zircon grains from 14 sandstones of the Alborz mountains, Zagros mountains, and central Iranian plateau provide an initial framework for understanding the Neoproterozoic to Cenozoic provenance history of Iran. The results place improved chronological constraints on the age of earliest sediment accumulation during Neoproterozoic–Cambrian time, the timing of the Mesozoic Iran–Eurasia collision and Cenozoic Arabia–Eurasia collision, and the contribution of various sediment sources of Gondwanan and Eurasian affinity during opening and closure of the Paleotethys and Neotethys oceans. The zircon age populations suggest that deposition of the extensive ~1 km-thick clastic sequence at the base of the cover succession commenced in latest Neoproterozoic and terminated by Middle Cambrian time. Comparison of the geochronological data with detrital zircon ages for northern Gondwana reveals that sediment principally derived from the East African orogen covered a vast region encompassing northern Africa and the Middle East. Although most previous studies propose a simple passive-margin setting for Paleozoic Iran, detrital zircon age spectra indicate Late Devonian–Early Permian and Cambrian–Ordovician magmatism. These data suggest that Iran was affiliated with Eurasian magmatic arcs or that rift-related magmatic activity during opening of Paleotethys and Neotethys was more pronounced than thought along the northern Gondwanan passive-margin. For a Triassic–Jurassic clastic overlap assemblage (Shemshak Formation) in the Alborz mountains, U–Pb zircon ages provide chronostratigraphic age control requiring collision of Iran with Eurasia by late Carnian–early Norian time (220–210 Ma). Finally, Cenozoic strata yield abundant zircons of Eocene age, consistent with derivation from arc magmatic rocks related to late-stage subduction and/or breakoff of the Neotethys slab. Together with the timing of foreland basin sedimentation in the Zagros, these detrital zircon ages help bracket the onset of the Arabia–Eurasia collision in Iran between middle Eocene and late Oligocene time.

Keywords: Iran; Detrital zircon geochronology; Alborz mountains; Zagros mountains; Collision

1. Introduction

Iran constitutes one of the largest tectonic provinces in the Middle East (Fig. 1) and occupies a poorly understood region connecting the Alpine and Himalayan orogenic systems (e.g., Gansser, 1955; Seber et al., 1997). In addition to the Cenozoic Arabia–Eurasia collision (Neotethys closure), Iran was involved in early Mesozoic collision of various Gondwanan terranes with Eurasia (Paleotethys closure) and in exhumation of the Neoproterozoic East African orogen (Berberian and King, 1981; Sengör, 1987). Given this diverse plate tectonic history and the limited number of geochronological studies, it is not

* Corresponding author.
E-mail address: horton@mail.utexas.edu (B.K. Horton).

0040-1951/$ - see front matter © 2008 Elsevier B.V. All rights reserved.
doi:10.1016/j.tecto.2007.11.063

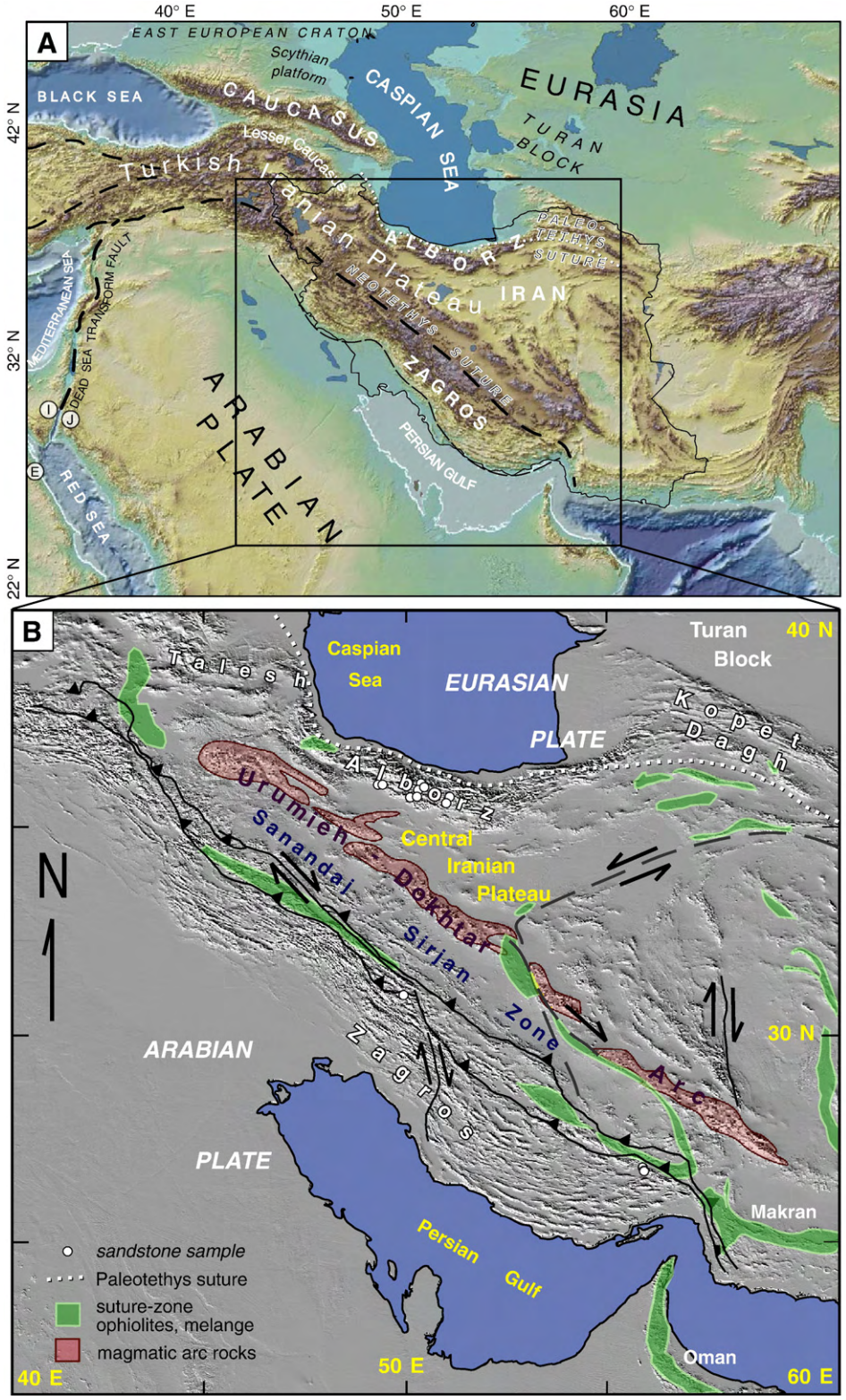

Fig. 1. (A) Regional map depicting topography, mountain belts, and tectonic features of the Middle East and south-central Eurasia (from Guest et al., 2006a). Locations of previous detrital zircon studies: I—Israel; J—Jordan; E—Egypt. (B) Geologic map of Iran and surrounding regions showing mountain belts, suture-zone ophiolites (green shading), the Urumieh–Dokhtar magmatic arc (red shading), and tectonomorphic provinces such as the Zagros fold-thrust belt, Sanandaj–Sirjan zone, and central Iranian plateau (after Guest et al., 2006b). White circles indicate sandstone sample locations.

surprising that fundamental questions persist on the timing of collisional events, nature of crystalline basement, and identity and past positions of individual terranes.

Iran has been considered part of Gondwana and commonly placed adjacent to Arabia in plate reconstructions for late Neoproterozoic–early Paleozoic time, largely on the basis of

similar sandstone units and less-extensive evaporites (Stöcklin, 1968). However, because sandstones of this age are distributed over a wide region from northern Africa to the Himalayas (Burke and Krauss, 2000; Avigad et al., 2003), their similarity does not demonstrate close proximity. Following presumed passive-margin conditions, an early Mesozoic collision is verified by the Paleotethys suture along the Alborz and Kopet Dagh mountains of northern Iran. It is unclear whether collision occurred with a consolidated Eurasia or an isolated Turan block (Fig. 1) later accreted to Eurasia (Stöcklin, 1974; Zonenshain et al., 1990; Lemaire et al., 1997; Besse et al., 1998). Equally uncertain is the timing of the Arabia–Eurasia collision recorded in the Zagros mountains of southern Iran, for which estimates range from Late Cretaceous to late Miocene time (Dewey et al., 1973; Hempton, 1987; Alavi, 1994; McQuarrie et al., 2003; Mohajjel et al., 2003; Alavi, 2004).

The goal of this paper is to use U–Pb detrital zircon geochronology to evaluate the provenance of Neoproterozoic to Cenozoic sedimentary rocks of the Alborz mountains, Zagros mountains, and central Iranian plateau. Detrital zircon provenance studies in other orogenic systems have clarified the collisional records of many continental blocks and accreted terranes (e.g., Gehrels et al., 1990; Thomas et al., 2004; Barbeau et al., 2005; Weislogel et al., 2006). Our preliminary findings, although limited in geographic extent and stratigraphic detail, are among the first detrital zircon ages reported for Iran and provide an initial chronological framework that refines the plate tectonic configuration, collisional timing, and sediment provenance history of Iran. In some cases, the zircon age spectra support previous paleogeographic reconstructions, but in other cases the results raise new questions that pose significant challenges to existing models. We anticipate that additional studies employing detrital zircon geochronology will shed further light on the varied tectonic and stratigraphic problems in Iran and surrounding regions.

2. Geological background and unresolved problems

2.1. Plate tectonic setting

Iran is regarded as a fragment of Gondwana and assumed to share a Neoproterozoic granitic basement analogous to the Arabian basement formed during and shortly after the 900–600 Ma Pan-African orogeny (Stöcklin, 1968; Becker et al., 1973; Berberian and King, 1981; Sengör, 1987; Davoudzadeh, 1997). With few exceptions (e.g., Ramezani and Tucker, 2003; Hassanzadeh et al., 2008-this volume), most crystalline basement in Iran has not been reliably dated. Broad lithostratigraphic similarities in the cover succession suggest a comparable history of Neoproterozoic to Cenozoic deposition for the Alborz, Zagros, and central Iranian plateau (Fig. 1). On the basis of proposed reconstructions (Stampfli and Borel, 2002; Golonka, 2004), this succession recorded initial rifting from Gondwana, subsequent collision with Eurasia, and final collision with Arabia. For simplicity in this paper, Eurasia generally refers to the southern and central parts of the present Eurasian plate, recognizing that these regions once constituted parts of Laurussia, Laurasia, and Pangea at different times during the Paleozoic and Mesozoic (Stampfli and Borel, 2002). The Iran plate refers to a collection of smaller blocks, of probable Gondwanan or peri-Gondwanan affinity, that made up part of the larger Cimmerian continent during evolution of the Paleotethys and Neotethys oceans (Sengör, 1987). In these discussions, continental collision is regarded as the elimination of oceanic lithosphere between two continents (e.g., Rowley, 1996).

Phases of plate separation and collision along the northern and southern margins of Iran are defined by potential passive-margin sequences, obducted ophiolites, and detrital overlap assemblages. Although initial rifting of various terranes from Gondwana may have occurred as early as late Neoproterozoic time, Iran lacks a thick miogeoclinal prism of early to middle Paleozoic age (Stöcklin, 1968). A late Paleozoic age is commonly favored for the main phase of rifting of Iran away from Gondwana and resulting growth of Neotethys (e.g., Berberian and King, 1981; Talbot and Alavi, 1996; Stampfli and Borel, 2002). Two suture zones delimit the principal collisional boundaries (Stöcklin, 1974; Haynes and McQuillan, 1974): the Paleotethys (north Iranian or Mashad) suture along the Alborz and Kopet Dagh mountains, and the Neotethys (south Iranian or Zagros) suture bordering the hinterland of the Zagros fold-thrust belt (Fig. 1). Although the existence and precise locations of these sutures are debated, most reconstructions indicate that closure of Paleotethys and collision along the northern margin occurred in Triassic or Jurassic time, whereas Neotethys was consumed between Arabia and Iran during the Late Cretaceous or Cenozoic.

2.2. Depositional history

2.2.1. Late Neoproterozoic–Cambrian

The oldest strata in Iran consist of sandstones with minor carbonates and volcanic rocks unconformably overlying granitic basement. On the basis of fossils and regional correlations, this ~1-km-thick, primarily clastic basal sequence (including, among others, the Kahar, Bayandor, Soltanieh, Barut, and Lalun formations; Fig. 2) is commonly assigned a late Neoproterozoic or Lower Cambrian age (Stöcklin, 1968, 1974; Berberian and King, 1981; Hamdi et al., 1989; Samani et al., 1994; Alavi, 1996).

The conventional model proposes Neoproterozoic granitic magmatism followed by minor to moderate rifting and strike–slip deformation that generated a post-magmatic Paleozoic passive-margin (Husseini, 1989; Kröner et al., 1992; Stern, 1985; Alsharhan and Kendall, 1986; Stern, 1994; Talbot and Alavi, 1996; Veevers, 2004). An alternative model suggests that newly dated latest Neoproterozoic–Cambrian calc–alkaline magmatism (Ramezani and Tucker, 2003; Hassanzadeh et al., 2008-this volume) may be part of a broader early Paleozoic active margin and contractional orogen potentially linked to a similar early Paleozoic system in the Himalayas (Stöcklin, 1980; DeCelles et al., 2000; Gehrels et al., 2003, 2006a,b; Cawood et al., 2007).

Constraining the provenance of the basal clastic sequence should place further limits on the northward extent of the East African (Pan-African) orogen and its associated clastic wedge

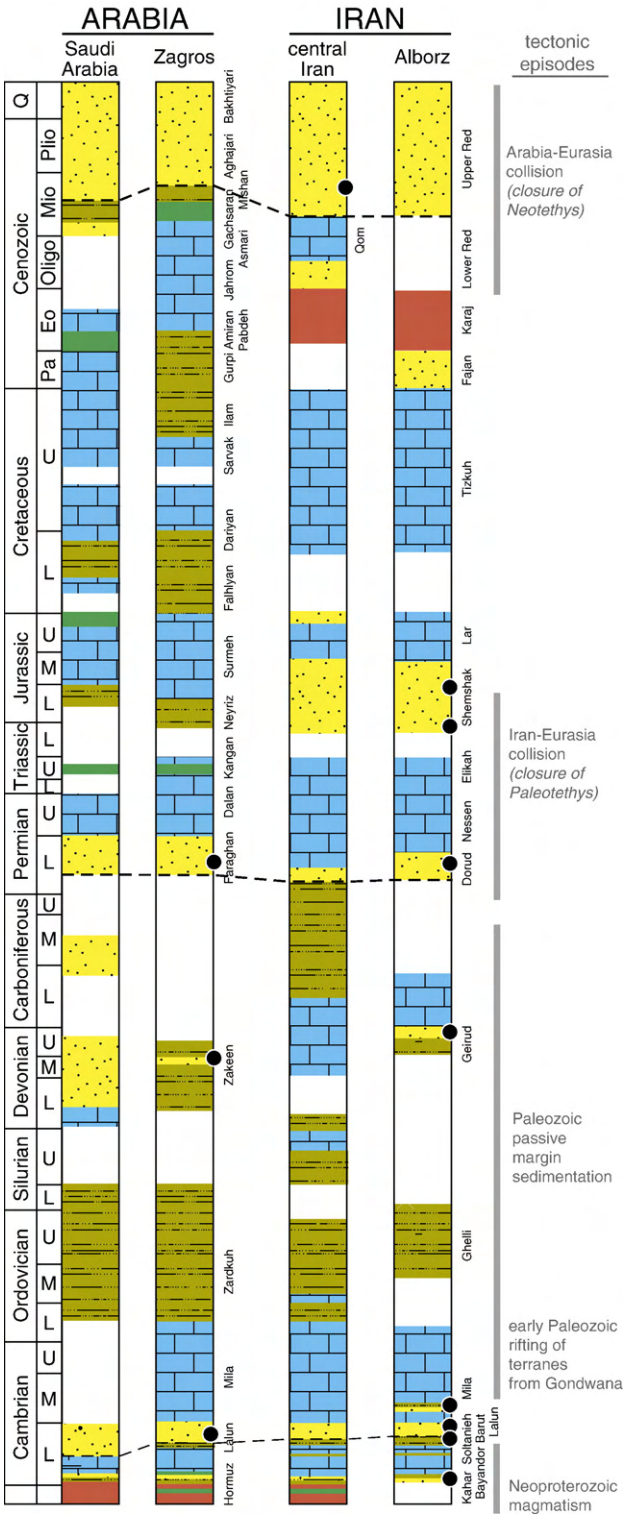

Fig. 2. Upper Neoproterozoic–Cenozoic stratigraphy of the Middle East. Individual columns are depicted for Arabia, southern Iran (Zagros mountains), central Iran, and northern Iran (Alborz mountains). Lithologic patterns include sandstone (yellow stipple), siltstone (brown dashed pattern), carbonate (blue block pattern), evaporite (green), volcanic rocks (orange), and sandstone sample locations (black circles). Stratigraphic gaps are shown by blank (white) intervals. Conventional interpretations and age assignments for tectonic episodes are depicted at the right (after Berberian and King, 1981).

(Jacobs and Thomas, 2004). Cambrian sandstones across northern Africa and western Arabia show derivation from this orogen (Burke and Krauss, 2000; Wilde and Youssef, 2002; Avigad et al., 2003; Kolodner et al., 2006). In addition, greater age control will improve plate reconstructions, placement of the Precambrian–Paleozoic boundary, and studies evaluating possible Neoproterozoic Snowball Earth conditions in the Middle East (e.g., Kimura et al., 1997; Brasier et al., 2000; Leather et al., 2002; Stern et al., 2006).

2.2.2. Paleozoic

The upper Neoproterozoic–Cambrian section is overlain conformably by an incomplete, relatively thin (<3 km) Paleozoic succession consisting of carbonate and clastic rocks (Stöcklin, 1968). Deposition is attributed to a platform setting in a poorly developed passive-margin characterized by limited, uneven subsidence. An incomplete and spatially variable Silurian–Carboniferous section across Iran (Fig. 2) suggests periods of nondeposition and erosion (e.g., Ghavidel-Syooki, 1995; Wendt et al., 2005; Ghavidel-Syooki, 2006). Of importance for this study are several units of regional extent. For northern and central Iran, these include the Geirud (Upper Devonian–Lower Carboniferous) and Dorud (Lower Permian) formations (Wendt et al., 2005). In the Zagros of southern Iran, clastic units include the Zakeen (Devonian) and Faraghan (Lower Permian) formations (Ghavidel-Syooki, 2003). Although southern Iran shares lithostratigraphic similarities with central and northern Iran, the proximity of these regions during Paleozoic sedimentation remains unclear. Nevertheless, with few exceptions (e.g., Sengör, 1990), most studies consider Paleozoic Iran to represent shallow-marine passive-margin sedimentation with no significant magmatism or deformation (James and Wynd, 1965; Stöcklin, 1968; Berberian and King, 1981; Berberian and Berberian, 1981; Alsharhan and Kendall, 1986).

2.2.3. Mesozoic

The Mesozoic succession contains basal carbonates capped by the extensive Shemshak Formation (Assereto, 1966). The up to 4-km-thick Shemshak (Fig. 2) represents a shift to primarily nonmarine conditions and is deemed the earliest signature of collision between Iran and the Turan block of southern Eurasia (Fig. 2) (Dercourt et al., 1986; Sengör, 1987). Shemshak sandstone, mudstone, and coal lithofacies were deposited across the Paleotethys suture (Stöcklin, 1974; Stampfli, 1978; Alavi, 1991, 1996), with distal facies in central to northern Iran and proximal synorogenic facies in the Turan block to the north. The age of Shemshak deposition, and therefore timing of syn- to post-collisional deformation, has been attributed to Late Triassic to Middle Jurassic time (Seyed-Emami et al., 2006). Capping the Shemshak is ~5 km of Middle Jurassic to Eocene carbonates (Fig. 2) representing a marine shelf across most of the Middle East (Koop and Stoneley, 1982; Alsharhan and Kendall, 1986; Stoneley, 1990; Haq and Al-Qahtani, 2005).

2.2.4. Cenozoic

Cenozoic strata record a transition from marine carbonate deposition to nonmarine clastic sedimentation (Fig. 2) related to

collision of Arabia with Iran along the southern margin of Eurasia. The timing of the Arabia–Eurasia collision is debated. In one model, collision is linked to southward ophiolite obduction onto the Arabian margin (including Oman) and coeval deposition of an Upper Cretaceous–lower Eocene clastic wedge (Gurpi–Amiran–Pabdeh succession) shed southward into a marine foreland basin (Glennie et al., 1973; Koop and Stoneley, 1982; Beydoun et al., 1992; Alavi, 1994, 2004; Sepehr and Cosgrove, 2004). In other models, collision is considered to occur significantly later during Eocene–Oligocene (Hempton, 1987; Yilmaz, 1993), early Miocene (Allen et al., 2004; Robertson et al., 2006), or late Miocene time (Axen et al., 2001; McQuarrie et al., 2003). Many studies attribute the coarse-grained Bakhtiyari Formation to collision-related uplift, but age estimates vary from the Pliocene (James and Wynd, 1965; Falcon, 1974; Homke et al., 2004) to late Oligocene–early Miocene (Fakhari et al., 2008-this volume). In the central Iranian plateau (Fig. 1), Oligocene to Pliocene strata of the Lower Red, Qom, and Upper Red formations contain erosional products from the Alborz to the north and the Urumieh–Dokhtar belt and Sanandaj–Sirjan zone to the south (Tillman et al., 1981; Amini, 1997; Guest et al., 2007). In addition to the detrital record, intense magmatism followed by a cessation of igneous activity in the Urumieh–Dokhtar belt of central Iran (Fig. 1) could provide a measure of final arc magmatism related to northward subduction and/or breakoff of the Neotethys slab (Berberian and Berberian, 1981; McQuarrie et al., 2003; Ghasemi and Talbot, 2006).

3. U–Pb geochronology

3.1. Methods

Detrital zircons were analyzed from 14 Neoproterozoic to Miocene medium-grained sandstones of the Alborz, Zagros, and central Iranian plateau (Table 1). U–Pb analyses were carried out using the Cameca IMS 1270 ion microprobe at the University of California, Los Angeles following procedures outlined by Schmitt et al. (2003a,b) and Quidelleur et al. (1997). Zircon grains were separated by standard heavy liquid and magnetic techniques, randomly selected, mounted in epoxy, and polished. Grain mounts were ultrasonically washed in 2 mol HCl for 2 min, rinsed with deionized water, then coated with ~100 Å of gold. Operating conditions involved a primary O^- ion beam focused to a spot of ~30 μm diameter, a secondary ion beam yielding a mass resolving power of 5000 with an energy window of 50 eV, and an analysis duration of 8–10 cycles with primary beam presputtering for 120–180 s. To enhance secondary ionization of Pb^+, the sample chamber was flooded with oxygen at $\sim 3\times10^{-5}$ Torr. Zircon standard AS-3 (1099± 0.5 Ma; Paces and Miller, 1993) was used to determine Pb/U relative sensitivity. Corrections for common Pb were made using measured ^{204}Pb (Stacey and Kramers, 1975) and ^{208}Pb, after correction for ^{232}Th-derived ^{208}Pb (Compston et al., 1984), as a proxy for common ^{206}Pb and ^{207}Pb. The corrections employed anthropogenic Pb compositions appropriate for the Los Angeles basin (Sanudo-Wilhelmy and Flegal, 1994).

A total of 589 concordant and discordant ages are presented, with age uncertainties reported at the 1σ level (Table 2). About 70% of analyses yielded concordant ages; the remaining ages exhibited >20% discordance. Systematic reverse discordance for some analyses is expressed as geologically unreasonable ^{207}Pb/^{206}Pb ages, typically much younger than the range of plausible depositional ages. This problem reflects the diminished signal of ^{207}Pb during in-situ analyses of Neoproterozoic-Phanerozoic zircons; for clarity, the most unreasonable ^{207}Pb/^{206}Pb ages are not reported. Less than 5% of the analyses were excluded due to measured UO/U and/or U/$^{94}Zr_2O$ ratios beyond the range observed in analyses of standard AS-3. The preferred ages generally represent ^{206}Pb/^{238}U ages for <1000 Ma grains and ^{207}Pb/^{206}Pb ages for >1000 Ma grains (Table 2). All reported ages are plotted on relative age probability diagrams, with results for each sample normalized to yield equal areas beneath probability curves. For one case (PC5, Table 1), due to limited analyses, we combine the age results of three samples (from the Lalun, Barut, and Mila formations). Although the individual results for these three samples are not drastically different, particular caution must be exercised in interpretation of composite

Table 1
Sample information

ID	Sample	N lat. (°)	E long. (°)	Formation (reported age)	Stratigraphic level
PC1	03AKHe3 (JH)	36.105	50.851	Kahar (1)	~150 m below top
PC2	05BY1 (JH)	36.568	48.403	Bayandor (1)	~30 m above base
PC3	BG5-19 (BG)	36.315	51.000	Lalun (1)	~100 m above base
PC4	LJ-13-10-6 (YG)	31.782	50.793	Lalun (1)	~150 m above base
PC5	KJ007 (DS)	36.061	51.310	Lalun (1)	~5 m above base
PC5	KJ008 (DS)	36.050	51.314	Barut (1)	~3 m above base
PC5	SH5-5 (BG)	36.348	50.942	Mila (2)	~80 m above base
PZ1	05MO1 (JH)	35.998	51.480	Geirud (4)	~100 m above base
PZ2	05DO1 (JH)	36.018	51.474	Dorud (5)	~100 m above base
PZ3	MZA-92 (MZ)	28.087	55.947	Zakeen (3)	~92 m above base
PZ4	MZA-217 (MZ)	28.090	55.940	Faraghan (5)	~60 m above base
MZ1	KJ006 (DS)	36.083	51.318	Shemshak (6)	~120 m above base
MZ2	ZJ004 (DS)	36.529	48.371	Shemshak (6)	~150 m above base
CZ1	20-35-2 (GA)	36.226	50.981	Upper Red equivalent (7)	~500 m above base

Stratigraphic ages (in parentheses): (1) Neoproterozoic–Lower Cambrian; (2) Middle Cambrian; (3) Devonian; (4) Upper Devonian–Lower Carboniferous; (5) Lower Permian; (6) Upper Triassic–Middle Jurassic; (7) Miocene.

Table 2
U–Pb results

Sample ID	$^{206}Pb^*/^{238}U$	$^{206}Pb^*/^{238}U$	$^{207}Pb^*/^{235}U$	$^{207}Pb^*/^{235}U$	$^{207}Pb^*/^{206}Pb$	$^{207}Pb^*/^{206}Pb$	% Radiogenic ^{206}Pb	Age (Ma) $^{206}Pb/^{238}U$	Age (Ma) $^{206}Pb/^{238}U$	Age (Ma) $^{207}Pb/^{235}U$	Age (Ma) $^{207}Pb/^{235}U$	Age (Ma) $^{207}Pb/^{206}Pb$	Age (Ma) $^{207}Pb/^{206}Pb$	U (ppm)	Th/U
		1 σ		1 σ		1 σ			1 σ		1 σ		1 σ		
PC1: Kahar Formation, Alborz Mountains, 03AKHe3 (JH). n = 52.															
g49	0.08370	0.00628	0.6230	0.0469	0.05399	0.00101	99.87	*518.1*	*37.4*	491.7	29.3	–	–	747	0.42
g40	0.08509	0.00557	0.6606	0.0458	0.05631	0.00125	99.86	*526.4*	*33.1*	515	28	–	–	228	0.21
g9	0.08594	0.00517	0.6714	0.0447	0.05666	0.00159	99.55	*531.5*	*30.7*	521.5	27.1	478.1	62.2	201	0.44
g19	0.08882	0.00589	0.6838	0.0589	0.05583	0.00228	99.63	*548.6*	*34.8*	529.1	35.5	–	–	178	0.15
g13	0.09020	0.00518	0.6786	0.0480	0.05456	0.00222	99.36	*556.7*	*30.6*	525.9	29.1	–	–	144	0.40
g8	0.09066	0.00516	0.7310	0.0449	0.05848	0.00092	99.79	*559.5*	*30.5*	557.1	26.3	547.7	34.4	329	0.35
g45	0.09114	0.00516	0.6784	0.0487	0.05399	0.00234	99.4	*562.3*	*30.5*	525.8	29.4	–	–	358	0.24
g12	0.09313	0.00565	0.7359	0.0467	0.05731	0.00116	99.68	*574.0*	*33.3*	560	27.3	503.4	44.6	554	0.09
g43	0.09324	0.00515	0.7230	0.0459	0.05624	0.00143	99.81	*574.7*	*30.4*	552.4	27.1	–	–	574	0.35
g39	0.09346	0.00700	0.7489	0.0648	0.05812	0.00260	99.72	*575.9*	*41.3*	567.6	37.6	534.1	98	115	0.37
g34	0.09349	0.00551	0.7496	0.0473	0.05815	0.00125	99.91	*576.2*	*32.5*	568	27.4	535.5	46.9	310	0.37
g37	0.09435	0.00588	0.7555	0.0486	0.05807	0.00118	99.96	*581.2*	*34.6*	571.4	28.1	532.5	44.5	231	0.35
g14	0.09480	0.00559	0.7854	0.0463	0.06009	0.00085	100	*583.9*	*32.9*	588.6	26.3	606.7	30.7	310	0.81
g54	0.09607	0.00517	0.7790	0.0422	0.05880	0.00048	99.92	*591.4*	*30.4*	584.9	24.1	559.8	17.9	2416	0.30
g15	0.09697	0.00585	0.8118	0.0551	0.06072	0.00223	99.86	*596.6*	*34.4*	603.4	30.9	629.2	79.1	100	0.45
g10	0.09702	0.00623	0.7560	0.0566	0.05651	0.00173	99.69	*596.9*	*36.6*	571.7	32.7	–	–	186	1.30
g18	0.09705	0.00600	0.7150	0.0841	0.05344	0.00519	98.12	*597.1*	*35.3*	547.7	49.8	–	–	185	0.28
g2	0.09730	0.00710	0.7885	0.0615	0.05878	0.00151	99.6	*598.5*	*41.7*	590.3	34.9	558.9	56	2604	0.27
g50	0.09731	0.00590	0.7837	0.0597	0.05841	0.00257	97.61	*598.6*	*34.6*	587.6	34	545.1	96	392	0.62
g27	0.09848	0.00607	0.8075	0.0521	0.05947	0.00110	99.84	*605.5*	*35.6*	601	29.3	584.3	40	636	0.93
g47	0.09952	0.00560	0.7931	0.0451	0.05780	0.00067	99.82	*611.6*	*32.9*	592.9	25.6	–	–	1208	0.38
g33	0.09955	0.00624	0.7864	0.0515	0.05729	0.00088	99.9	*611.8*	*36.6*	589.1	29.3	–	–	409	0.59
g28	0.09976	0.00622	0.7966	0.0696	0.05791	0.00361	99.36	*613.0*	*36.5*	594.9	39.3	526.4	137	109	0.62
g22	0.10070	0.00621	0.7898	0.0556	0.05689	0.00232	99.6	*618.5*	*36.4*	591.1	31.6	–	–	105	0.65
g26	0.10070	0.00566	0.8398	0.0486	0.06047	0.00098	99.9	*618.7*	*33.1*	619.1	26.8	620.4	35	432	0.36
g38	0.10140	0.00578	0.7943	0.0455	0.05684	0.00088	99.74	*622.3*	*33.9*	593.6	25.7	–	–	706	0.55
g55	0.10140	0.00624	0.8164	0.0523	0.05840	0.00100	99.84	*622.5*	*36.5*	606.1	29.2	–	–	669	0.09
g44	0.10190	0.00583	0.8322	0.0492	0.05924	0.00113	99.78	*625.4*	*34.1*	614.8	27.3	576	41.6	376	0.22
g36	0.10220	0.00644	0.8520	0.0566	0.06047	0.00152	99.78	*627.2*	*37.7*	625.7	31.1	620.3	54.1	201	0.46
g53	0.10240	0.00598	0.8380	0.0533	0.05933	0.00129	99.71	*628.7*	*34.9*	618	29.5	579.3	47.3	533	0.70
g24	0.10250	0.00567	0.8308	0.0462	0.05880	0.00095	99.85	*628.9*	*33.1*	614.1	25.6	559.8	35.2	935	0.73
g29	0.10310	0.00753	0.8578	0.0688	0.06037	0.00234	99.86	*632.3*	*44.0*	628.9	37.6	616.8	83.6	134	1.80
g17	0.10470	0.00619	0.8411	0.0505	0.05827	0.00091	99.95	*641.9*	*36.1*	619.7	27.9	–	–	512	0.50
g1	0.10520	0.00936	0.8064	0.1364	0.05558	0.00738	98.12	*644.9*	*54.6*	600.4	76.7	–	–	687	0.08
g5	0.10640	0.00911	0.9162	0.4221	0.06246	0.02670	90.8	*651.7*	*53.1*	660.3	224	–	–	582	0.61
g20	0.10810	0.00678	0.8684	0.0561	0.05827	0.00173	99.81	*661.6*	*39.4*	634.7	30.5	–	–	244	0.16
g4	0.10990	0.01048	1.0550	0.5509	0.06961	0.03348	92.43	*672.4*	*60.9*	731.5	272	–	–	154	0.61
g31	0.12010	0.00825	1.0090	0.0744	0.06094	0.00172	99.63	*731.1*	*47.5*	708.4	37.6	637	60.6	167	0.24
g21	0.13880	0.00854	1.2740	0.0792	0.06657	0.00137	99.78	*837.7*	*48.3*	834.1	35.3	824.4	43	609	0.32
g35	0.14580	0.00851	1.3730	0.0820	0.06829	0.00097	99.93	*877.2*	*47.9*	877.3	35.1	877.4	29.2	577	0.29
g46	0.14740	0.00910	1.3120	0.0881	0.06454	0.00151	99.81	*886.6*	*51.1*	851	38.7	–	–	316	0.28
g30	0.14810	0.00899	1.4010	0.0850	0.06863	0.00070	99.98	*890.1*	*50.5*	889.4	35.9	887.6	21.1	650	0.63
g25	0.14850	0.00969	1.4290	0.0974	0.06979	0.00156	99.99	*892.6*	*54.4*	901.1	40.7	922.1	46.1	262	0.59
g6	0.15180	0.00831	1.4570	0.0837	0.06963	0.00098	99.9	*911.0*	*46.5*	912.9	34.6	917.3	28.8	424	0.45
g23	0.15440	0.00834	1.4860	0.0837	0.06980	0.00087	99.87	*925.6*	*46.6*	924.7	34.2	922.5	25.8	435	0.22
g16	0.15620	0.00924	1.5780	0.0964	0.07323	0.00110	99.89	*935.9*	*51.5*	961.4	38	–	–	210	0.08
g3	0.19140	0.01758	2.0160	0.3923	0.07639	0.01153	97.41	*1129*	*95.1*	1121	132	1105	302	102	0.16
g42	0.32030	0.02157	4.8930	0.3342	0.11080	0.00139	99.9	1791	105	1801	57.6	*1812*	*22.9*	678	0.43
g32	0.30460	0.01904	4.8290	0.3057	0.11500	0.00093	99.87	1714	94.1	1790	53.3	*1880*	*14.5*	649	0.07
g48	0.27300	0.01792	4.6540	0.3322	0.12360	0.00202	99.97	1556	90.8	1759	59.7	*2009*	*28.9*	211	0.63
g11	0.50160	0.03723	12.0600	0.9061	0.17440	0.00138	99.76	2621	160	2609	70.4	*2600*	*13.2*	145	0.15
g7	0.53900	0.03522	19.1400	1.2550	0.25750	0.00365	99.77	2779	148	3049	63.3	*3231*	*22.4*	52	0.56
PC2: Bayandor Formation, Alborz Mountains, 05BY1 (JH). n = 39.															
by-3	0.08807	0.00544	0.6946	0.0498	0.05720	0.00169	99.43	*542.9*	*30.8*	534.5	28.9	499.2	65	214	0.53
by-14	0.09102	0.00516	0.7181	0.0492	0.05722	0.00200	98.47	*559.9*	*29*	548.3	28.1	500.1	76.8	594	0.35
by-6	0.09148	0.00562	0.7998	0.0521	0.06341	0.00166	99.36	*563*	*31.7*	595.6	28.2	–	–	296	0.26

by-19	0.09211	0.00592	0.6297	0.0577	0.04958	0.00309	98.26	*566.9*	*33.4*	495.1	35.2	–	–	124	0.52
by-2	0.09208	0.00642	0.7473	0.0541	0.05887	0.00106	99.68	*567.4*	*36.3*	566.3	30.2	562.1	39.4	310	0.10
by-12	0.09371	0.00655	0.5679	0.1542	0.04395	0.01114	95.92	*576.3*	*37.3*	455.9	99.5	–	–	116	0.85
by-g9	0.09460	0.00511	0.7193	0.0401	0.05515	0.00100	99.82	*582.7*	*30.1*	550.2	23.7	–	–	760	0.68
by-20	0.09630	0.00609	0.6257	0.0563	0.04712	0.00291	97.87	*591.4*	*34.3*	492.5	34.4	–	–	287	0.57
by-4	0.09699	0.00568	0.7755	0.0482	0.05799	0.00119	99.46	*595.2*	*31.8*	581.8	26.4	529.5	44.8	388	0.71
by-10	0.09738	0.00639	0.7325	0.0534	0.05456	0.00169	99.41	*598.2*	*35.8*	557.4	30.1	–	–	333	0.54
by-8	0.09761	0.00563	0.7171	0.0542	0.05329	0.00246	98.83	*598.7*	*31.5*	547.8	31.2	–	–	183	0.69
by-26	0.09777	0.00533	0.7399	0.0545	0.05489	0.00249	99.01	*599.3*	*29.8*	560.8	31	–	–	660	0.61
by-11	0.09915	0.00667	0.6642	0.0710	0.04858	0.00399	97.33	*607.5*	*37.8*	515.8	42.7	–	–	161	1.40
by-g5	0.09908	0.00601	0.7784	0.0505	0.05698	0.00099	99.69	*609.0*	*35.2*	584.6	28.8	–	–	416	0.32
by-16	0.09946	0.00564	0.7908	0.0472	0.05767	0.00099	98.93	*609.6*	*31.4*	590.4	25.6	–	–	791	0.50
by-21	0.10050	0.00737	0.8574	0.1251	0.06185	0.00746	99.56	*615.9*	*42.1*	627.5	67.9	669.6	258	56	1.20
by-g6	0.10110	0.00653	0.8207	0.0530	0.05888	0.00149	99.8	*620.9*	*38.2*	608.5	29.5	562.5	55.2	349	1.00
by-24	0.10330	0.00576	0.8590	0.0501	0.06032	0.00115	98.96	*631.8*	*32*	628.1	26.2	615	41.2	1321	0.58
by-g4	0.10900	0.00878	0.9411	0.0838	0.06262	0.00180	99.24	*667.0*	*51.0*	673.5	43.8	695.3	61.2	216	0.59
by-g14	0.10950	0.00674	0.8846	0.0569	0.05858	0.00140	99.65	*670.0*	*39.2*	643.5	30.6	–	–	244	0.59
by-g10	0.11080	0.00740	0.8579	0.0594	0.05614	0.00113	99.94	*677.6*	*42.9*	629	32.4	–	–	365	0.42
by-g13	0.11260	0.00997	0.8757	0.0746	0.05640	0.00162	99.83	*687.9*	*57.7*	638.7	40.4	–	–	682	0.32
by-25	0.11320	0.00629	1.0490	0.0601	0.06719	0.00127	99.32	*688.6*	*34.9*	726.1	28.7	–	–	473	0.16
by-g2	0.11600	0.00775	0.9057	0.0694	0.05662	0.00214	99.52	*707.5*	*44.8*	654.7	37	–	–	401	0.31
by-7	0.11760	0.00668	0.8097	0.0608	0.04992	0.00232	98.38	*714.9*	*36.7*	600.9	33.2	–	–	499	0.42
by-g12	0.12550	0.00905	1.0360	0.0796	0.05989	0.00125	99.59	*762.2*	*51.9*	722.1	39.7	–	–	312	0.23
by-g11	0.12710	0.00944	1.0450	0.0812	0.05967	0.00147	99.85	*771.1*	*54.0*	726.6	40.3	–	–	331	0.42
by-g7	0.13090	0.01067	1.0750	0.0873	0.05958	0.00125	99.79	*793.1*	*60.8*	741.4	42.7	–	–	251	0.58
by-5	0.13390	0.00982	1.0760	0.0846	0.05830	0.00168	98.98	*809.4*	*53.7*	741.4	40	–	–	619	0.61
by-g8	0.13660	0.01237	1.1880	0.1202	0.06309	0.00284	98.21	*825.5*	*70.1*	795.2	55.8	711.2	95.6	189	0.80
by-17	0.13900	0.00829	1.1600	0.0807	0.06056	0.00199	98.71	*836.8*	*44.7*	780.8	36.6	–	–	305	0.56
by-g1	0.20790	0.01490	2.0860	0.1493	0.07280	0.00080	100	1217	79.5	1144	49.1	*1008*	*22.3*	346	1.20
by-22	0.35300	0.02382	5.6460	0.3785	0.11600	0.00163	99.48	1946	109	1922	55.6	*1896*	*25.3*	262	0.68
by-15	0.36570	0.02449	6.0010	0.4102	0.11900	0.00149	99.52	2006	111	1974	57.5	*1941*	*22.4*	123	0.67
by-g15	0.27120	0.01402	4.5860	0.2379	0.12270	0.00075	99.74	1547	71.1	1747	43.2	*1995*	*10.9*	638	1.90
by-13	0.27950	0.01665	4.8400	0.2919	0.12560	0.00089	99.75	1585	80.1	1790	48.6	*2037*	*12.5*	591	0.21
by-g3	0.53580	0.04453	11.6200	0.9722	0.15730	0.00128	99.76	2766	187	2575	78.2	*2427*	*13.8*	389	0.26
by-18	0.38390	0.02990	10.2100	0.7967	0.19280	0.00247	99.27	2091	136	2452	70.5	*2767*	*21*	158	0.56
by-9	0.43740	0.02673	12.1100	0.7379	0.20080	0.00121	99.89	2334	115	2610	54.7	*2832*	*9.8*	416	0.10
PC3: Lalun Formation, Alborz Mountains, BG5-19 (BG). n = 47.															
19-g46	0.08545	0.00702	0.6501	0.0538	0.05518	0.00105	99.75	*528.6*	*41.7*	508.5	33.1	–	–	249	0.62
19-g35	0.08581	0.00743	0.7648	0.0755	0.06464	0.00308	99.06	*530.7*	*44.1*	576.8	43.5	–	–	69	1.10
19-g1	0.08738	0.00668	0.6924	0.0560	0.05747	0.00110	99.96	*540*	*39.6*	534.3	33.6	509.8	42	178	0.40
19-g37	0.09102	0.00873	0.7496	0.0689	0.05973	0.00148	99.88	*561.6*	*51.6*	568	40	593.7	53.8	83	0.32
19-g24	0.09145	0.00733	0.7847	0.0692	0.06224	0.00261	99.32	*564.1*	*43.3*	588.2	39.4	682.2	89.7	67	0.69
19-g15	0.09297	0.00720	0.7556	0.0629	0.05894	0.00192	99.8	*573.1*	*42.5*	571.5	36.4	565	71	108	1.30
19-g50	0.09373	0.00700	0.7988	0.0641	0.06182	0.00195	98.91	*577.5*	*41.2*	596.2	36.2	667.7	67.4	165	1.10
19-g14	0.10050	0.00776	0.8522	0.0666	0.06151	0.00081	99.9	*617.2*	*45.4*	625.8	36.5	657.3	28.4	199	0.75
19-g32	0.10330	0.00883	0.8748	0.0767	0.06141	0.00094	99.87	*633.9*	*51.6*	638.2	41.5	653.6	32.9	199	0.37
19-g16	0.10790	0.00996	0.9069	0.0837	0.06096	0.00082	99.73	*660.5*	*57.9*	655.4	44.5	637.8	28.9	655	0.28
19-g26	0.10890	0.00736	0.9945	0.0684	0.06621	0.00108	99.93	*666.6*	*42.8*	701	34.8	–	–	190	0.61
19-g22	0.10930	0.00844	1.0070	0.0765	0.06681	0.00182	99.29	*668.7*	*49*	707.3	38.7	–	–	201	1.20
19-g45	0.11460	0.01127	0.9676	0.0926	0.06125	0.00123	99.9	*699.3*	*65.2*	687.2	47.8	647.9	43	103	0.34
19-g33	0.11710	0.01037	0.9338	0.0920	0.05785	0.00196	98.8	*713.7*	*59.9*	669.6	48.3	–	–	115	0.67
19-g48	0.11810	0.00949	1.0600	0.0862	0.06510	0.00073	99.92	*719.6*	*54.7*	733.8	42.5	777.5	23.5	243	0.46
19-g38	0.12080	0.01051	1.0460	0.0978	0.06281	0.00169	99.72	*735*	*60.5*	726.8	48.5	701.7	57.2	103	0.46
19-g29	0.12300	0.00846	1.1090	0.0780	0.06542	0.00140	99.22	*747.6*	*48.5*	757.7	37.6	787.9	45	142	0.51
19-g25	0.12390	0.00952	1.1730	0.0917	0.06865	0.00121	99.94	*753.1*	*54.6*	788	42.9	–	–	184	0.38
19-g23	0.12670	0.01143	1.1070	0.1106	0.06341	0.00214	99.75	*768.8*	*65.4*	757	53.3	722.1	71.7	48	0.89
19-g18	0.12780	0.00981	1.1580	0.0892	0.06573	0.00066	99.93	*775*	*56.1*	781	42	797.9	21.2	411	0.67
19-g42	0.12780	0.01252	1.1100	0.1090	0.06298	0.00148	99.77	*775.5*	*71.6*	758.3	52.4	707.7	50	61	1.10
19-g28	0.13160	0.01254	1.1730	0.1135	0.06468	0.00068	99.87	*796.7*	*71.5*	788.2	53	764	22.2	279	0.30
19-g39	0.13230	0.01400	1.1720	0.1276	0.06425	0.00153	99.93	*801.1*	*79.7*	787.6	59.6	749.7	50.2	168	0.72
19-g13	0.13640	0.01229	1.2120	0.1104	0.06444	0.00123	99.58	*824.3*	*69.7*	806.1	50.7	756	40.3	111	0.84
19-g7	0.14030	0.01256	1.3130	0.1313	0.06787	0.00215	99.74	*846.5*	*71*	851.6	57.6	864.6	65.5	54	0.56
19-g31	0.14350	0.01541	1.2980	0.1464	0.06560	0.00123	99.93	*864.6*	*86.9*	845	64.7	793.6	39.4	146	0.44
19-g8	0.14400	0.01102	1.3500	0.1009	0.06798	0.00108	99.96	*867.2*	*62.1*	867.4	43.6	867.8	32.9	150	0.59

(continued on next page)

Table 2 (*continued*)

Sample ID	$^{206}Pb^*/^{238}U$	$^{206}Pb^*/^{238}U$	$^{207}Pb^*/^{235}U$	$^{207}Pb^*/^{235}U$	$^{207}Pb^*/^{206}Pb$	$^{207}Pb^*/^{206}Pb$	% Radiogenic ^{206}Pb	Age (Ma) $^{206}Pb/^{238}U$	Age (Ma) $^{206}Pb/^{238}U$	Age (Ma) $^{207}Pb/^{235}U$	Age (Ma) $^{207}Pb/^{235}U$	Age (Ma) $^{207}Pb/^{206}Pb$	Age (Ma) $^{207}Pb/^{206}Pb$	U (ppm)	Th/U
		1 σ		1 σ		1 σ			1 σ		1 σ		1 σ		
19-g40	0.14480	0.01342	1.3350	0.1293	0.06687	0.00152	99.9	*872*	*75.6*	861.3	56.2	833.8	47.4	107	0.86
19-g17	0.15350	0.01276	1.4690	0.1230	0.06943	0.00075	99.96	*920.4*	*71.3*	917.8	50.6	911.6	22.2	234	0.29
19-g20	0.15450	0.01367	1.4710	0.1320	0.06906	0.00085	99.98	*926*	*76.4*	918.5	54.2	900.6	25.5	149	0.71
19-g19	0.15940	0.01272	1.5890	0.1281	0.07232	0.00082	99.98	*953.2*	*70.7*	965.9	50.2	994.9	23	179	0.33
19-g9	0.15960	0.01555	1.4230	0.1407	0.06467	0.00138	99.65	*954.7*	*86.5*	898.8	58.9	–	–	94	0.76
19-g2	0.18110	0.01777	1.7340	0.1726	0.06944	0.00117	99.76	1073	97	1021	64.1	*911.8*	*34.6*	303	0.29
19-g47	0.16260	0.01383	1.5750	0.1364	0.07028	0.00119	99.81	971.1	76.7	960.5	53.8	*936.5*	*34.7*	75	1.00
19-g3	0.20500	0.02071	2.0870	0.2111	0.07385	0.00091	99.96	1202	111	1145	69.4	*1037*	*25*	154	0.35
19-g5	0.28880	0.02888	4.3070	0.4307	0.10820	0.00087	99.84	1636	144	1695	82.4	*1769*	*14.8*	271	0.27
19-g36	0.40230	0.04439	6.9400	0.8177	0.12510	0.00326	99.76	2179	204	2104	105	*2031*	*46.1*	45	0.84
19-g4	0.35830	0.03143	6.3450	0.5487	0.12840	0.00132	99.97	1974	149	2025	75.9	*2077*	*18.1*	177	0.52
19-g21	0.26370	0.02374	5.4280	0.4914	0.14930	0.00124	99.82	1509	121	1889	77.6	*2338*	*14.2*	722	0.62
19-g43	0.32870	0.02690	6.8190	0.5564	0.15050	0.00066	99.99	1832	131	2088	72.3	*2351*	*7.5*	223	0.45
19-g44	0.41800	0.03905	9.3060	0.8612	0.16150	0.00292	99.96	2251	178	2369	84.8	*2471*	*30.5*	22	11.0
19-g49	0.40640	0.03033	9.1980	0.6936	0.16420	0.00182	100	2198	139	2358	69.1	*2499*	*18.7*	74	1.10
19-g12	0.41700	0.03692	9.4840	0.8357	0.16500	0.00122	99.86	2247	168	2386	80.9	*2507*	*12.4*	332	0.57
19-g11	0.48040	0.04070	10.9400	0.9307	0.16510	0.00121	99.79	2529	177	2518	79.2	*2509*	*12.4*	166	0.35
19-g30	0.38440	0.02944	8.8890	0.6836	0.16770	0.00161	99.94	2097	137	2327	70.2	*2535*	*16.1*	83	1.20
19-g41	0.51760	0.04334	13.9800	1.1790	0.19590	0.00147	99.86	2689	184	2748	79.9	*2792*	*12.3*	95	0.93
19-g6	0.62560	0.05411	21.0400	1.8220	0.24390	0.00236	99.96	3132	215	3140	84	*3146*	*15.3*	119	0.48
PC4: Lalun Formation, Zagros Mountains, LJ-13-10-6 (YG). n=49.															
g7-32	0.08863	0.00706	0.7170	0.0995	0.05867	0.00615	98.4	*547.4*	*41.8*	548.9	58.8	555	229	30	0.90
g7-44	0.09066	0.00359	0.7417	0.0299	0.05933	0.00139	99.88	*559.5*	*21.2*	563.4	17.4	579.2	50.9	122	1.60
g7-33	0.09326	0.00614	0.7128	0.0701	0.05543	0.00379	98.55	*574.8*	*36.2*	546.4	41.5	429.6	152	58	0.72
g7-26	0.09436	0.00342	0.7644	0.0354	0.05875	0.00185	99.72	*581.3*	*20.2*	576.5	20.3	557.8	68.5	139	0.82
g7-30	0.09545	0.00426	0.7904	0.0395	0.06006	0.00162	99.71	*587.7*	*25*	591.4	22.4	605.6	58.2	105	0.23
g7-19	0.09572	0.00370	0.7705	0.0314	0.05838	0.00093	99.87	*589.3*	*21.8*	580	18	544	34.7	198	0.47
g7-35	0.09783	0.00527	0.8021	0.0446	0.05946	0.00141	99.86	*601.7*	*31*	598	25.1	583.9	51.6	164	0.94
g7-29	0.09857	0.00498	0.8406	0.0624	0.06185	0.00419	99.09	*606*	*29.2*	619.5	34.4	668.9	145	45	0.61
g7-50	0.09974	0.00361	0.8090	0.0297	0.05883	0.00110	99.83	*612.9*	*21.2*	601.9	16.6	560.8	40.7	153	0.58
g7-13	0.10070	0.00400	0.8055	0.0453	0.05804	0.00170	99.6	*618.3*	*23.4*	599.9	25.4	531.2	64.2	146	0.50
g7-40	0.10080	0.00484	0.8524	0.0699	0.06136	0.00373	99.03	*618.8*	*28.3*	625.9	38.3	651.8	131	55	1.00
g7-51	0.10310	0.00451	0.8658	0.0414	0.06091	0.00096	99.94	*632.4*	*26.4*	633.3	22.5	636.2	34	187	0.89
g-7-1	0.10380	0.00809	0.8105	0.0789	0.05660	0.00341	99.08	*636.9*	*47.2*	602.7	44.3	–	–	51	0.51
g-7-2	0.10390	0.00477	0.8610	0.0472	0.06011	0.00131	99.7	*637.2*	*27.8*	630.7	25.8	607.5	47	141	0.46
g-7-4	0.10530	0.00727	0.8990	0.0712	0.06189	0.00179	99.73	*645.7*	*42.4*	651.2	38.1	670.3	61.9	70	0.46
g7-45	0.11080	0.00433	0.9232	0.0548	0.06044	0.00222	99.34	*677.2*	*25.2*	664	28.9	619.5	79.3	105	0.30
g7-39	0.12150	0.00605	1.0760	0.0635	0.06426	0.00174	99.72	*739.2*	*34.8*	741.9	31.1	750.1	57.1	110	0.64
g7-37	0.12340	0.00630	1.0730	0.0539	0.06306	0.00117	99.73	*750.1*	*36.1*	740.1	26.4	710.2	39.5	168	1.10
g7-18	0.12470	0.00539	1.0770	0.0551	0.06264	0.00118	99.69	*757.3*	*30.9*	742.1	26.9	696.2	40	176	0.24
g7-34	0.12490	0.00475	1.0800	0.0444	0.06270	0.00123	99.72	*758.8*	*27.2*	743.6	21.7	698.1	41.7	148	0.83
g7-46	0.12580	0.00829	1.1390	0.0856	0.06571	0.00252	99.6	*763.7*	*47.5*	772.3	40.6	797.1	80.4	54	0.81
g7-25	0.12710	0.00512	1.1290	0.0551	0.06444	0.00161	99.76	*771.1*	*29.3*	767.3	26.3	756.2	52.8	119	0.58
g7-12	0.12730	0.00713	1.1100	0.0830	0.06323	0.00313	99.1	*772.4*	*40.8*	758.1	40	716.1	105	51	0.62
g7-49	0.12860	0.00567	1.1410	0.0581	0.06438	0.00173	99.56	*779.9*	*32.4*	773.2	27.5	754	56.7	91	0.64
g7-6	0.13250	0.00748	1.1420	0.0786	0.06253	0.00280	98.21	*802.1*	*42.6*	773.6	37.3	692.2	95.3	81	0.83
g7-28	0.13660	0.00549	1.2690	0.0597	0.06738	0.00143	99.8	*825.6*	*31.1*	832.1	26.7	849.5	44	122	1.00
g7-16	0.14130	0.00900	1.2570	0.0846	0.06453	0.00216	99.35	*852.1*	*50.9*	826.7	38.1	759.1	70.7	64	0.39
g7-8	0.14170	0.00473	1.3320	0.0441	0.06815	0.00092	99.95	*854.4*	*26.7*	859.6	19.2	873.3	28	167	0.66
g7-17	0.14280	0.00860	1.3710	0.1281	0.06961	0.00485	99.35	*860.6*	*48.5*	876.5	54.9	916.7	143	36	0.65
g-7-5	0.14610	0.00808	1.3700	0.1030	0.06803	0.00323	99.39	*879.1*	*45.5*	876.4	44.1	869.5	98.3	32	0.62
g7-15	0.15000	0.00631	1.4450	0.0632	0.06986	0.00079	99.85	901	35.4	907.8	26.2	*924.1*	*23.1*	284	1.10
g7-7	0.15510	0.01852	1.5330	0.1974	0.07170	0.00535	99.21	929.3	103	943.7	79.1	*977.4*	*152*	13	0.92
g7-48	0.20650	0.00737	2.2910	0.0868	0.08046	0.00063	99.86	1210	39.4	1209	26.8	*1208*	*15.4*	321	0.47
g7-23	0.33450	0.01860	4.9510	0.2998	0.10740	0.00150	99.23	1860	89.8	1811	51.1	*1755*	*25.5*	174	0.62
g7-42	0.32440	0.01742	5.0150	0.2786	0.11210	0.00297	99.37	1811	84.8	1822	47	*1834*	*48*	35	1.40
g7-11	0.30560	0.01279	4.8400	0.2059	0.11490	0.00074	99.94	1719	63.1	1792	35.8	*1878*	*11.7*	335	0.88
g7-41	0.38740	0.01873	6.7240	0.3420	0.12590	0.00262	98.82	2111	87	2076	45	*2041*	*36.8*	66	1.00

g7-21	0.28800	0.00950	5.6070	0.1851	0.14120	0.00085	99.9	1631	47.5	1917	28.4	*2242*	*10.4*	473	0.94
g7-27	0.42550	0.01661	8.4540	0.3341	0.14410	0.00079	99.95	2286	75.1	2281	35.9	*2277*	*9.44*	205	0.71
g7-10	0.43830	0.02018	9.4150	0.4462	0.15580	0.00262	98.64	2343	90.5	2379	43.5	*2410*	*28.6*	51	0.33
g7-43	0.44220	0.01687	9.7120	0.3977	0.15930	0.00223	98.89	2361	75.4	2408	37.7	*2448*	*23.7*	91	0.53
g7-38	0.47820	0.03911	10.5500	0.9172	0.16000	0.00283	98.86	2519	171	2484	80.7	*2455*	*29.9*	39	0.72
g7-24	0.49750	0.03557	11.0100	0.7974	0.16050	0.00239	99.35	2603	153	2524	67.4	*2461*	*25.2*	46	0.57
g7-31	0.40620	0.03331	9.0300	0.7146	0.16120	0.00290	99.37	2198	153	2341	72.3	*2468*	*30.4*	46	0.76
g7-20	0.47230	0.01746	10.6600	0.4201	0.16370	0.00244	99.25	2494	76.4	2494	36.6	*2494*	*25.1*	74	0.49
g7-9	0.46480	0.01908	10.6000	0.4400	0.16530	0.00137	99.69	2461	84	2488	38.5	*2511*	*13.9*	225	0.59
g7-47	0.41180	0.01393	9.4610	0.3137	0.16660	0.00071	99.98	2223	63.6	2384	30.5	*2524*	*7.17*	249	0.62
g7-22	0.49960	0.02987	11.7800	0.7173	0.17100	0.00136	99.45	2612	128	2587	57	*2568*	*13.3*	280	0.16
g-7-3	0.54960	0.02391	14.3700	0.6064	0.18970	0.00136	99.7	2824	99.5	2775	40	*2739*	*11.8*	76	0.42
PC5: Lalun Formation, Alborz Mountains, KJ007 (DS). n = 19.															
12-3l1	0.08436	0.00243	0.6606	0.0319	0.05679	0.00205	97.92	*522.1*	*14.4*	515	19.5	483.5	79.5	466	0.52
12-3g1	0.09081	0.00271	0.7564	0.0283	0.06041	0.00142	99.79	*560.3*	*16*	572	16.3	618.4	50.7	376	0.75
12-3c1	0.09646	0.00300	0.7403	0.0525	0.05566	0.00362	99.43	*593.6*	*17.7*	562.6	30.6	-	-	131	0.97
12-3j1	0.09742	0.00354	0.7934	0.0465	0.05907	0.00317	99.52	*599.2*	*20.8*	593.1	26.3	569.5	117	114	0.66
12-3k1	0.10230	0.00378	0.9028	0.0472	0.06401	0.00280	99.74	*627.8*	*22.1*	653.2	25.2	742	92.4	62	0.61
12-4l1	0.10510	0.00604	0.8430	0.0508	0.05820	0.00124	99.62	*644*	*35.3*	620.8	28	–	–	133	0.35
12-4e1	0.11620	0.00490	0.9413	0.1009	0.05875	0.00543	97.91	*708.7*	*28.3*	673.6	52.8	557.7	202	49	0.41
12-3m1	0.12520	0.00489	1.0550	0.0502	0.06108	0.00195	99.88	*760.7*	*28*	731.3	24.8	–	–	69	0.71
12-4k1	0.12690	0.01137	1.0450	0.1471	0.05975	0.00631	98.1	*770.1*	*65*	726.6	73	594.6	229	24	0.99
12-3f1	0.12920	0.00376	1.2020	0.0515	0.06748	0.00218	99.7	*783.5*	*21.5*	801.7	23.7	852.8	67	99	1.40
12-4g1	0.12990	0.00661	1.1580	0.0706	0.06464	0.00156	99.7	*787.3*	*37.7*	780.9	33.2	762.5	51	132	0.75
12-3d1	0.15040	0.00448	1.3330	0.0604	0.06426	0.00260	99.46	*903.2*	*25.1*	860	26.3	–	–	111	0.50
12-4b1	0.28980	0.01243	3.8780	0.1829	0.09705	0.00135	99.44	1641	62.1	1609	38.1	*1568*	*26.1*	156	1.10
12-4i1	0.26630	0.00964	3.8850	0.1606	0.10580	0.00167	99.88	1522	49.1	1611	33.4	*1729*	*28.9*	353	0.11
12-4d1	0.41580	0.01421	7.8420	0.2804	0.13680	0.00118	99.85	2242	64.7	2213	32.2	*2187*	*15*	128	0.50
12-3i1	0.47800	0.01866	10.410	0.3746	0.15790	0.00371	99.81	2519	81.4	2472	33.3	*2433*	*39.8*	34	0.76
12-3e1	0.49550	0.01517	11.2000	0.3566	0.16400	0.00191	99.38	2594	65.4	2540	29.7	*2497*	*19.6*	107	0.60
12-3b1	0.46700	0.01355	10.5700	0.3142	0.16420	0.00203	99.89	2470	59.6	2486	27.6	*2499*	*20.8*	160	1.00
12-3h1	0.47670	0.01559	11.250	0.3515	0.17120	0.00257	99.97	2513	68.1	2544	29.1	*2570*	*25.1*	70	1.10
PC5: Barut Formation, Alborz Mountains, KJ008 (DS). n = 9.															
13-6b1	0.09288	0.00235	0.7548	0.0232	0.05894	0.00132	99.44	*572.6*	*13.9*	571	13.4	564.9	48.9	360	0.58
13-6g1	0.09752	0.00252	0.8569	0.0289	0.06373	0.00144	99.73	*599.8*	*14.8*	628.4	15.8	–	–	198	0.59
13-6d1	0.09896	0.00310	0.8435	0.0366	0.06182	0.00236	99.89	*608.3*	*18.2*	621.1	20.2	667.8	81.6	91	0.96
13-6c1	0.14310	0.00436	1.3800	0.0522	0.06993	0.00189	99.74	*862.3*	*24.6*	880.4	22.3	926.3	55.5	218	0.28
13-5e1	0.16610	0.00865	1.3910	0.0844	0.06073	0.00185	99.88	*990.7*	*47.8*	885.1	35.9	–	–	158	0.41
13-6h1	0.17170	0.00566	1.7040	0.0686	0.07198	0.00160	99.9	*1022*	*31.1*	1010	25.8	985.3	45.4	124	1.10
13-6e1	0.17940	0.00527	1.8540	0.0933	0.07493	0.00315	99.88	1064	28.8	1065	33.2	*1067*	*84.5*	143	0.57
13-6g1-2	0.18130	0.00761	1.9400	0.0900	0.07759	0.00111	99.53	1074	41.5	1095	31.1	*1136*	*28.5*	168	0.41
13-6i1	0.24700	0.00727	3.8440	0.1176	0.11290	0.00143	99.84	1423	37.6	1602	24.6	*1846*	*23*	261	0.52
PC5: Mila Formation, Alborz Mountains, SH5-5 (BG). n = 11.															
5-g1	0.08599	0.00731	0.6875	0.0622	0.05798	0.00128	99.79	*531.8*	*43.4*	531.3	37.4	529.1	48.2	154	0.50
5-g4	0.10430	0.00975	0.8703	0.0837	0.06051	0.00096	99.97	*639.7*	*56.9*	635.7	45.4	621.8	34.4	189	0.45
5-g7	0.12010	0.01385	0.9542	0.1246	0.05764	0.00307	99.21	*731*	*79.7*	680.3	64.7	–	–	51	0.64
5-g9	0.12300	0.00999	1.1920	0.0968	0.07027	0.00206	99.22	*747.9*	*57.3*	796.9	44.8	–	–	91	3.00
5-g5	0.13870	0.01343	1.2620	0.1234	0.06601	0.00119	99.78	*837.1*	*76*	828.8	55.4	806.6	37.8	139	0.26
5-g10	0.14060	0.01069	1.3800	0.1049	0.07116	0.00047	99.81	*848.1*	*60.4*	880.3	44.7	–	–	848	0.23
5-g11	0.14060	0.01261	1.2880	0.1160	0.06641	0.00122	99.79	*848.2*	*71.3*	840.2	51.5	819.3	38.4	99	0.43
5-g2	0.17620	0.01671	1.7220	0.1643	0.07087	0.00060	99.79	1046	91.6	1017	61.3	*953.6*	*17.2*	503	0.18
5-g6	0.40600	0.03932	9.1580	0.8844	0.16360	0.00171	99.54	2197	180	2354	88.4	*2493*	*17.6*	45	1.28
5-g8	0.45240	0.03978	10.2100	0.8966	0.16370	0.00066	99.94	2406	177	2454	81.2	*2494*	*6.81*	233	0.37
5-g3	0.49380	0.04380	11.1400	0.9892	0.16370	0.00072	99.96	2587	189	2535	82.7	*2494*	*7.45*	613	0.46
PZ1: Geirud Formation, Alborz Mountains, 05MO1 (JH). n = 50.															
gr-g23	0.05395	0.00393	0.3904	0.0323	0.05247	0.00290	99.67	*338.7*	*24*	334.6	23.6	–	–	98	0.48
gr-g33	0.05552	0.00345	0.3766	0.1000	0.04920	0.01211	73.61	*348.3*	*21*	324.5	73.8	–	–	251	0.75
gr-g15	0.05554	0.00381	0.4006	0.1265	0.05232	0.01554	89.65	*348.4*	*23.3*	342.1	91.7	–	–	101	0.47
gr-g27	0.05589	0.00354	0.3267	0.0519	0.04240	0.00606	97.66	*350.6*	*21.6*	287.1	39.7	–	–	88	0.47
gr-g45	0.05610	0.00348	0.4346	0.0386	0.05618	0.00317	99.63	*351.9*	*21.2*	366.4	27.3	459.5	125	76	0.40
gr-g5	0.05618	0.00386	0.3722	0.0341	0.04804	0.00258	98.98	*352.4*	*23.6*	321.3	25.2	–	–	212	0.61
gr-g3	0.05660	0.00460	0.3830	0.0501	0.04908	0.00501	97.75	*354.9*	*28*	329.2	36.8	–	–	107	0.47
gr-g1	0.05733	0.00433	0.4314	0.0405	0.05458	0.00297	99.6	*359.3*	*26.4*	364.2	28.7	395.2	122	105	0.47

(continued on next page)

Table 2 (*continued*)

Sample ID	$^{206}Pb^*/^{238}U$	$^{206}Pb^*/^{238}U$	$^{207}Pb^*/^{235}U$	$^{207}Pb^*/^{235}U$	$^{207}Pb^*/^{206}Pb$	$^{207}Pb^*/^{206}Pb$	% Radiogenic ^{206}Pb	Age (Ma) $^{206}Pb/^{238}U$	Age (Ma) $^{206}Pb/^{238}U$	Age (Ma) $^{207}Pb/^{235}U$	Age (Ma) $^{207}Pb/^{235}U$	Age (Ma) $^{207}Pb/^{206}Pb$	Age (Ma) $^{207}Pb/^{206}Pb$	U (ppm)	Th/U
		1 σ		1 σ		1 σ			1 σ		1 σ		1 σ		
gr-g17	0.05746	0.00380	0.4269	0.0389	0.05388	0.00306	99.27	*360.2*	*23.2*	360.9	27.7	365.9	128	119	0.49
gr-g36	0.05854	0.00323	0.4308	0.0269	0.05337	0.00146	99.85	*366.8*	*19.6*	363.7	19.1	344.4	61.7	210	0.45
gr-g24	0.05865	0.00405	0.3812	0.0333	0.04714	0.00234	99.37	*367.4*	*24.6*	327.9	24.5	–	–	159	0.53
gr-g28	0.05876	0.00390	0.4231	0.0375	0.05222	0.00337	99.62	*368.1*	*23.7*	358.3	26.7	–	–	60	0.34
gr-g26	0.05903	0.00335	0.4194	0.0304	0.05153	0.00230	99.07	*369.8*	*20.4*	355.6	21.8	–	–	159	0.44
gr-g47	0.05968	0.00358	0.4120	0.0331	0.05007	0.00302	99.35	*373.7*	*21.8*	350.3	23.8	–	–	95	0.85
gr-g7	0.05972	0.00404	0.4265	0.0357	0.05179	0.00244	99.65	*373.9*	*24.5*	360.7	25.4	–	–	117	0.46
gr-g12	0.05973	0.00357	0.4202	0.0375	0.05102	0.00363	99.4	*374*	*21.7*	356.2	26.8	–	–	128	0.47
gr-g20	0.06063	0.00356	0.4445	0.0292	0.05317	0.00152	99.6	*379.4*	*21.6*	373.4	20.5	–	–	417	0.36
gr-g46	0.06212	0.00459	0.4275	0.0405	0.04991	0.00294	99.75	*388.5*	*27.8*	361.4	28.8	–	–	77	0.45
gr-g43	0.06236	0.00378	0.4721	0.0307	0.05491	0.00116	99.93	*389.9*	*22.9*	392.6	21.1	408.4	47.2	421	0.51
gr-g6	0.06315	0.00448	0.4518	0.0387	0.05189	0.00230	98.54	*394.7*	*27.1*	378.5	27.1	–	–	360	0.48
gr-g49	0.06496	0.00460	0.4670	0.0399	0.05214	0.00207	99.66	*405.7*	*27.8*	389.1	27.6	–	–	213	0.55
gr-g50	0.06720	0.00521	0.5119	0.0453	0.05524	0.00189	100	*419.3*	*31.5*	419.7	30.4	422.1	76.3	90	0.45
gr-g25	0.08584	0.00517	0.6514	0.0811	0.05504	0.00550	99.01	*530.9*	*30.7*	509.4	49.9	–	–	37	0.84
gr-g2	0.08728	0.00645	0.6718	0.0511	0.05583	0.00113	99.85	*539.4*	*38.3*	521.8	31	–	–	534	0.07
gr-g4	0.09193	0.00636	0.7308	0.0574	0.05765	0.00247	99.81	*567*	*37.6*	557	33.7	516.5	93.9	82	0.30
gr-g13	0.09320	0.00546	0.7591	0.0635	0.05907	0.00354	99.54	*574.4*	*32.2*	573.5	36.7	569.7	130	54	0.80
gr-g44	0.09572	0.00592	0.8072	0.0564	0.06116	0.00248	99.73	*589.3*	*34.8*	600.9	31.7	644.9	87.1	56	1.30
gr-g10	0.09865	0.00608	0.8274	0.0543	0.06083	0.00242	99.91	*606.5*	*35.6*	612.2	30.2	633.2	85.6	86	0.71
gr-g11	0.10180	0.00879	0.7206	0.1105	0.05136	0.00587	98.42	*624.8*	*51.4*	551	65.2	–	–	31	2.10
gr-g31	0.11040	0.00619	0.9019	0.0617	0.05927	0.00223	98.14	*674.9*	*35.9*	652.8	32.9	576.9	81.9	343	0.62
gr-g39	0.11100	0.00650	0.9193	0.0553	0.06008	0.00114	99.91	*678.4*	*37.7*	662	29.2	606.4	41.1	229	0.18
gr-g34	0.12280	0.00781	1.1110	0.0783	0.06564	0.00145	99.88	*746.7*	*44.8*	758.9	37.6	794.9	46.3	123	1.10
gr-g37	0.12500	0.00740	1.1150	0.0708	0.06469	0.00111	99.91	*759.1*	*42.4*	760.4	34	764.1	36	122	0.40
gr-g18	0.12640	0.00788	1.1100	0.0735	0.06371	0.00145	99.83	*767.3*	*45.1*	758.4	35.4	732.1	48.1	189	0.80
gr-g40	0.12730	0.01008	1.1440	0.0870	0.06517	0.00325	99.91	*772.3*	*57.6*	774.2	41.2	779.8	105	52	0.81
gr-g29	0.12930	0.00764	1.1300	0.0716	0.06340	0.00131	99.83	*783.9*	*43.6*	767.9	34.1	721.8	44	153	0.79
gr-g14	0.13030	0.00911	1.1160	0.0894	0.06212	0.00260	99.71	*789.5*	*52*	761	42.9	678.2	89.5	73	0.54
gr-g48	0.13270	0.00753	1.2350	0.0776	0.06752	0.00222	99.91	*803.1*	*42.9*	816.7	35.3	853.9	68.1	139	0.76
gr-g30	0.13430	0.00819	1.2090	0.0778	0.06532	0.00096	99.89	*812.1*	*46.6*	804.8	35.7	784.6	30.8	287	0.95
gr-g21	0.13770	0.00956	1.2380	0.0993	0.06525	0.00289	99.6	*831.4*	*54.2*	818.2	45	782.4	93	52	0.62
gr-g38	0.13900	0.00940	1.2620	0.0885	0.06588	0.00179	99.82	*838.8*	*53.2*	828.9	39.7	802.5	56.8	72	0.40
gr-g19	0.14070	0.01265	1.1930	0.1665	0.06150	0.00584	99.05	*848.8*	*71.5*	797.5	77.1	656.6	204	22	0.40
gr-g51	0.15150	0.01071	1.3340	0.0981	0.06386	0.00111	99.91	*909.4*	*60*	860.6	42.7	–	–	146	0.90
gr-g52	0.17160	0.01105	1.5940	0.1163	0.06739	0.00220	99.41	1021	60.8	968	45.5	*849.9*	*67.9*	118	0.32
gr-g9	0.17660	0.01469	1.6700	0.1458	0.06857	0.00358	99.66	1048	80.5	997.1	55.5	*885.9*	*108*	37	0.43
gr-g8	0.16900	0.01171	1.6270	0.1183	0.06983	0.00106	99.92	1007	64.5	980.9	45.7	*923.2*	*31.2*	321	0.52
gr-g35	0.17090	0.00926	1.7090	0.0943	0.07252	0.00071	99.92	1017	51	1012	35.4	*1000*	*19.8*	543	0.33
gr-g41	0.17520	0.01071	1.7770	0.1136	0.07354	0.00095	99.96	1041	58.8	1037	41.5	*1029*	*26*	187	0.46
gr-g16	0.23980	0.01499	3.4940	0.2274	0.10570	0.00147	99.83	1385	77.9	1526	51.4	*1726*	*25.5*	169	0.18
gr-g42	0.54220	0.03384	15.1100	0.9433	0.20210	0.00160	99.94	2793	141	2822	59.5	*2843*	*12.9*	109	1.90
PZ2: Dorud Formation, Alborz Mountains, 05DO1 (JH). n = 51.															
do-g22	0.04284	0.00325	0.2917	0.0734	0.04939	0.01086	97.8	*270.4*	*20.1*	259.9	57.7	–	–	34	0.35
do-g29	0.04471	0.00338	0.3425	0.0323	0.05555	0.00290	99.81	*282*	*20.9*	299	24.4	–	–	130	0.56
do-g46	0.04551	0.00517	0.3054	0.0460	0.04866	0.00504	99.31	*286.9*	*31.9*	270.6	35.8	–	–	49	0.35
do-g6	0.04880	0.00313	0.3524	0.0284	0.05238	0.00268	99.72	*307.1*	*19.3*	306.5	21.3	–	–	210	0.44
do-g18	0.04951	0.00287	0.3136	0.0277	0.04594	0.00294	98.98	*311.5*	*17.6*	277	21.4	–	–	201	0.55
do-g12	0.05017	0.00346	0.4023	0.0431	0.05816	0.00486	99.56	*315.6*	*21.3*	343.3	31.2	–	–	47	0.41
do-g3	0.05065	0.00345	0.4065	0.0571	0.05821	0.00686	99.49	*318.5*	*21.2*	346.3	41.2	–	–	64	0.49
do-g41	0.05084	0.00329	0.3286	0.0310	0.04688	0.00371	100	*319.7*	*20.2*	288.5	23.7	–	–	31	0.51
do-g36	0.05088	0.00327	0.3727	0.0408	0.05313	0.00423	99.5	*319.9*	*20.1*	321.7	30.1	–	–	154	0.50
do-g43	0.05146	0.00287	0.3655	0.0255	0.05151	0.00207	99.66	*323.5*	*17.6*	316.3	18.9	–	–	330	0.29
do-g23	0.05163	0.00394	0.3568	0.0372	0.05012	0.00453	99.49	*324.5*	*24.2*	309.8	27.8	–	–	90	0.54
do-g27	0.05180	0.00308	0.3484	0.0283	0.04878	0.00294	99.49	*325.6*	*18.9*	303.5	21.3	–	–	252	0.55
do-g32	0.05184	0.00422	0.4015	0.0967	0.05617	0.01254	97.32	*325.8*	*25.9*	342.7	70	–	–	106	0.51
do-g44	0.05185	0.00340	0.4145	0.0392	0.05798	0.00449	99.59	*325.8*	*20.9*	352.1	28.1	–	–	82	0.59
do-g21	0.05259	0.00380	0.3780	0.0404	0.05213	0.00411	99.54	*330.4*	*23.3*	325.6	29.8	–	–	95	0.76

do-g48	0.05264	0.00356	0.3642	0.0340	0.05017	0.00275	99.6	*330.7*	*21.8*	315.3	25.3	–	–	232	0.53
do-g2	0.05265	0.00320	0.3837	0.0264	0.05285	0.00167	99.64	*330.8*	*19.6*	329.8	19.4	–	–	342	0.72
do-g19	0.05285	0.00430	0.3880	0.0510	0.05325	0.00492	99.39	*332*	*26.3*	332.9	37.3	–	–	115	0.51
do-g5	0.05361	0.00354	0.4456	0.0475	0.06029	0.00481	99.4	*336.6*	*21.7*	374.2	33.4	–	–	80	0.70
do-g53	0.05409	0.00530	0.3774	0.0798	0.05061	0.00937	98.14	*339.6*	*32.4*	325.1	58.9	–	–	35	0.51
do-g7	0.05427	0.00382	0.3849	0.0432	0.05143	0.00392	99.26	*340.7*	*23.3*	330.6	31.7	–	–	118	0.69
do-g35	0.05630	0.00409	0.4172	0.0554	0.05375	0.00602	99.15	*353.1*	*24.9*	354.1	39.7	–	–	82	0.41
do-g17–2	0.06249	0.00657	0.4972	0.0822	0.05771	0.00765	97.11	*390.8*	*39.9*	409.8	55.7	–	–	49	0.51
do-g42	0.07029	0.00372	0.5786	0.0371	0.05970	0.00178	99.94	*437.9*	*22.4*	463.6	23.8	592.8	64.5	242	0.43
do-g40	0.07439	0.00568	0.3424	0.1991	0.03338	0.01851	96.23	*462.6*	*34.1*	299	151	–	–	24	2.90
do-g15	0.08582	0.00570	0.7057	0.0859	0.05964	0.00648	99.45	*530.8*	*33.9*	542.2	51.1	590.6	236	45	0.40
do-g26	0.08686	0.00554	0.7010	0.0761	0.05853	0.00455	99.63	*536.9*	*32.8*	539.4	45.4	549.8	170	38	1.50
do-g49	0.08954	0.00501	0.6619	0.0492	0.05362	0.00261	99.62	*552.8*	*29.6*	515.8	30.1	–	–	101	1.20
do-g9	0.09417	0.00615	0.7517	0.0541	0.05789	0.00174	99.94	*580.2*	*36.2*	569.2	31.4	525.5	65.9	167	1.90
do-g39	0.09685	0.00946	0.8264	0.1187	0.06188	0.00668	98.56	*595.9*	*55.6*	611.6	66	670	231	36	0.73
do-g28	0.09769	0.00623	0.8142	0.0658	0.06045	0.00305	99.86	*600.9*	*36.6*	604.8	36.8	619.6	109	91	1.10
do-g4	0.09971	0.01485	1.2430	0.2443	0.09042	0.01004	100	*612.7*	*87*	820.3	111	–	–	14	0.81
do-g47	0.10040	0.00853	0.8351	0.0888	0.06033	0.00413	99.48	*616.7*	*50*	616.5	49.1	615.6	148	59	0.56
do-g51	0.10350	0.00652	0.8572	0.0647	0.06007	0.00206	99.94	*634.9*	*38.1*	628.6	35.4	606	74	143	0.68
do-g37	0.10450	0.00864	0.7962	0.1008	0.05524	0.00424	99.23	*641*	*50.4*	594.7	57	–	–	130	0.79
do-g33	0.11270	0.00711	0.9662	0.0676	0.06219	0.00193	99.94	*688.3*	*41.2*	686.5	34.9	680.5	66.4	140	0.27
do-g13	0.11360	0.00905	0.9715	0.1028	0.06201	0.00381	99.57	*693.7*	*52.4*	689.2	52.9	674.5	132	42	0.42
do-g8	0.11710	0.00651	1.0110	0.1147	0.06261	0.00626	98.88	*713.7*	*37.6*	709.2	57.9	695	213	40	0.59
do-g50	0.12060	0.00745	1.1440	0.0816	0.06882	0.00187	99.84	*733.8*	*42.9*	774.5	38.6	–	–	187	0.32
do-g1	0.13030	0.01122	1.0920	0.1678	0.06079	0.00710	98.76	*789.8*	*64*	749.7	81.4	631.8	251	23	0.40
do-g30	0.13090	0.01146	1.0330	0.1553	0.05722	0.00693	98.73	*793.2*	*65.3*	720.5	77.6	–	–	62	0.81
do-g45	0.13470	0.00782	1.2800	0.0949	0.06893	0.00365	99.56	*814.8*	*44.4*	837.1	42.3	896.7	109	76	0.46
do-g16	0.13960	0.00962	1.2320	0.0999	0.06399	0.00290	99.7	*842.3*	*54.4*	815	45.5	741.2	95.9	99	0.52
do-g34	0.14760	0.00942	1.3960	0.0990	0.06858	0.00170	99.76	*887.5*	*52.9*	887.1	42	886	51.3	160	0.42
do-g52	0.14990	0.00943	1.2930	0.1064	0.06256	0.00294	99.45	*900.3*	*52.9*	842.5	47.1	–	–	107	0.56
do-g24	0.17220	0.01099	1.6170	0.1371	0.06808	0.00369	98.67	*1024*	*60.4*	976.7	53.2	870.9	112	259	0.81
do-g31	0.34750	0.02485	5.2560	0.3895	0.10970	0.00185	99.51	1923	119	1862	63.2	*1794*	*30.6*	228	0.01
do-g25	0.33230	0.02279	5.1030	0.3635	0.11140	0.00129	99.89	1850	110	1837	60.5	*1822*	*21.1*	253	0.33
do-g20	0.36980	0.03026	5.6850	0.4955	0.11150	0.00191	99.66	2029	142	1929	75.3	*1824*	*31.1*	208	0.67
do-g11	0.34490	0.02243	5.6320	0.3766	0.11840	0.00126	99.93	1910	108	1921	57.7	*1933*	*19.1*	156	0.18
do-g10	0.46200	0.03169	10.5700	0.7665	0.16590	0.00325	99.76	2449	140	2486	67.3	*2517*	*32.9*	23	0.91
PZ3: Zakeen Formation, Zagros Mountains, −92 (MZ). n = 49.															
92-g54	0.07471	0.00636	0.6083	0.0540	0.05904	0.00133	98.87	*464.5*	*38.2*	482.5	34.1	–	–	925	0.85
92-g53	0.07569	0.00442	0.5687	0.0351	0.05450	0.00114	99.97	*470.3*	*26.5*	457.2	22.7	–	–	523	0.87
92-g48	0.07676	0.00640	0.5811	0.0721	0.05491	0.00497	99.37	*476.7*	*38.3*	465.2	46.3	408.7	202	34	1.60
92-g4	0.08058	0.00445	0.6683	0.0437	0.06015	0.00187	99.93	*499.6*	*26.6*	519.7	26.6	–	–	93	0.69
92-g42	0.08066	0.00414	0.6348	0.0411	0.05708	0.00256	99.94	*500.1*	*24.7*	499.1	25.5	494.5	99	169	1.30
92-g18	0.08181	0.00557	0.6582	0.0503	0.05834	0.00220	100	*506.9*	*33.2*	513.5	30.8	542.7	82.3	74	0.89
92-g37	0.08499	0.00492	0.7090	0.0441	0.06050	0.00156	99.96	*525.9*	*29.2*	544.2	26.2	–	–	186	0.44
92-g41	0.08724	0.00620	0.7390	0.0762	0.06144	0.00433	100	*539.2*	*36.8*	561.8	44.5	654.5	151	33	1.60
92-g60	0.08772	0.00619	0.7008	0.0501	0.05794	0.00100	99.85	*542*	*36.7*	539.3	29.9	527.5	37.7	304	0.45
92-g56	0.08945	0.00576	0.7007	0.0515	0.05681	0.00171	99.63	*552.3*	*34.1*	539.2	30.7	484.3	66.4	185	2.80
92-g2	0.09091	0.00526	0.7564	0.0448	0.06035	0.00076	99.63	*560.9*	*31.1*	572	25.9	616	27	753	0.81
92-g25	0.09349	0.01124	0.7573	0.0903	0.05875	0.00089	99.88	*576.1*	*66.3*	572.5	52.2	557.9	33.1	198	0.33
92-g50	0.09454	0.00561	0.7543	0.0511	0.05787	0.00259	99.61	*582.3*	*33*	570.7	29.6	524.8	98.3	170	0.66
92-g43	0.09511	0.00633	0.7382	0.0601	0.05629	0.00289	99.59	*585.7*	*37.3*	561.3	35.1	464	114	83	0.63
92-g15	0.09561	0.00785	0.7340	0.0665	0.05568	0.00178	99.81	*588.6*	*46.2*	558.9	38.9	–	–	102	1.40
92-g46	0.09568	0.00528	0.7761	0.0435	0.05883	0.00096	99.86	*589*	*31.1*	583.3	24.9	561	35.5	415	0.46
92-g24	0.09685	0.00730	0.7724	0.0642	0.05784	0.00122	99.87	*595.9*	*42.9*	581.1	36.8	523.6	46.2	207	2.00
92-g14	0.09746	0.00660	0.8423	0.0621	0.06268	0.00204	99.87	*599.5*	*38.8*	620.4	34.2	697.4	69.4	74	0.42
92-g49	0.09811	0.00701	0.7906	0.0579	0.05844	0.00270	99.81	*603.3*	*41.2*	591.5	32.8	546.4	101	96	0.28
92-g35	0.09880	0.00544	0.8088	0.0491	0.05937	0.00130	99.94	*607.4*	*31.9*	601.8	27.5	580.8	47.4	135	0.35
92-g8	0.10280	0.00856	0.8367	0.0731	0.05904	0.00162	99.72	*630.6*	*50*	617.3	40.4	568.7	59.8	91	0.38
92-g32	0.10480	0.00672	0.8683	0.0586	0.06007	0.00121	99.9	*642.7*	*39.2*	634.6	31.8	606	43.5	173	0.43
92-g61	0.10920	0.00820	0.8993	0.0798	0.05973	0.00254	99.88	*668.1*	*47.6*	651.4	42.7	593.7	92	64	0.43
92-g34	0.10990	0.00683	0.9349	0.0690	0.06168	0.00237	99.84	*672.3*	*39.7*	670.2	36.2	663.2	82.2	68	0.14
92-g9	0.11130	0.00775	0.9616	0.0668	0.06265	0.00092	99.93	*680.4*	*44.9*	684.1	34.6	696.5	31.4	390	0.06
92-g27	0.11510	0.00943	0.9936	0.0878	0.06259	0.00189	99.87	*702.5*	*54.5*	700.6	44.7	694.2	64.3	67	0.77

(continued on next page)

Table 2 (*continued*)

Sample ID	$^{206}Pb^*/^{238}U$	$^{206}Pb^*/^{238}U$	$^{207}Pb^*/^{235}U$	$^{207}Pb^*/^{235}U$	$^{207}Pb^*/^{206}Pb$	$^{207}Pb^*/^{206}Pb$	% Radiogenic ^{206}Pb	Age (Ma) $^{206}Pb/^{238}U$	Age (Ma) $^{206}Pb/^{238}U$	Age (Ma) $^{207}Pb/^{235}U$	Age (Ma) $^{207}Pb/^{235}U$	Age (Ma) $^{207}Pb/^{206}Pb$	Age (Ma) $^{207}Pb/^{206}Pb$	U (ppm)	Th/U
		1 σ		1 σ		1 σ			1 σ		1 σ		1 σ		
92-g20	0.11540	0.00874	0.9745	0.0758	0.06125	0.00119	99.89	*704*	*50.5*	690.8	39	647.9	41.8	172	0.22
92-g47	0.12320	0.00627	1.2240	0.0711	0.07208	0.00215	99.91	*749*	*36*	811.8	32.4	–	–	54	0.60
92-g3	0.12330	0.00784	1.0750	0.0821	0.06321	0.00266	100	*749.5*	*45*	741	40.2	715.2	89.2	58	0.31
92-g36	0.12710	0.01008	1.0820	0.0899	0.06177	0.00156	99.85	*771.2*	*57.6*	744.8	43.8	–	–	101	0.47
92-g62	0.13010	0.01021	1.1610	0.0930	0.06468	0.00171	99.82	*788.6*	*58.2*	782.2	43.7	763.9	55.8	148	0.41
92-g63	0.13290	0.00899	1.2630	0.0879	0.06895	0.00096	99.82	*804.3*	*51.2*	829.3	39.4	–	–	319	0.85
92-g59	0.13710	0.00924	1.2160	0.0836	0.06434	0.00134	99.89	*828*	*52.4*	807.9	38.3	752.7	44	131	0.56
92-g21	0.13820	0.00982	1.2410	0.0952	0.06511	0.00193	99.69	*834.4*	*55.6*	819.2	43.1	778	62.4	67	0.57
92-g58	0.13930	0.01278	1.2540	0.1200	0.06530	0.00212	99.87	*840.6*	*72.3*	825.2	54	783.9	68.1	35	0.96
92-g44	0.14440	0.00823	1.3700	0.0809	0.06880	0.00098	99.96	*869.8*	*46.3*	876.3	34.6	892.8	29.3	383	0.56
92-g29	0.14980	0.01314	1.3800	0.1485	0.06679	0.00362	99.53	*900.1*	*73.7*	880.4	63.4	831.3	113	22	0.64
92-g6	0.15090	0.00895	1.4120	0.0850	0.06784	0.00076	99.98	906.1	50.1	893.9	35.8	*863.8*	*23.1*	330	0.13
92-g23	0.15030	0.00984	1.4240	0.0949	0.06870	0.00135	99.92	902.8	55.1	899	39.8	*889.6*	*40.6*	104	0.30
92-g17	0.17440	0.01215	1.6820	0.1222	0.06996	0.00110	99.95	1036	66.7	1002	46.3	*927.3*	*32.1*	150	0.60
92-g1	0.15610	0.00922	1.5350	0.0941	0.07128	0.00124	99.98	935.2	51.4	944.3	37.7	*965.6*	*35.4*	108	0.62
92-g16	0.15490	0.01036	1.5350	0.1202	0.07185	0.00254	100	928.6	57.8	944.5	48.1	*981.8*	*72.1*	28	0.34
92-g45	0.17540	0.01233	1.7450	0.1357	0.07216	0.00163	99.88	1042	67.6	1025	50.2	*990.5*	*45.8*	131	0.39
92-g10	0.17920	0.01192	1.8170	0.1221	0.07353	0.00062	99.93	1063	65.2	1052	44	*1029*	*17.2*	457	0.84
92-g11	0.46170	0.04006	9.7130	0.8425	0.15260	0.00264	99.97	2447	177	2408	79.9	*2375*	*29.5*	44	0.98
92-g33	0.48290	0.03166	10.6800	0.7058	0.16040	0.00135	99.94	2540	138	2496	61.3	*2460*	*14.2*	149	1.40
92-g31	0.30210	0.02041	6.7700	0.4548	0.16260	0.00224	99.85	1701	101	2082	59.4	*2482*	*23.2*	104	2.10
92-g51	0.37920	0.02865	8.8990	0.7019	0.17020	0.00397	99.71	2073	134	2328	72	*2560*	*39*	52	0.19
92-g28	0.48440	0.04271	12.2200	1.1050	0.18290	0.00332	99.9	2546	185	2621	84.9	*2680*	*30*	29	0.41
PZ4: Faraghan Formation, Zagros Mountains, 217 (MZ). March 2005 n = 37. March 2006 n = 12. TOTAL n = 49.															
217-g16	0.07492	0.00456	0.7129	0.0437	0.06901	0.00070	99.69	*465.7*	*27.4*	546.5	25.9	–	–	802	0.60
217-g31	0.07900	0.00622	0.6337	0.0543	0.05818	0.00147	100	*490.2*	*37.2*	498.4	33.7	536.4	55.3	78	1.10
217-g26	0.07967	0.00631	0.6503	0.0530	0.05920	0.00089	99.53	*494.1*	*37.6*	508.7	32.6	–	–	874	0.56
217-5	0.08716	0.00580	0.7611	0.0538	0.06333	0.00126	99.75	*537.9*	*33*	573.9	29.9	–	–	364	0.88
217-g32	0.08774	0.00720	0.6816	0.0574	0.05634	0.00135	99.8	*542.2*	*42.7*	527.7	34.7	465.7	53.1	247	0.32
217-g37	0.09417	0.00859	0.7688	0.0710	0.05921	0.00083	99.93	*580.2*	*50.6*	579.1	40.7	574.8	30.6	417	0.88
217-8	0.09472	0.00696	0.7330	0.0683	0.05613	0.00294	99.03	*582.4*	*39.7*	557.5	39.2	–	–	63	2.50
217-10	0.09846	0.00662	0.7781	0.0539	0.05732	0.00089	99.67	*604.8*	*37.1*	584	29.5	–	–	644	0.15
217-3	0.09880	0.00679	0.7827	0.0589	0.05745	0.00149	99.63	*606.5*	*38.3*	586.3	32.5	–	–	127	0.38
217-g33	0.10360	0.00929	0.8360	0.0768	0.05850	0.00102	99.89	*635.7*	*54.3*	616.9	42.5	–	–	146	0.34
217-12	0.10480	0.00656	0.8479	0.0551	0.05868	0.00089	99.7	*641.5*	*36.4*	622.7	28.9	–	–	464	0.22
217-g9	0.10490	0.01242	0.8266	0.0983	0.05717	0.00088	99.88	*642.9*	*72.5*	611.7	54.6	–	–	310	1.20
217-1	0.10860	0.00691	0.8849	0.0599	0.05911	0.00115	99.63	*663.2*	*38.4*	642.6	31	–	–	255	0.32
217-g4	0.11000	0.01506	0.8648	0.1170	0.05700	0.00133	99.79	*673*	*87.4*	632.7	63.7	–	–	164	0.73
217-g39	0.11050	0.01092	0.9626	0.0957	0.06319	0.00120	99.89	*675.6*	*63.4*	684.6	49.5	714.6	40.4	514	1.00
217-g7	0.11180	0.01334	0.9318	0.1113	0.06043	0.00123	99.79	*683.4*	*77.3*	668.6	58.5	618.9	44	133	0.18
217-g21	0.11350	0.01231	0.9571	0.1053	0.06116	0.00104	99.89	*693*	*71.3*	681.8	54.6	644.9	36.5	106	0.26
217-g17	0.11410	0.01439	0.8920	0.1136	0.05670	0.00106	99.86	*696.5*	*83.3*	647.4	61	–	–	211	0.36
217-g22	0.11570	0.01268	0.9546	0.1054	0.05982	0.00083	99.83	*706*	*73.3*	680.5	54.8	–	–	392	0.17
217-g18	0.12090	0.01490	1.0050	0.1282	0.06030	0.00148	99.85	*735.5*	*85.7*	706.2	65	–	–	103	0.49
217-g19	0.12200	0.01012	1.1000	0.0903	0.06540	0.00110	99.88	*741.8*	*58.2*	753.2	43.7	787.1	35.3	204	1.10
217-g8	0.12280	0.01121	1.0890	0.0999	0.06431	0.00062	99.98	*746.5*	*64.4*	747.9	48.6	752	20.5	279	0.37
217-g11	0.12610	0.01633	0.9868	0.1346	0.05677	0.00213	99.84	*765.4*	*93.5*	697.1	68.8	–	–	77	1.60
217-g3	0.12670	0.00852	1.2860	0.0884	0.07360	0.00077	99.88	*769.3*	*48.7*	839.7	39.3	–	–	296	0.32
217-9	0.13020	0.00842	1.1570	0.0829	0.06449	0.00149	99.64	*787.4*	*45.9*	779.7	37.7	757.7	48.8	106	0.70
217-g5	0.13370	0.02349	1.0440	0.2008	0.05667	0.00413	99.04	*808.8*	*134*	726.1	99.7	–	–	42	0.06
217-g1	0.13520	0.01345	1.2290	0.1219	0.06595	0.00072	99.98	*817.3*	*76.4*	813.9	55.5	804.7	22.9	216	1.00
217-7	0.13950	0.00949	1.2430	0.0869	0.06464	0.00094	99.76	*840.6*	*51.5*	819.5	37.8	762.7	30.7	236	1.30
217-g27	0.14220	0.01240	1.4570	0.1309	0.07430	0.00238	99.66	*857.2*	*70*	912.8	54.1	–	–	29	0.65
217-g38	0.14430	0.01279	1.3110	0.1170	0.06593	0.00096	99.87	*868.7*	*72.1*	850.7	51.4	804.1	30.5	212	0.53
217-g13	0.14880	0.01668	1.3500	0.1501	0.06582	0.00118	99.88	*894.3*	*93.6*	867.8	64.9	800.7	37.7	90	0.69
217-g40	0.15470	0.01488	1.4290	0.1377	0.06701	0.00066	99.9	*927.3*	*83*	901.3	57.5	–	–	351	0.42
217-13	0.15550	0.01420	1.5910	0.1703	0.07419	0.00407	99.25	*930.5*	*78*	965.7	66	1047	111	25	0.55
217-g10	0.16490	0.01677	1.8180	0.1903	0.07994	0.00146	99.84	*984.1*	*92.8*	1052	68.6	–	–	83	2.00

217-g12	0.18520	0.03187	1.5120	0.2617	0.05921	0.00097	99.53	1096	173	935.4	106	*574.9*	*35.5*	557	0.86
217-4	0.15800	0.00993	1.5020	0.0972	0.06897	0.00124	99.63	943.8	52.7	930.1	37.8	*897.9*	*37*	172	0.34
217-6	0.17370	0.01525	1.6710	0.1500	0.06976	0.00132	98.91	1035	80.7	998.9	55	*921.3*	*39*	380	2.30
217-g2	0.18290	0.01962	1.7830	0.1917	0.07069	0.00063	99.96	1083	107	1039	69.9	*948.4*	*18.3*	311	0.10
217-g6	0.18770	0.02299	1.8370	0.2286	0.07101	0.00145	99.83	1109	125	1059	81.8	*957.8*	*41.7*	84	0.54
217-11	0.16830	0.01109	1.6690	0.1098	0.07192	0.00062	99.85	1002	58.4	996	39.9	*983.7*	*17.6*	358	0.34
217-g28	0.20280	0.01982	2.0370	0.2081	0.07287	0.00140	99.87	1190	106	1128	69.6	*1010*	*39*	128	0.64
217-g23	0.17780	0.01729	1.7940	0.1774	0.07320	0.00087	99.95	1055	94.7	1043	64.5	*1020*	*24*	332	0.60
217-2	0.19640	0.01447	2.0000	0.1562	0.07388	0.00165	99.64	1155	75.1	1115	51.1	*1038*	*45*	112	1.50
217-g25	0.19580	0.03305	2.0810	0.3202	0.07707	0.00441	99.88	1153	178	1142	106	*1123*	*114*	166	0.75
217-g15	0.19600	0.01730	2.9670	0.2614	0.10980	0.00203	99.95	1154	93.2	1399	66.9	*1796*	*33.6*	441	0.58
217-g24	0.42200	0.04044	7.7010	0.7392	0.13240	0.00064	99.99	2270	183	2197	86.3	*2129*	*8.49*	439	0.38
217-g35	0.40340	0.03154	8.9160	0.6987	0.16030	0.00075	99.97	2185	145	2329	71.5	*2459*	*7.88*	493	0.46
217-g30	0.50500	0.04682	11.3600	1.0490	0.16320	0.00127	99.96	2635	201	2554	86.1	*2489*	*13.1*	351	0.32
217-g36	0.36400	0.03160	8.4530	0.7481	0.16840	0.00231	99.98	2001	149	2281	80.4	*2542*	*23*	64	1.40
MZ1: Shemshak Formation (East), Alborz Mountains, KJ006 (DS). n = 54.															
11-2j1	0.03239	0.00093	0.2234	0.0118	0.05002	0.00226	99.56	*205.5*	*5.79*	204.7	9.83	–	–	234	0.60
11-1a1	0.03384	0.00100	0.2249	0.0142	0.04820	0.00285	99.42	*214.5*	*6.25*	206	11.8	–	–	194	0.42
11-1k2	0.03402	0.00098	0.2140	0.0137	0.04563	0.00254	98.32	*215.6*	*6.12*	196.9	11.4	–	–	564	0.34
11-g12	0.03418	0.00276	0.2532	0.0221	0.05371	0.00177	99.84	*216.7*	*17.2*	229.1	17.9	–	–	199	0.67
11-1g1	0.03428	0.00097	0.2204	0.0132	0.04663	0.00239	99.37	*217.3*	*6.02*	202.2	11	–	–	393	0.50
11-2k1	0.03509	0.00098	0.2462	0.0082	0.05089	0.00098	99.83	*222.3*	*6.09*	223.5	6.71	–	–	743	0.28
11-2b1	0.03583	0.00108	0.2359	0.0182	0.04776	0.00332	99	*226.9*	*6.71*	215.1	14.9	–	–	169	0.54
11-2a1	0.03756	0.00106	0.2410	0.0098	0.04654	0.00140	99.45	*237.7*	*6.58*	219.2	8.03	–	–	558	0.32
11-g15	0.03800	0.00363	0.2564	0.0264	0.04893	0.00204	99.58	*240.5*	*22.5*	231.7	21.3	–	–	194	0.54
11-g8	0.03806	0.00308	0.2748	0.0231	0.05235	0.00110	99.96	*240.8*	*19.1*	246.5	18.4	–	–	375	0.43
11-2n1	0.04030	0.00114	0.2726	0.0159	0.04906	0.00237	99.76	*254.7*	*7.07*	244.7	12.7	–	–	418	0.51
11-2c1	0.04086	0.00118	0.2847	0.0117	0.05053	0.00151	99.77	*258.2*	*7.28*	254.4	9.21	–	–	366	0.43
11-2p1	0.04102	0.00116	0.2801	0.0151	0.04952	0.00223	99.83	*259.2*	*7.16*	250.7	12	–	–	398	0.32
11-2q1	0.04363	0.00146	0.2863	0.0268	0.04759	0.00419	99.43	*275.3*	*9*	255.7	21.1	–	–	133	0.35
11-1c1	0.04693	0.00130	0.3188	0.0290	0.04928	0.00406	98.97	*295.6*	*8*	281	22.3	–	–	163	0.45
11-1d1	0.05294	0.00152	0.3751	0.0190	0.05139	0.00205	99.63	*332.5*	*9.28*	323.4	14	–	–	389	0.37
11-g3	0.05581	0.00460	0.4145	0.0349	0.05387	0.00115	99.77	*350.1*	*28.1*	352.1	25.1	365.5	48	238	0.39
11-1b1	0.05757	0.00163	0.4275	0.0287	0.05386	0.00338	99.7	*360.8*	*9.95*	361.4	20.4	365	141	118	1.30
11-g2	0.06716	0.00545	0.4989	0.0405	0.05388	0.00070	99.83	*419.1*	*32.9*	411	27.5	–	–	1251	0.10
11-g16	0.07556	0.00623	0.5585	0.0477	0.05361	0.00114	99.79	*469.6*	*37.3*	450.6	31.1	–	–	237	0.44
11-1f2	0.08606	0.00222	0.6954	0.0219	0.05861	0.00098	99.28	*532.2*	*13.2*	536.1	13.1	552.6	36.4	1261	0.13
11-g9	0.08686	0.00669	0.6972	0.0551	0.05821	0.00102	99.61	*537*	*39.7*	537.1	33	537.7	38.2	774	0.17
11-g17	0.09763	0.00820	0.7837	0.0675	0.05821	0.00094	99.87	*600.5*	*48.2*	587.6	38.4	537.9	35.3	241	0.30
11-2m1	0.09903	0.00305	0.7716	0.0447	0.05650	0.00264	99.78	*608.7*	*17.9*	580.7	25.6	–	–	87	0.44
11-2l1	0.11010	0.00341	0.8742	0.0470	0.05761	0.00269	99.44	*673.1*	*19.8*	637.8	25.4	–	–	147	0.13
11-g5	0.11160	0.00929	0.8765	0.0764	0.05695	0.00152	99.54	*682.1*	*53.9*	639.1	41.3	–	–	274	0.48
11-1i1	0.11250	0.00397	0.8160	0.0918	0.05261	0.00529	97.4	*687.3*	*23*	605.8	51.3	–	–	74	0.25
11-g6	0.11730	0.01153	0.9327	0.1000	0.05765	0.00231	99.46	*715.2*	*66.5*	669	52.5	–	–	100	1.20
11-g14	0.12290	0.01168	1.0130	0.0966	0.05978	0.00073	99.75	*747.3*	*67.1*	710.5	48.7	–	–	1138	0.14
11-1e1	0.12400	0.00366	1.1520	0.0402	0.06739	0.00110	99.91	*753.5*	*21*	778.2	19	–	–	172	0.61
11-2i1	0.12430	0.00331	1.1150	0.0424	0.06509	0.00174	99.85	*755.2*	*19*	760.8	20.3	777.3	56.2	123	0.60
11-1f1	0.12880	0.00331	1.1450	0.0354	0.06445	0.00123	99.41	*781*	*18.9*	774.7	16.7	756.6	40.2	276	0.32
11-g10	0.13630	0.01163	1.2420	0.1104	0.06611	0.00157	99.45	*823.7*	*66*	820	50	809.9	49.8	283	0.62
11-1h2	0.15170	0.00453	1.4360	0.0650	0.06864	0.00219	99.47	*910.5*	*25.4*	904	27.1	888	65.9	108	0.48
11-g18	0.15350	0.01251	1.3930	0.1687	0.06580	0.00538	98.22	*920.7*	*69.9*	885.9	71.6	800	171	183	1.10
11-1l2	0.16120	0.00493	2.1850	0.0894	0.09830	0.00314	99.42	*963.4*	*27.4*	1176	28.5	1592	59.6	88	0.51
11-g11	0.16990	0.01506	1.5770	0.1492	0.06731	0.00203	99.48	1012	83	961.2	58.8	*847.3*	*62.8*	68	0.64
11-2f1	0.21000	0.00740	2.3350	0.1038	0.08063	0.00273	99.41	1229	39.4	1223	31.6	*1212*	*66.7*	74	0.88
11-2o1	0.29590	0.01002	4.0980	0.1602	0.10040	0.00182	99.73	1671	49.8	1654	31.9	*1632*	*33.7*	69	0.69
11-g1	0.30520	0.02670	4.5460	0.4052	0.10800	0.00137	99.93	1717	132	1739	74.2	*1766*	*23.2*	80	0.65
11-2e1	0.35230	0.00997	5.3500	0.1566	0.11010	0.00084	99.63	1945	47.5	1877	25	*1802*	*13.8*	619	0.33
11-g20	0.32590	0.02544	5.0430	0.3918	0.11220	0.00072	99.97	1819	124	1827	65.8	*1836*	*11.5*	245	0.24
11-1n1	0.33340	0.00907	5.1880	0.1469	0.11290	0.00080	99.9	1855	43.8	1851	24.1	*1846*	*12.8*	343	0.15
11-2g1	0.31350	0.00846	4.8940	0.1341	0.11320	0.00089	99.64	1758	41.5	1801	23.1	*1852*	*14.3*	660	0.24
11-1p1	0.30450	0.00820	4.7660	0.1481	0.11350	0.00150	99.74	1714	40.5	1779	26.1	*1856*	*23.9*	537	0.12
11-2d1	0.32140	0.00872	5.0660	0.1409	0.11430	0.00059	99.93	1797	42.5	1830	23.6	*1869*	*9.34*	375	0.18
11-1p2-1	0.32970	0.00867	5.2040	0.1364	0.11450	0.00058	99.83	1837	42	1853	22.3	*1872*	*9.1*	510	0.10

(continued on next page)

Table 2 (*continued*)

Sample ID	$^{206}Pb^*/^{238}U$	$^{206}Pb^*/^{238}U$	$^{207}Pb^*/^{235}U$	$^{207}Pb^*/^{235}U$	$^{207}Pb^*/^{206}Pb$	$^{207}Pb^*/^{206}Pb$	% Radiogenic ^{206}Pb	Age (Ma) $^{206}Pb/^{238}U$	Age (Ma) $^{206}Pb/^{238}U$	Age (Ma) $^{207}Pb/^{235}U$	Age (Ma) $^{207}Pb/^{235}U$	Age (Ma) $^{207}Pb/^{206}Pb$	Age (Ma) $^{207}Pb/^{206}Pb$	U (ppm)	Th/U
		1 σ		1 σ		1 σ			1 σ		1 σ		1 σ		
11-1m1	0.33750	0.00921	5.3430	0.1520	0.11480	0.00090	99.85	1875	44.4	1876	24.3	*1877*	*14.2*	412	0.11
11-2h1	0.33310	0.00925	5.4290	0.1511	0.11820	0.00075	99.92	1853	44.7	1889	23.9	*1929*	*11.4*	291	0.63
11-g7	0.31530	0.02512	5.7330	0.4559	0.13190	0.00049	99.86	1767	123	1936	68.8	*2123*	*6.46*	974	0.27
11-1o1	0.44090	0.01567	9.1040	0.3379	0.14980	0.00306	99.9	2355	70.1	2349	34	*2343*	*34.9*	32	0.83
11-1j1	0.39010	0.01246	8.9710	0.2829	0.16680	0.00202	99.84	2123	57.8	2335	28.8	*2526*	*20.3*	115	0.97
11-g13	0.50730	0.04728	12.5600	1.1850	0.17960	0.00398	99.98	2645	202	2648	88.7	*2650*	*36.7*	525	0.33
11-g4	0.16920	0.11960	11.2900	0.9203	0.48420	0.33960	99.6	1008	659	2548	76	*4194*	*1040*	784	0.23
MZ2: Shemshak Formation (West), Alborz Mountains, ZJ004 (DS). n = 51.															
27-7k1	0.03775	0.00184	0.2189	0.0707	0.04206	0.01295	97.41	*238.9*	*11.4*	201	58.9	–	–	25	0.39
27-g4	0.04237	0.00607	0.2805	0.0445	0.04801	0.00233	99.75	*267.5*	*37.6*	251	35.3	–	–	177	0.84
27-7b1	0.05083	0.00145	0.3703	0.0142	0.05283	0.00137	99.82	*319.6*	*8.88*	319.8	10.5	–	–	389	0.54
27-8k1	0.05106	0.00214	0.3250	0.0407	0.04616	0.00596	99.23	*321*	*13.1*	285.7	31.2	–	–	61	0.50
27-7e1	0.05145	0.00178	0.3576	0.0362	0.05041	0.00479	99.27	*323.4*	*10.9*	310.4	27.1	–	–	91	0.35
27-g1	0.05199	0.00979	0.3678	0.0690	0.05130	0.00166	99.87	*326.7*	*60*	318	51.2	–	–	390	0.17
27-7o1	0.05860	0.00169	0.4359	0.0143	0.05396	0.00085	99.92	*367.1*	*10.3*	367.4	10.1	369.2	35.3	603	0.60
27-7i1	0.06301	0.00472	0.5455	0.0748	0.06279	0.00734	100	*393.9*	*28.6*	442	49.1	–	–	10	0.02
27-g11	0.06361	0.00530	0.4298	0.0548	0.04900	0.00481	98.66	*397.5*	*32.1*	363	38.9	–	–	44	0.30
27-8i1	0.06639	0.00198	0.5089	0.0227	0.05559	0.00178	99.84	*414.4*	*12*	417.7	15.3	436	71.5	274	0.98
27-8m1	0.06694	0.00204	0.4640	0.0277	0.05027	0.00254	99.25	*417.7*	*12.3*	387	19.2	–	–	170	0.77
27-7a1	0.07025	0.00235	0.5405	0.0241	0.05581	0.00169	99.89	*437.7*	*14.2*	438.8	15.9	444.6	67.5	246	0.56
27-7c1	0.07212	0.00224	0.5513	0.0177	0.05544	0.00085	99.92	*448.9*	*13.5*	445.9	11.6	430.2	34.3	448	0.12
27-g12	0.07295	0.00550	0.5509	0.0481	0.05477	0.00236	99.11	*453.9*	*33.1*	445.6	31.5	402.9	96.3	91	0.53
27-g14	0.07940	0.00712	0.5721	0.0600	0.05226	0.00319	97.62	*492.5*	*42.5*	459.4	38.7	–	–	408	1.60
27-8n1	0.08296	0.00281	0.6870	0.0487	0.06005	0.00436	99.76	*513.8*	*16.7*	531	29.3	605.5	157	47	1.30
27-7d2	0.08526	0.00243	0.7310	0.0222	0.06219	0.00093	100	*527.4*	*14.4*	557.2	13	–	–	396	0.20
27-7j1	0.08821	0.00249	0.7146	0.0225	0.05875	0.00097	99.99	*544.9*	*14.8*	547.5	13.3	557.9	36	826	0.34
27-7l1	0.09818	0.00323	0.8676	0.0713	0.06409	0.00512	99.85	*603.7*	*18.9*	634.2	38.8	744.6	169	61	0.44
27-7n1	0.09960	0.00283	0.8192	0.0251	0.05965	0.00084	100	*612.1*	*16.6*	607.6	14	591.1	30.4	526	0.26
27-8a1	0.09980	0.00312	0.8005	0.0478	0.05817	0.00303	99.66	*613.2*	*18.3*	597.1	27	536.2	114	71	0.29
27-8o1	0.10090	0.00373	0.8196	0.0399	0.05889	0.00176	99.6	*619.9*	*21.8*	607.8	22.3	562.9	65.2	128	0.58
27-8h1	0.10160	0.00413	0.7371	0.0399	0.05260	0.00215	99.75	*623.9*	*24.2*	560.7	23.3	–	–	67	0.34
27-g7	0.10220	0.01997	0.8488	0.1633	0.06023	0.00152	99.91	*627.3*	*117*	624	89.7	612	54.3	1864	0.02
27-7g1	0.10290	0.00312	0.8398	0.0296	0.05920	0.00116	99.92	*631.3*	*18.2*	619	16.3	574.5	42.5	334	0.10
27-g9	0.10300	0.00920	0.8293	0.0750	0.05842	0.00083	99.71	*631.8*	*53.8*	613.3	41.6	–	–	1002	0.19
27-8l1	0.11280	0.00361	0.9369	0.0644	0.06025	0.00342	99.39	*688.8*	*20.9*	671.2	33.8	612.6	122	64	0.63
27-g10	0.11330	0.01011	0.9203	0.0819	0.05890	0.00096	99.87	*692*	*58.6*	662.5	43.3	–	–	282	0.30
27-g26	0.12040	0.00803	1.0920	0.0729	0.06573	0.00105	99.53	*733.1*	*46.2*	749.2	35.4	797.7	33.5	1240	0.19
27-g6	0.12560	0.03155	1.0270	0.2502	0.05932	0.00132	99.88	*762.8*	*181*	717.6	125	–	–	266	0.90
27-g2	0.12960	0.01665	1.1700	0.1579	0.06546	0.00204	99.57	*785.5*	*95*	786.5	73.9	789.3	65.2	86	1.90
27-g23	0.13710	0.01158	1.2270	0.1158	0.06491	0.00226	99.52	*828.4*	*65.7*	813.1	52.8	771.5	73.4	95	0.98
27-7f1	0.15570	0.00563	1.4770	0.0669	0.06882	0.00199	99.77	*932.7*	*31.4*	921.1	27.4	893.5	59.8	73	0.74
27-g16	0.15950	0.01377	1.5330	0.1327	0.06971	0.00124	99.77	954.2	76.5	943.9	53.2	*919.8*	*36.6*	169	0.33
27-g22	0.16850	0.01552	1.6210	0.1509	0.06978	0.00061	99.95	1004	85.6	978.5	58.4	*921.8*	*18*	604	0.22
27-g5	0.15510	0.02275	1.4970	0.2256	0.07001	0.00103	99.86	929.5	127	929.3	91.7	*928.7*	*30.1*	247	0.26
27-g3	0.15130	0.01529	1.4930	0.1497	0.07156	0.00210	99.92	908.2	85.6	927.4	61	*973.4*	*59.8*	150	0.40
27-g8	0.18500	0.01677	1.9070	0.1793	0.07474	0.00125	99.97	1094	91.2	1084	62.6	*1062*	*33.7*	128	0.52
27-g19	0.18510	0.01480	1.9380	0.1556	0.07594	0.00061	99.94	1095	80.5	1094	53.8	*1093*	*16.2*	490	0.04
27-g20	0.33950	0.02612	5.1890	0.4032	0.11080	0.00125	99.61	1884	126	1851	66.1	*1813*	*20.5*	568	0.42
27-g24	0.33760	0.02590	5.1800	0.4049	0.11130	0.00148	99.59	1875	125	1849	66.5	*1821*	*24.1*	350	0.30
27-g25	0.35360	0.02776	5.4770	0.4356	0.11230	0.00108	99.62	1952	132	1897	68.3	*1838*	*17.3*	526	0.27
27-8f1	0.34430	0.01001	5.3670	0.1635	0.11310	0.00117	99.83	1907	48	1880	26.1	*1849*	*18.7*	270	0.28
27-g15	0.35500	0.03144	5.5920	0.5014	0.11420	0.00133	99.89	1959	150	1915	77.2	*1868*	*21.1*	96	0.60
27-8b1	0.34050	0.01012	5.4310	0.1630	0.11570	0.00099	99.89	1889	48.7	1890	25.7	*1891*	*15.3*	420	0.24
27-7h1	0.32960	0.00975	5.5300	0.1663	0.12170	0.00084	99.97	1837	47.3	1905	25.9	*1981*	*12.2*	395	0.12
27-g17	0.34250	0.02517	5.8160	0.4347	0.12310	0.00169	99.49	1899	121	1949	64.8	*2002*	*24.3*	189	1.00
27-7m1	0.43040	0.01320	9.3940	0.2884	0.15830	0.00154	99.98	2307	59.5	2377	28.2	*2438*	*16.4*	173	0.68
27-g21	0.45880	0.03434	10.0900	0.7577	0.15960	0.00077	99.83	2434	152	2443	69.4	*2451*	*8.18*	592	0.53
27-g18	0.36370	0.02800	8.4090	0.6498	0.16770	0.00090	99.95	2000	132	2276	70.1	*2535*	*9.04*	459	0.56
27-g13	0.52560	0.05292	12.1600	1.2270	0.16790	0.00196	99.71	2723	224	2617	94.6	*2536*	*19.6*	101	0.64

CZ1: Upper Red Formation, Alborz Mountains, 20-35-2 (GA). n = 59.

21-g33	0.00517	0.00110	–	–	–	–	29.81	*33.25*	*7.05*	–	–	–	–	234	1.60
21-g13	0.00730	0.00100	–	–	–	–	88.09	*46.89*	*6.37*	–	–	–	–	177	0.70
21-g7	0.00733	0.00071	0.0389	0.0069	0.03849	0.00558	98.75	*47.08*	*4.55*	38.75	6.73	–	–	599	1.70
21-g3	0.00733	0.00064	0.0506	0.0167	0.05006	0.01516	97.18	*47.1*	*4.08*	50.13	16.2	–	–	78	0.78
21-g1	0.00750	0.00062	0.0285	0.0212	0.02752	0.01983	95.56	*48.17*	*3.97*	28.49	20.9	–	–	139	0.59
21-g23	0.00770	0.00074	0.0476	0.0072	0.04483	0.00512	99.01	*49.41*	*4.73*	47.18	7.01	–	–	228	0.68
21-g5	0.00771	0.00066	0.0395	0.0116	0.03714	0.01016	97.47	*49.51*	*4.22*	39.31	11.3	–	–	183	0.61
I-9g1	0.00772	0.00038	0.0567	0.0281	0.05332	0.02503	95.72	*49.55*	*2.44*	56.03	27	–	–	142	0.43
21-g11	0.00788	0.00067	0.0555	0.0100	0.05107	0.00772	98.49	*50.6*	*4.3*	54.84	9.61	–	–	282	0.32
21-43	0.00803	0.00085	0.0329	0.0119	0.02969	0.01011	97.11	*51.56*	*5.43*	32.85	11.7	–	–	217	0.60
21-g29	0.00849	0.00116	–	–	–	–	89.37	*54.47*	*7.43*	–	–	–	–	123	0.66
21-g17	0.00993	0.00126	0.0514	0.0162	0.03753	0.01037	97.58	*63.67*	*8.02*	50.85	15.6	–	–	159	0.74
I-9l1	0.01833	0.00149	0.1183	0.0439	0.04680	0.01640	96.14	*117.1*	*9.41*	113.5	39.8	–	–	44	0.54
I-9k1	0.02234	0.00806	–	–	–	–	88.11	*142.4*	*50.8*	–	–	–	–	124	0.72
21-g18	0.03678	0.00297	0.2594	0.0220	0.05114	0.00123	99.85	*232.8*	*18.4*	234.1	17.7	–	–	343	0.45
21-g15	0.03999	0.00390	0.2748	0.0277	0.04983	0.00184	99.66	*252.8*	*24.2*	246.5	22	–	–	238	0.43
21-22	0.05111	0.00630	0.3026	0.0492	0.04294	0.00409	98.52	*321.3*	*38.6*	268.4	38.3	–	–	89	1.10
21-g34	0.05280	0.00476	0.3658	0.0436	0.05025	0.00376	99.4	*331.7*	*29.1*	316.6	32.4	–	–	203	0.66
21-g9	0.05714	0.00537	0.4033	0.0401	0.05119	0.00154	99.84	*358.2*	*32.7*	344.1	29	–	–	354	0.74
21-g25	0.05743	0.00626	0.3901	0.0447	0.04926	0.00172	98.94	*360*	*38.1*	334.4	32.7	–	–	540	0.34
xm9-9n2	0.06992	0.00216	0.5335	0.1021	0.05534	0.00973	96.24	*435.6*	*13*	434.1	67.6	–	–	256	0.35
xm9-9v1	0.07095	0.00235	0.5090	0.1408	0.05204	0.01350	94.73	*441.9*	*14.2*	417.8	94.7	–	–	218	0.34
xm9-9f1	0.07135	0.00175	0.4625	0.0500	0.04701	0.00468	96.8	*444.3*	*10.6*	386	34.7	–	–	74	0.74
21-g12	0.07305	0.00616	0.5277	0.0596	0.05239	0.00338	99.37	*454.5*	*37*	430.3	39.6	–	–	44	0.95
xm9-9w1	0.07360	0.00210	0.5510	0.0768	0.05430	0.00687	97.03	*457.8*	*12.6*	445.7	50.3	–	–	328	0.53
xm9-9t1	0.07393	0.00204	0.5303	0.0598	0.05203	0.00528	97.21	*459.8*	*12.2*	432	39.7	–	–	335	0.33
21-g35	0.09270	0.00787	0.7732	0.0654	0.06050	0.00080	99.19	*571.5*	*46.4*	581.6	37.5	621.4	28.5	1294	0.50
21-g14	0.09292	0.00756	0.7219	0.0620	0.05634	0.00140	99.57	*572.8*	*44.6*	551.8	36.6	–	–	144	0.65
21-g31	0.10020	0.00853	0.7434	0.0698	0.05379	0.00209	99.16	*615.7*	*50*	564.4	40.6	–	–	166	0.29
21-g39	0.10170	0.00912	0.7907	0.0740	0.05641	0.00146	99.44	*624.1*	*53.4*	591.6	42	–	–	915	0.01
21-g4	0.10370	0.00846	0.8205	0.0679	0.05739	0.00106	99.61	*636*	*49.4*	608.3	37.9	–	–	239	1.00
21-g16	0.11210	0.01114	0.8787	0.0998	0.05687	0.00288	98.92	*684.6*	*64.6*	640.3	53.9	–	–	97	0.25
21-g20	0.11880	0.01322	0.9819	0.1123	0.05995	0.00106	99.76	*723.5*	*76.2*	694.6	57.5	–	–	259	1.60
I-9c2	0.12150	0.00392	1.9280	0.1159	0.11510	0.00505	99.18	*739*	*22.5*	1091	40.2	–	–	167	0.77
21-g36	0.12910	0.01332	1.1860	0.1268	0.06668	0.00153	99.37	*782.5*	*76*	794.3	58.9	827.7	47.9	378	0.45
I-9e1	0.12920	0.00496	1.2180	0.0669	0.06837	0.00272	99.13	*783.3*	*28.3*	808.8	30.6	879.7	82.1	177	1.70
21-26	0.13030	0.01670	1.1970	0.1526	0.06661	0.00141	98.78	*789.7*	*95.2*	799.2	70.5	825.7	44.2	613	0.65
21-g8	0.13180	0.01482	0.8926	0.1116	0.04911	0.00267	98.61	*798.2*	*84.4*	647.7	59.9	–	–	144	0.91
21-g2	0.13190	0.01032	1.1520	0.0994	0.06333	0.00202	99.58	*798.7*	*58.7*	778.1	46.9	719.4	67.7	81	0.89
21-21	0.13640	0.01789	1.0780	0.1422	0.05735	0.00229	99.65	*824.1*	*102*	742.7	69.5	–	–	81	0.21
xm8-1a2	0.14920	0.00384	1.2180	0.0397	0.05922	0.00110	97.78	*896.5*	*21.5*	809	18.2	–	–	771	0.24
xm5-8o1	0.15300	0.00407	1.4290	0.0925	0.06773	0.00353	98.44	*917.9*	*22.8*	901.2	38.6	860.4	108	365	0.22
xm5-8t1	0.15990	0.00444	1.4150	0.1835	0.06419	0.00753	96.32	*955.9*	*24.7*	895.1	77.2	747.8	248	171	0.43
xm8-1a1	0.16320	0.00438	1.5460	0.0493	0.06871	0.00112	99.29	*974.3*	*24.3*	948.8	19.7	–	–	957	0.13
21-g30	0.17000	0.01959	1.4860	0.1737	0.06340	0.00186	99.56	1012	108	924.6	71	*721.6*	*62.1*	145	0.39
21-41	0.25100	0.06492	2.2090	0.5789	0.06383	0.00145	98.34	1444	335	1184	183	*736*	*48.2*	603	0.40
21-g37	0.14370	0.01332	1.3470	0.1249	0.06799	0.00114	99.8	865.6	75.1	866.4	54	*868.3*	*34.7*	97	0.34
21-g28	0.18180	0.01888	1.8050	0.1925	0.07199	0.00107	99.88	1077	103	1047	69.7	*985.7*	*30.3*	163	0.92
21-g38	0.18530	0.01753	2.2540	0.2177	0.08824	0.00114	99.84	1096	95.3	1198	67.9	*1388*	*24.9*	1015	0.13
21-40	0.20510	0.02322	2.6040	0.2943	0.09208	0.00071	99.76	1202	124	1302	82.9	*1469*	*14.6*	579	0.18
I-9i1	0.28120	0.01651	3.8280	0.2543	0.09874	0.00244	99.66	1597	83.1	1599	53.5	*1600*	*46.2*	58	0.45
21-42	0.33080	0.03456	4.9080	0.5144	0.10760	0.00074	99.77	1842	167	1804	88.4	*1759*	*12.5*	645	0.05
21-g6	0.34170	0.02787	5.2540	0.4280	0.11150	0.00102	99.73	1895	134	1861	69.5	*1824*	*16.7*	205	0.19
I-9d1	0.34490	0.01558	5.8800	0.3262	0.12370	0.00289	99.09	1910	74.7	1958	48.1	*2010*	*41.4*	82	0.59
21-g24	0.17410	0.01352	3.1640	0.2671	0.13180	0.00391	99.92	1035	74.2	1448	65.1	*2122*	*52*	352	0.20
21-g19	0.44560	0.04810	8.2640	0.8901	0.13450	0.00115	99.9	2376	214	2260	97.6	*2158*	*14.9*	162	0.45
21-g32	0.29500	0.02445	6.1290	0.5165	0.15070	0.00180	99.92	1666	122	1994	73.6	*2354*	*20.4*	98	0.51
21-g10	0.41730	0.02987	9.5400	0.6930	0.16580	0.00131	99.82	2248	136	2391	66.8	*2516*	*13.3*	193	0.08
I-9f1	0.55940	0.01777	15.6700	0.5061	0.20310	0.00117	99.9	2864	73.5	2857	30.8	*2852*	*9.41*	352	1.30

Italics indicate preferred age.

sample PC5. A more general consideration for this dataset pertains to the number of grains analyzed per sample. An attempt was made to obtain acceptable ages for 50 zircons per sample. However, provided 50 single-grain analyses, there remains a possibility that potentially significant age components within the sample were not identified (e.g., Dodson et al., 1988; Fedo et al., 2003).

To address the depositional age of sampled stratigraphic levels, a mean U–Pb age was calculated for the youngest zircon age population observed in each sample. In all but one case, the five youngest grains identified in each sample yield a unimodal age probability distribution, suggesting a single robust population. For the exception (sample MZ2), the five youngest grains define two separate populations. In all cases, the calculated mean age is considered to represent the maximum depositional age of the sampled horizon. Therefore, although the age of deposition can be no older than the calculated mean age (and reported 2σ error), it could be considerably younger. Nevertheless, as discussed below, the calculated mean ages likely approximate the true depositional age in several cases where the mean ages correspond to previously assigned stratigraphic ages and/or sampled units were deposited during synchronous magmatic activity (e.g., Fildani et al., 2003; DeCelles et al., 2007). The discussion of reported ages uses the timescale of Gradstein et al. (2004).

3.2. Late Neoproterozoic–Cambrian

Similar detrital zircon ages for the oldest stratigraphic units in Iran are suggestive of a common sediment source during late Neoproterozoic–Cambrian sedimentation. Four Alborz sandstones (PC1–PC3 and PC5) and one Zagros sandstone (PC4) from the Kahar, Bayandor, Barut, Lalun, and Mila formations yield primary age probability peaks at 600 Ma with a concentration of ages from 950 to 550 Ma (Fig. 3), including peaks at 780 and 860 Ma. Secondary age peaks occur (in order of decreasing magnitude) at 2500, 1880, and 1020 Ma. Several upsection trends are observed: (1) the 780 and 2500 Ma peaks become emergent from lower to upper levels; and (2) whereas the two lower samples both reveal a unimodal age distribution with a 600 Ma peak, the three upper samples show a more cosmopolitan distribution (Fig. 3; Table 2). These trends are attributed to unroofing of regions that contributed a progressively greater variety of zircons from older provinces.

The maximum depositional ages are represented by the mean U–Pb ages of the five youngest zircons in samples PC1–PC5: 537±29 Ma, 559±28 Ma, 544±38 Ma, 573±22 Ma, and 559±36 Ma. Because these mean ages are younger than previously reported stratigraphic ages and coincide with syndepositional

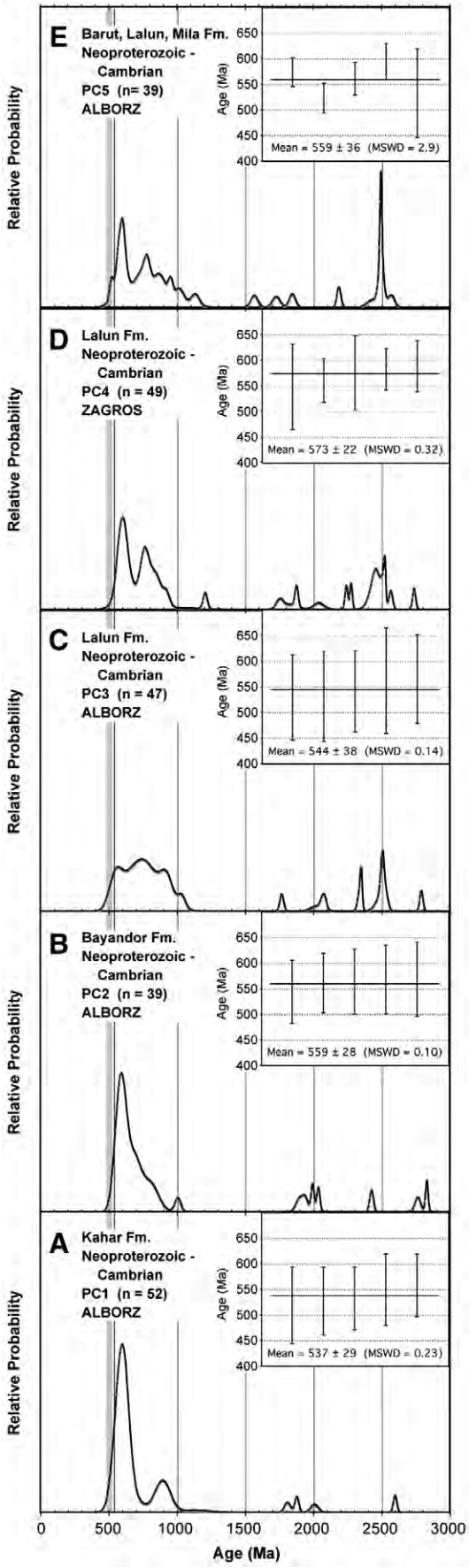

Fig. 3. Relative age probability diagrams displaying the U–Pb detrital zircon age distributions for upper Neoproterozoic–Cambrian sandstone samples PC1–PC5. Diagrams are arranged in chronostratigraphic order (older strata at the base), with vertical gray bands indicating previously assigned depositional ages. Inset plots depict individual U–Pb ages of the five youngest zircons for each sample. (A) Kahar Formation (Alborz). (B) Bayandor Formation (Alborz). (C) Lalun Formation (Alborz). (D) Lalun Formation (Zagros). (E) Barut–Lalun–Mila formations (Alborz).

volcanism (Stöcklin, 1968, 1974; Berberian and King, 1981; Samani et al., 1994), we regard them as approximations of true depositional ages. Although an upsection age progression is not observed, the mean ages all overlap within error, suggesting accumulation of the entire sampled interval during the very latest Neoproterozoic and Early Cambrian. Considering the relatively large age errors, we tentatively suggest that earliest sediment accumulation commenced in the latest Neoproterozoic prior to the Precambrian–Cambrian boundary (542 Ma). Deposition of the basal clastic sequence was complete by the end of Early Cambrian time (513 Ma), in agreement with the Middle to Late Cambrian age assigned for overlying fossiliferous carbonates (Ghavidel-Syooki, 2006). However, given the overlapping ages, we cannot rule out deposition of the entire basal clastic sequence over a shorter interval in the latest Proterozoic–Early Cambrian. The lack of an exposed basal contact for the lowermost unit (Kahar Formation) of the basal clastic sequence further precludes definitive statements regarding the precise onset of sediment accumulation in the region. Nevertheless, the data are in agreement with a depositional age constrained between 627 Ma and 533 Ma for the Tashk Formation in central Iran, a lateral equivalent of the Kahar Formation (Ramezani and Tucker, 2003).

U–Pb ages for PC1–PC5 approximately match detrital zircon results for upper Neoproterozoic–Cambrian sandstones of Israel, Jordan, and possibly Egypt (Fig. 4) (Kröner et al., 1990; Wilde and Youssef, 2002; Avigad et al., 2003; Kolodner et al., 2006). Cumulative age probability distributions for Iran and the Elat region of Israel (Fig. 4D) highlight their similarity in terms of age probabilities in the 950 to 550 Ma range and concentrations at 600 Ma and 2500 Ma. The observed age populations for Iran (PC1–PC5), Israel, Jordan, and Egypt correspond to the Arabian–Nubian shield of the western Arabian peninsula and northeastern Africa (Fig. 1A). Basement rocks of this shield exhibit a preponderance of 900–600 Ma ages (Johnson and Woldehaimanot, 2003), consistent with crustal growth during and after the main (Pan-African) phase of construction of the East African orogen (Stern, 1994; Jacobs and Thomas, 2004). Although less prevalent, a concentration of 2600–2400 Ma ages revealed by isotopic and geochronologic evidence from the Arabian–Nubian shield (Windley et al., 1996; Collins and Pisarevsky, 2005; Hargrove et al., 2006; Stoeser and Frost, 2006) is further compatible with a secondary peak observed in our samples.

The similarity of Iranian detrital zircon ages reported here to age-equivalent deposits presently >2000 km to the west and south (Fig. 1A) suggests several possibilities. First, sediment may have been provided by multiple local sediment sources in Iran that share a basement similar to the Arabian–Nubian shield. However, emerging U–Pb data for the Alborz and central Iran suggest a relatively uniform basement limited to latest Neoproterozoic–Early Cambrian age, from roughly 600 to 520 Ma (Lam, 2002; Ramezani and Tucker, 2003; Hassanzadeh et al., 2008-this volume). The lack of a significant population of older, pre-600 Ma ages and the uniform regional stratigraphy for the Neoproterozoic–Cambrian section (Stöcklin, 1968; Berberian and King, 1981) is inconsistent with many localized sources areas. Therefore, we favor an alternative explanation in which

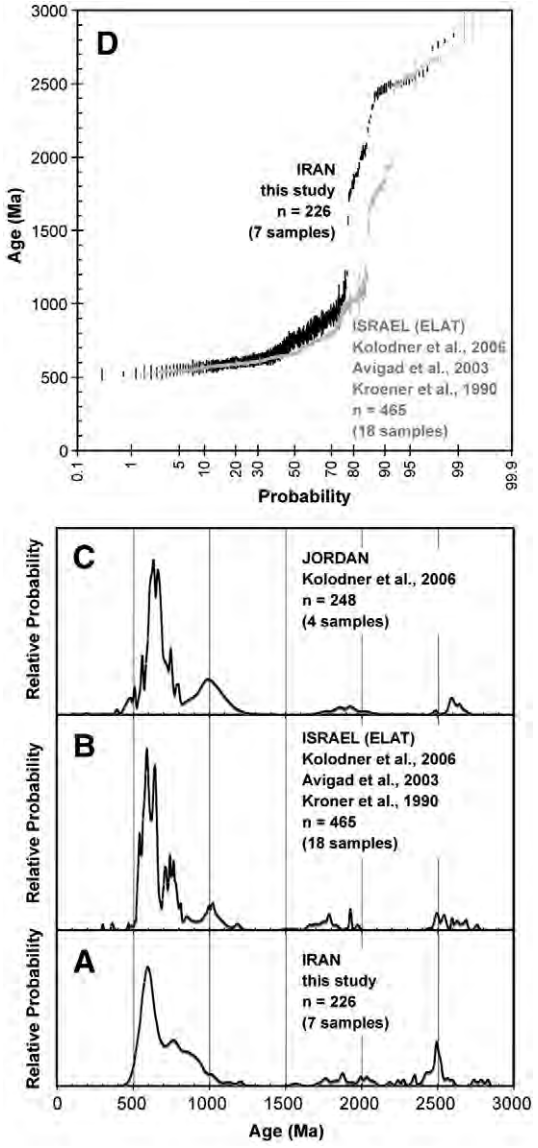

Fig. 4. (A–D) Relative age probability diagrams displaying U–Pb detrital zircon age distributions for Neoproterozoic–Cambrian sandstones from (A) Iran (samples PC1–PC5), (B) Elat region of Israel, and (C) Jordan. (D) Cumulative age probability distributions of U–Pb ages for Iran (this study) and the Elat region of Israel, depicting the same data plotted in (A) and (B).

late Neoproterozoic–Cambrian unroofing of the Arabian–Nubian shield and other parts of the East African orogen influenced a vast area across northern Africa and the Middle East. Such source regions contain significant quantities of not only latest Neoproterozoic–Cambrian but also pre-600 Ma igneous rocks (Stern, 1994; Johnson and Woldehaimanot, 2003). Because the age of earliest sedimentation is older in northern Africa (e.g., Shalaby et al., 2006), this interpretation suggests northward and eastward expansion of clastic depositional systems from the East African orogen toward Iran.

3.3. Middle to Late Paleozoic

Detrital zircon analyses of four Devonian to Lower Permian samples (PZ1–PZ4) reveal evidence of Paleozoic magmatism in

Iran. Two Alborz sandstones from the Upper Devonian–Lower Carboniferous Geirud Formation (PZ1) and Lower Permian Dorud Formation (PZ2) reveal unimodal U–Pb age spectra in which the largest population of grains is defined by zircons slightly older or indistinguishable from the assigned depositional age of the host unit. Specifically, the Geirud and Dorud formations yield unimodal age probability peaks of 370 and 325 Ma, and mean U–Pb ages for the five youngest zircons of 348±19 Ma and 294±18 Ma, respectively (Fig. 5A and B). We attribute these age patterns to derivation from youthful igneous sources during Late Devonian to Early Permian time. The lateral extent of these mature quartzose sandstone units throughout the Alborz and the dominance of youthful sources suggest that detrital zircons were first-cycle grains derived from an igneous source of regional importance. Most previous reports of igneous rocks in the Alborz are limited to basaltic lava flows in the Devonian to Carboniferous section (Wensink et al., 1978; Wendt et al., 2005) and clasts of granite and andesite in conglomerates intercalated within the Silurian Soltan Meydan basalt flows (Jenny, 1977; Stampfli, 1978; Delaloye et al., 1981). East of the Alborz, local occurrences of Silurian–Devonian igneous rocks have been reported north of the Paleotethys suture in the Kopet Dagh mountains (Fig. 1) (Lyberis et al., 1998). West of the Alborz, Devonian metamorphic rocks are known in the Talesh Mountains (Berberian and King, 1981; Sengör, 1990). Additional, but much smaller, peaks in the zircon age spectra occur at 580, 800, 1010, and 1820 Ma (Fig. 5A and B).

In the Zagros, Devonian and Lower Permian sandstones (PZ3, PZ4) yield consistent zircon age spectra suggestive of Neoproterozoic sources and a previously undocumented igneous source of early Paleozoic age. Both samples yield age spectra with peaks at 595, 760, 870, 950, and 2460 Ma (Fig. 5C and D), corresponding to the principally Neoproterozoic ages reported above for uppermost Neoproterozoic–Cambrian rocks (Fig. 3). However, a presence of Paleozoic zircons is defined by the mean ages of the five youngest zircons for the Devonian Zakeen (PZ3) and Lower Permian Faraghan (PZ4) formations: 486±26 Ma and 500±30 Ma, respectively. These ages are attributed to Cambrian and possibly Ordovician magmatism in the source area(s). To our knowledge, no reliable evidence for significant Paleozoic magmatism after 550 Ma has been presented for the Zagros or Arabian margin (e.g., Berberian and Berberian, 1981; Sengör, 1990). We tentatively suggest derivation from magmatic sources of limited extent in the Zagros, other parts of Arabia, or possibly northeast Africa where Ordovician anorogenic intrusions are observed (Guiraud et al., 2005).

3.4. Mesozoic

U–Pb detrital zircon ages for lower Mesozoic strata of the Alborz reveal an important shift in provenance. Two samples of the Triassic–Jurassic Shemshak Formation (MZ1, MZ2) display notable age peaks, including Carboniferous–Early Triassic (320–220 Ma) and late Paleoproterozoic (1900–1800 Ma) ages

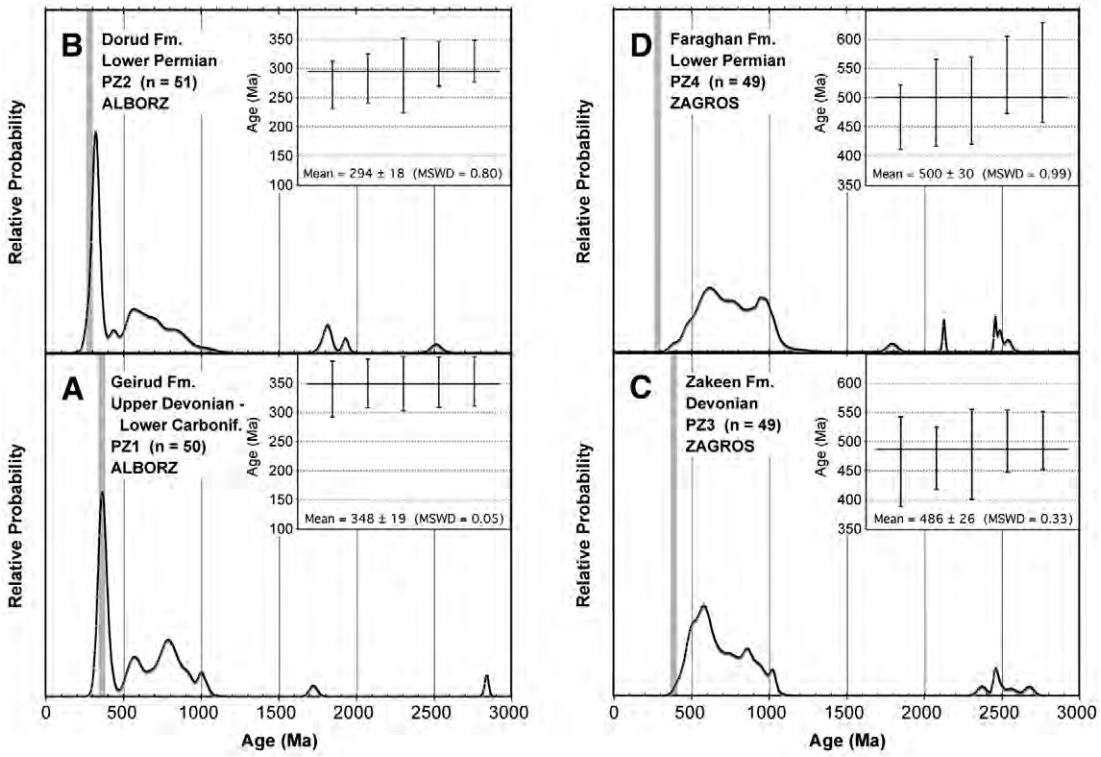

Fig. 5. Relative age probability diagrams displaying the U–Pb detrital zircon age distributions for Devonian to Permian sandstone samples PZ1–PZ4. Diagrams are arranged in chronostratigraphic order (older strata at the base), with vertical gray bands indicating previously assigned depositional ages. Inset plots depict individual U–Pb ages of the five youngest zircons for each sample. (A) Geirud Formation (Alborz). (B) Dorud Formation (Alborz). (C) Zakeen Formation (Zagros). (D) Faraghan Formation (Zagros).

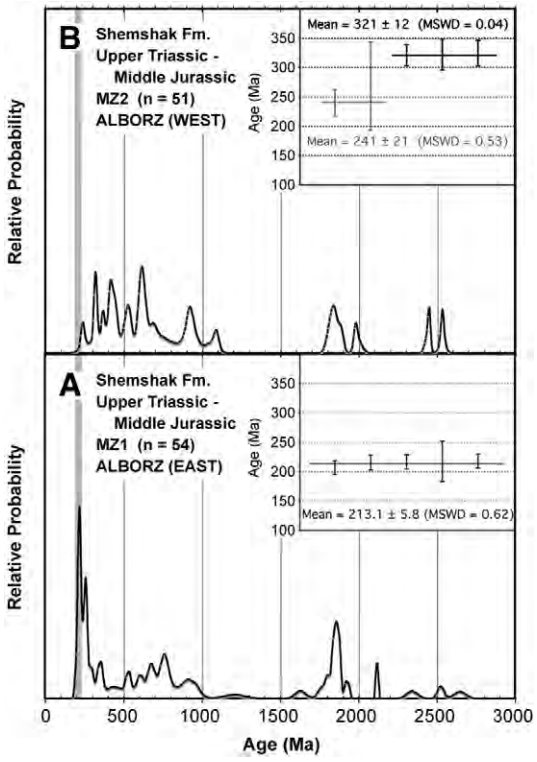

Fig. 6. Relative age probability diagrams displaying the U–Pb detrital zircon age distributions for Mesozoic sandstone samples MZ1 and MZ2. Diagrams are arranged in chronostratigraphic order (older strata at the base), with vertical gray bands indicating previously assigned depositional ages. Inset plots depict individual U–Pb ages of the five youngest zircons for each sample. (A) Shemshak Formation (eastern Alborz). (B) Shemshak Formation (western Alborz).

(Fig. 6). These ages are rarely observed in adjacent regions of Gondwana, but are consistent with magmatism in the Caucasus mountains and parts of the East European craton (including the Scythian platform; Fig. 1A) of south-central Eurasia (Nikishin et al., 1996). Such evidence supports collision of Iran with Eurasia by the time of Shemshak deposition. Whereas the eastern Shemshak sample (MZ1) exhibits prominent age peaks at 220, 260, and 1860 Ma, the western sample (MZ2) has age peaks at 320, 610, 425, 525, and 1840 Ma (Fig. 6). Furthermore, whereas MZ1 yields a mean U–Pb age of 213±5.8 Ma (early Late Triassic) for the five youngest zircons, MZ2 yields two young populations of Carboniferous and Early Triassic age (Fig. 6). These spatial variations in Shemshak provenance are attributed to two northern sediment sources in Eurasia (Fig. 1): (1) a probable northeastern source composed of principally Triassic magmatic arc rocks in the Turan block north of the Kopet Dagh mountains (Rastsvetaev, 1997; Thomas et al., 1999; Garzanti and Gaetani, 2002); and (2) a probable northwestern source involving prolonged middle to late Paleozoic magmatic arcs near the Caucasus mountains along the border of the Scythian platform (Khain and Koronousky, 1997; Allen et al., 2006). These results are consistent with facies trends suggesting generally southward transport of Shemshak sediment (Assereto, 1966; Dercourt et al., 1986; Alavi, 1996). The data, however, do not rule out additional contributions from local sediment sources such as Late Triassic plutons reported in east-central Iran (Ramezani and Tucker, 2003).

For sample MZ1, the youngest age peak of 220 Ma and a mean age for the five youngest zircons of 213±5.8 Ma (Fig. 6A) are indistinguishable from the oldest reported depositional age of late Carnian–early Norian (early Late Triassic) for the lower Shemshak Formation (Assereto, 1966; Stöcklin, 1974; Stampfli, 1978). We therefore consider these young zircon ages to accurately represent the timing of early Shemshak deposition, thus providing a minimum estimate for the age of the Iran–Eurasia collision.

3.5. Cenozoic

A single Cenozoic sample from north-central Iran helps define the exhumation record of the Alborz and/or Urumieh–Dokhtar belt during regional uplift driven by the Arabia collision. The Miocene sandstone (CZ1) is from the Taleghan basin of the southernmost Alborz (Table 1), which shared a depositional history similar to the Upper Red Formation of the central Iranian plateau (Guest et al., 2007). Detrital zircons from this sandstone reveal a single substantial age probability peak of 50 Ma (Fig. 7). The calculated mean U–Pb age of the five youngest zircons is 46.1±4.2 Ma, including a single-grain age of 33.3±7.1 Ma (Table 2), These data are consistent with a major contribution of zircon from well-known Eocene volcanic rocks of the Alborz mountains to the north and/or the Urumieh–Dokhtar belt to the south (Fig. 1). This volcanism may be attributed to late-stage northward subduction and/or breakoff of the Neotethys or related slab (Hassanzadeh et al., 2002; McQuarrie et al., 2003; Hassanzadeh et al., 2004; Ghasemi and Talbot, 2006). The pronounced shortage of Oligocene–Miocene zircon populations within the Miocene sandstone is consistent with roughly late Eocene termination of major volcanism due to the Arabia collision.

A secondary peak at 450 Ma (Fig. 7) is in agreement with evidence presented above for Ordovician zircon crystallization expressed in Paleozoic sandstones of the Zagros. During the Cenozoic, however, these Ordovician zircons may also have

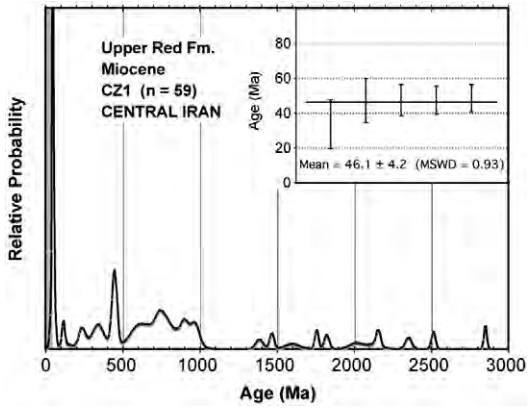

Fig. 7. Relative age probability diagram displaying the U–Pb detrital zircon age distribution for Cenozoic sandstone sample CZ1 from north-central Iran. Vertical gray band indicates previously assigned depositional age. Inset plot depicts individual U–Pb ages of the five youngest zircons.

originated from a non-Gondwanan sediment source such as the Paleozoic arc rocks of the Eurasian plate to the north. A suite of minor peaks include the following ages (in order of decreasing magnitude): 750, 905, 970, 120, 345, and 240 Ma. The large range of Late Archean to Cretaceous ages in this sample probably reflects recycling of older strata to the north in the Alborz or to the south in the Urumieh–Dokhtar belt or Sanandaj–Sirjan zone (Fig. 1). Although sediment sources exist to both the north and south, clast compositions and paleocurrent data suggest that the sampled interval was derived from uplifted parts of the Alborz (Amini, 1997; Guest et al., 2007).

4. Discussion

4.1. Pan-African signatures in Iran

Some plate reconstructions propose late Neoproterozoic–Cambrian extension with possible rifting of peri-Gondwanan terranes away from Arabia and/or Iran (Fig. 8A) (Stöcklin, 1968; Falcon, 1974; Berberian and King, 1981; Husseini, 1989; Talbot and Alavi, 1996). However, the U–Pb detrital zircon ages reported here for upper Neoproterozoic–Cambrian sandstones of Iran are comparable to zircon age spectra from age-equivalent units presently >2000 km to the west and south in Israel (Elat region), Jordan, and Egypt (Fig. 4). All of these units are dominated by Pan-African (900–600 Ma) sources with similar pre-Neoproterozoic signatures. One possibility is that Iran shares a Pan-African basement similar to these other regions and exposed basement sources within Iran supplied sediment to localized Neoproterozoic–Cambrian basins. The available basement ages for Iran (Ramezani and Tucker, 2003; Hassanzadeh et al., 2008-this volume), however, lack the significant pre-600 Ma signatures observed in the detrital age populations. Therefore, although Iranian basement may have contributed some sediment, the main sources were likely located in basement provinces of Arabia and Africa, particularly the Arabian–Nubian shield. In this scenario, Iran, Arabia, and northern Africa were all part of an extensive clastic wedge sharing source regions of similar age. The ultimate sources consisted of basement provinces of the East African orogen uplifted during Neoproterozoic collision of East and West Gondwana during the Pan-African orogeny (Stern, 1994; Jacobs and Thomas, 2004; Cox et al., 2004; Fitzsimons and Hulscher, 2005). The new U–Pb geochronological data indicate that Iran was near Arabia and constituted part of Gondwana during the early Paleozoic. Although in conflict with some reconstructions, little or no separation of Iran from Gondwana during late Neoproterozoic to Permian time (Fig. 8A) is consistent with the principally shallow-marine facies and limited thickness of the Paleozoic succession of the Alborz, Zagros, and central Iranian plateau (Stöcklin, 1968).

Although the broad extent of Pan-African magmatism and subsequent shelf deposition may suggest a passive-margin setting, a lack of evidence for substantial rifting or continuous subsidence in latest Precambrian to early Paleozoic Iran is considered more compatible with recent models suggesting a subduction zone boundary and contractional orogenic belt along the Gondwanan margin from Iran (Fig. 8B) (e.g., Ramezani and Tucker, 2003; Hassanzadeh et al., 2008-this volume) to the Himalayas (Stöcklin, 1980; DeCelles et al., 2000; Gehrels et al., 2003, 2006a,b; Cawood et al., 2007). Furthermore, such an active margin may explain emerging evidence for early Paleozoic igneous activity, including the proportion of <550 Ma detrital zircons identified in this study.

4.2. Sources of Paleozoic magmatic rocks

U–Pb detrital zircon ages for middle to late Paleozoic strata in the Alborz and Zagros mountains reveal an unexpected contribution from Paleozoic igneous sources (Fig. 5). Most notable is the dominance of zircon ages nearly indistinguishable from the Late Devonian to Early Permian depositional ages of the Geirud and Dorud formations in northern Iran. The unimodal age spectra indicate a significant supply of first-cycle igneous detritus ranging from roughly 390 to 280 Ma (Fig. 5A and B; Table 2). In the Zagros, sandstones of Late Devonian to Early Permian age exhibit a much smaller fraction of Paleozoic igneous grains which cluster around 500 Ma (Table 2). The collective results for the Alborz and Zagros conflict with conventional models in which Iran was dominated by an amagmatic passive margin throughout the Paleozoic (Fig. 8C).

We envision three scenarios to explain the Alborz data. First, igneous grains may have been transported long distances from Paleozoic magmatic arcs in southern and eastern Gondwana (e.g., Sengör, 1987; Metcalfe, 1996). This model would require transport of primary arc detritus thousands of kilometers without significant dilution by other source areas, a prediction contrary to the sediment mixing behavior of large river systems (e.g., DeGraaff-Surpless et al., 2003; Mapes et al., 2005). Second, the igneous grains may have been derived from southern Eurasia, where the Caucasus mountains and Turan block contain remnants of middle to late Paleozoic magmatic arcs (Khain and Koronousky, 1997; Thomas et al., 1999; Garzanti and Gaetani, 2002; Allen et al., 2006). This model would place the Alborz in close proximity to Eurasia by roughly 350 Ma, ~150 My earlier than assumed (Stampfli and Borel, 2002). In this case, the Alborz would be of Eurasian rather than Gondwanan affinity and the poorly located Paleotethys suture would lie along the southern rather than northern margin of the Alborz (compare Stöcklin, 1974 with Ruttner, 1993). Alternatively, a third possibility is that poorly identified Paleozoic magmatism affected the Alborz or

Fig. 8. Simplified plate reconstructions depicting conventional models (left column) and alternative models (right column) relevant to interpretation of detrital zircon ages for Iran. (A) Neoproterozoic rifting and Paleozoic passive-margin subsidence. (B) Neoproterozoic–early Paleozoic subduction along northern Gondwanan margin. (C) Paleozoic northward motion of Iran during amagmatic opening of Paleotethys. (D) Paleozoic magmatism related to Paleotethy rifting and/or poorly documented arc systems. (E) Late Triassic Iran–Eurasia collision and Paleotethys closure. (F) Eurasia collision in which northern Iran (Alborz) was attached to the Turan block (southern Eurasia) prior to collision with central Iran. (G) Arabia–Eurasia collision and Neotethys closure during late Miocene time. (H) Middle Eocene to Oligocene Arabia–Eurasia collision following intensified magmatism in the Urumieh–Dokhtar arc. Modified from Berberian and King (1981); Dercourt et al. (1986); Stern (1994); Stampfli and Borel (2002); Ramezani and Tucker (2003); Jacobs and Thomas (2004). See text for discussion.

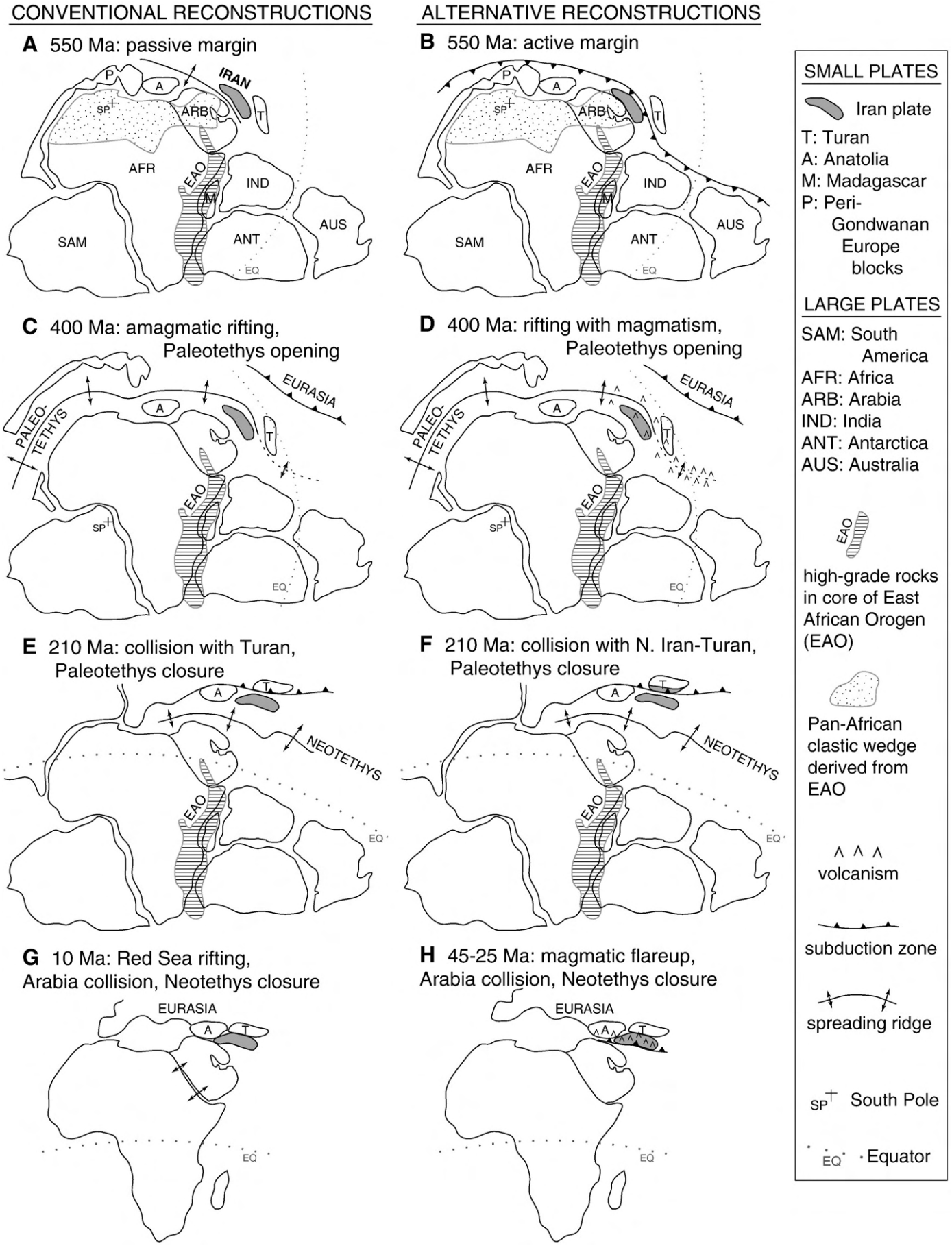
CONVENTIONAL RECONSTRUCTIONS
ALTERNATIVE RECONSTRUCTIONS
A 550 Ma: passive margin
B 550 Ma: active margin
C 400 Ma: amagmatic rifting, Paleotethys opening
D 400 Ma: rifting with magmatism, Paleotethys opening
E 210 Ma: collision with Turan, Paleotethys closure
F 210 Ma: collision with N. Iran-Turan, Paleotethys closure
G 10 Ma: Red Sea rifting, Arabia collision, Neotethys closure
H 45-25 Ma: magmatic flareup, Arabia collision, Neotethys closure
P
A
IRAN
T
SP
ARB
AFR
EAO
M
IND
SAM
ANT
AUS
EQ
PALEO-TETHYS
EURASIA
NEOTETHYS
SMALL PLATES
Iran plate
T: Turan
A: Anatolia
M: Madagascar
P: Peri-Gondwanan Europe blocks
LARGE PLATES
SAM: South America
AFR: Africa
ARB: Arabia
IND: India
ANT: Antarctica
AUS: Australia
high-grade rocks in core of East African Orogen (EAO)
Pan-African clastic wedge derived from EAO
volcanism
subduction zone
spreading ridge
South Pole
Equator

bordering regions (Fig. 8D). Minor, principally mafic, extrusive and intrusive rocks of Ordovician–Carboniferous age have been reported (Wensink et al., 1978; Stampfli et al., 1991; Alavi, 1996; Wendt et al., 2005), but there are few candidates for significant igneous centers capable of supplying the dominant zircon age populations. Nevertheless, we tentatively favor this third model and postulate that poorly dated igneous rocks may include a record of Paleozoic zircon crystallization in the Alborz. This model is consistent with Paleozoic paleobotanical evidence and basement ages indicating a Gondwanan affinity for the Alborz (Ghavidel-Syooki, 1995, 2006; Hassanzadeh et al., 2008-this volume). Although poorly understood, middle to late Paleozoic magmatism may be the product of intra-arc or back-arc spreading related to opening of Paleotethys (e.g., Stampfli et al., 1991; Nikishin et al., 1996; Kostyuchenko et al., 2004) and northward transport of peri-Gondwanan and Cimmerian terranes across Paleotethys (Fig. 8D) (e.g., Stampfli and Borel, 2002; Keppie et al., 2003; von Raumer et al., 2003; Murphy et al., 2004).

4.3. Timing of Iran–Eurasia collision

Collisional tectonics in Iran commenced with early Mesozoic northward accretion of Iran to the Turan block (Stöcklin, 1974; Zonenshain et al 1990). At this time, Turan (Fig. 1) may have been part of an amalgamated Eurasia or an isolated block to the south (Zonenshain et al., 1990; Lemaire et al., 1997; Besse et al., 1998; Golonka, 2004). Detrital zircon signatures reported here for the Shemshak overlap assemblage in northern Iran are dominated by a range of 360–210 Ma ages (Fig. 6), consistent with derivation from Carboniferous–Triassic magmatic arcs forming part of the Variscan basement of the Turan block (Rastsvetaev, 1997; Thomas et al., 1999; Garzanti and Gaetani, 2002) (Fig. 8E). An alternative or additional contributor of zircon may have included similar basement rocks comprising the Scythian platform and Caucasus mountains west of the Caspian Sea (Fig. 1) (Natal'in and Sengör, 2005; Allen et al., 2006).

The presence of 1700–2700 Ma detrital zircons in the Shemshak Formation (Fig. 6) demonstrates an additional sediment source beyond the Turan block and Scythian platform. The likeliest source of these older grains is the East European Craton to the north (Fig. 1), which contains some of the only known Archean and Paleoproterozoic basement in the broader Caspian region (Nikishin et al., 1996; Claesson et al., 2001; Kostyuchenko et al., 2004; Allen et al., 2006). Such a source would require collision of the Turan block with Eurasia prior to Shemshak deposition. As outlined in the second of three models mentioned above (Section 4.2), one could envision collision of northern Iran with the Turan block prior to final collision with Eurasia by Late Triassic time (Fig. 8F). However, such a history would be at odds with stratigraphic and paleomagnetic data for the late Paleozoic–early Mesozoic record (e.g., Stöcklin, 1974; Stampfli, 1978; Besse et al., 1998). We therefore favor the conventional model (Fig. 8E), as outlined by Hassanzadeh et al. (2008-this volume).

The Shemshak has long been recognized as an overlap assemblage recording the Turan–Iran collision, but the reported age assignments span >60 Myr from Late Triassic to Middle Jurassic time (e.g., Seyed-Emami et al., 2006). The zircon ages reported here constrain the maximum age of Shemshak deposition. A mean age of 213±5.8 Ma for the five youngest U–Pb ages (Fig 6) indicates that deposition was underway by late Carnian–early Norian (early Late Triassic) time and provides a new estimate for the timing of the Iran–Eurasia collision. Because the Shemshak overlaps the Paleotethys suture, these young zircons require that collision was complete by ~220–210 Ma. When combined with the age of the pre-collisional early Carnian (~228–222 Ma) carbonate platform (Stampfli, 1978), the Iran–Eurasia collision is restricted to late Carnian–early Norian time (roughly 222–210 Ma), in agreement with the age proposed for the suture zone farther east (Alavi et al., 1997).

4.4. Eocene arc magmatism and Arabia–Eurasia collision

Detrital zircon ages for Miocene strata in north-central Iran demonstrate the dominant contribution of Paleogene volcanic rocks and place rough limits on the cessation of arc magmatism following the Arabia–Eurasia collision. Eocene volcanic rocks are prevalent on both flanks of the central Iranian plateau: to the north along the southern Alborz and to the south in the Urumieh–Dokhtar belt (Fig. 1). The five youngest zircons from the analyzed sample yield a mean U–Pb age of 46.1±4.2 Ma (Fig. 7), indicating arc magmatism of Eocene age. The mean age likely represents late-stage arc magmatism and may be considered a maximum approximation for the age of initial contact between continental lithosphere of the Arabian plate and the Iran block of southern Eurasia. Independent age control on early foreland basin fill in the Zagros fold-thrust belt suggests that collision-related shortening was underway by late Oligocene–early Miocene time (Fakhari et al., 2008-this volume). Given these bounds, we place the timing of the Arabia–Eurasia collision between roughly 45 and 25 Ma (Fig. 8E). Although this estimate lacks precision, it is significantly older than many previous studies that rely on the late Miocene–Pliocene age of coarse-grained deposits in the modern Zagros foreland (e.g., James and Wynd, 1965; Falcon, 1974). Finally, it should be noted that although a middle Eocene to late Oligocene collision appears most likely, the main phase of rapid horizontal shortening expressed in the Zagros (McQuarrie, 2004) may have been delayed until after ~10 Ma (Hessami et al., 2001; Mouthereau et al., 2006).

5. Conclusions

1. U–Pb detrital zircon geochronology of selected clastic intervals in the uppermost Neoproterozoic to Miocene succession of Iran indicate evolving sediment source areas linked to construction of the East African (Pan-African) orogen followed by successive opening and closing of the Paleotethys and Neotethys oceans.
2. A basal clastic succession representing the earliest sedimentary record in Iran displays provenance age signatures dominated by Pan-African (900–600 Ma) rocks. Similar detrital zircon age spectra for age-equivalent strata of Israel, Jordan, and Egypt suggest that a clastic wedge derived from the East African orogen covered a huge region encompassing

most of northern Africa and the Middle East. In Iran, the youngest observed zircon ages within five Neoproterozoic–Cambrian sandstones suggest deposition of most of the basal clastic succession during very latest Neoproterozoic and Early Cambrian time.

3. Middle to upper Paleozoic sandstones reveal evidence of poorly documented Paleozoic magmatism in Iran and its surrounding regions. Detrital zircon ages indicate Late Devonian–Early Permian and Cambrian–Ordovician zircon crystallization that could reflect magmatic activity related to subduction of Paleotethys or related oceanic lithosphere. Alternatively, these zircons may be the product of rift-related magmatism during opening of Paleotethys and Neotethys.
4. The timing of the Iran–Eurasia collision is defined by the depositional age of the overlap assemblage comprised of the Upper Triassic–Middle Jurassic Shemshak Formation. The calculated mean U–Pb age of the youngest zircon population from the Shemshak indicates a late Carnian–early Norian (early Late Triassic) age, requiring continental collision and closure of Paleotethys by 220–210 Ma. The Shemshak data are further consistent with studies demonstrating that the Paleotethys suture is situated north of the Alborz (e.g., Hassanzadeh et al., 2008-this volume).
5. Detrital zircon ages for Miocene sandstones help constrain the age of some of the youngest products of major magmatism related to late-stage subduction and/or breakoff of the Neotethys slab. A major pulse of Eocene magmatism is well represented in the detrital age spectra, with most young zircons clustering around 50–45 Ma. On the basis of these ages and the timing of initial synorogenic sedimentation in the Zagros foreland basin, we place the Arabia–Eurasia collision in Iran between the middle Eocene and late Oligocene.

Acknowledgements

This research was supported by U.S. National Science Foundation grants EAR-0337775 (awarded to Horton and Axen) and EAR-9902932 (awarded to Axen). We thank Axel Schmitt and David Gingrich for assistance with ion-microprobe analyses and Sasan Bagheri, Yann Gavillot, and Martin Timmerman for informative discussions. Constructive reviews were provided by David Barbeau, Jahandar Ramezani, Gérard Stampfli, Amy Weislogel, and editors Ezat Heydari and Rasoul Sorkhabi.

References

Alavi, M., 1991. Sedimentary and structural characteristics of the Paleo–Tethys remnants in northeastern Iran. Geological Society of America Bulletin 103, 983–992.

Alavi, M., 1994. Tectonics of the Zagros orogenic belt of Iran: new data and interpretations. Tectonophysics 229, 211–238.

Alavi, M., 1996. Tectonostratigraphic synthesis and structural style of the Alborz mountain system in northern Iran. Journal of Geodynamics 21, 1–33.

Alavi, M., 2004. Regional stratigraphy of the Zagros fold-thrust belt of Iran and its proforeland evolution. American Journal of Science 304, 1–20.

Alavi, M., Vaziri, H., Seyed-Emami, K., Lasemi, Y., 1997. The Triassic and associated rocks of the Nakhlak and Aghdarband areas in central and northeastern Iran as remnants of the southern Turanian active continental margin. Geological Society of America Bulletin 109, 1563–1575.

Allen, M., Jackson, J., Walker, R., 2004. Late Cenozoic reorganization of the Arabia–Eurasia collision and the comparison of short-term and long-term deformation rates. Tectonics 23, 2008. doi:10.1029/2003TC001530.

Allen, M.B., Morton, A.C., Fanning, C.M., Ismail-Zadeh, A.J., Kroonenberg, S.B., 2006. Zircon age constraints on sediment provenance in the Caspian region. Journal of the Geological Society of London 163, 647–655.

Alsharhan, A.S., Kendall, C.G.S.C., 1986. Precambrian to Jurassic rocks of Arabian Gulf and adjacent areas: their facies, depositional setting, and hydrocarbon habitat. American Association of Petroleum Geologists Bulletin 70, 977–1002.

Amini, A., 1997. Provenance and depositional environment of Upper Red Formation, central zone, Iran. Ph.D. thesis, University of Manchester, 320 pp.

Assereto, R., 1966. The Jurassic Shemshak Formation in central Elburz (Iran). Rivista Italiana di Paleontologia e Stratigrafia 72, 1133–1182.

Avigad, D., Kolodner, K., McWilliams, M., Persing, H., Weissbrod, T., 2003. Origin of northern Gondwana Cambrian sandstone revealed by detrital zircon SHRIMP dating. Geology 31, 227–230.

Axen, G.J., Lam, P.J., Grove, M., Stockli, D.F., Hassanzadeh, J., 2001. Exhumation of the west-central Alborz Mountains, Iran, Caspian subsidence, and collision-related tectonics. Geology 29, 559–562.

Barbeau, D.L., Ducea, M.N., Gehrels, G.E., Kidder, S., Wetmore, P.H., 2005. U–Pb detrital-zircon geochronology of northern Salinian basement and cover rocks. Geological Society of America Bulletin 117, 466–481.

Becker, H., Förster, H., Soffel, H., 1973. Central Iran, a former part of Gondwanaland? Paleomagnetic evidence from Infracambrian rocks and iron ores of the Bafq area, Central Iran. Zeitschrift für Geophysik 39, 953–963.

Berberian, F., Berberian, M., 1981. Tectono-plutonic episodes in Iran. In: Gupta, H.K., Delany, F.M. (Eds.), Zagros-Hindu Kush-Himalaya Geodynamic Evolution. Geodynamics Series, vol. 3. American Geophysical Union, Washington, D.C., pp. 5–32.

Berberian, M., King, G.C.P., 1981. Towards a paleogeography and tectonic evolution of Iran. Cananadian Journal of Earth Sciences 18, 210–265.

Besse, J., Torcq, F., Gallet, Y., Ricou, L.E., Krystyn, L., Saidi, A., 1998. Late Permian to Late Triassic palaeomagnetic data from Iran: constraints on the migration of the Iranian block through the Tethyan Ocean and initial destruction of Pangaea. Geophysical Journal International 135, 77–92.

Beydoun, Z.R., Clarke, M.W.H., Stoneley, R., 1992. Petroleum in the Zagros Basin: a late Tertiary foreland basin overprinted onto the outer edge of a vast hydrocarbon-rich Paleozoic–Mesozoic passive-margin shelf. In: Macqueen, R.W., Leckie, D.A. (Eds.), Foreland Basins and Fold Belts, American Association of Petroleum Geologists. Memoir, vol. 55, pp. 309–339.

Brasier, M., McCarron, G., Tucker, R., Leather, J., Allen, P., Shields, G., 2000. New U–Pb zircon dates for the Neoproterozoic Ghubrah glaciation and for the top of the Huqf Supergroup, Oman. Geology 28, 175–178.

Burke, K., Krauss, J.U., 2000. Deposition of immense Cambro–Ordovician sandstone bodies, now exposed mainly in N. Africa and Arabia, during the aftermath of the final assembly of Gondwana. Geological Society of America Abstracts with Programs 32 (7), 249.

Cawood, P.A., Johnson, M.R.W., Nemchin, A.A., 2007. Early Palaeozoic orogenesis along the Indian margin of Gondwana: tectonic response to Gondwana assembly. Earth and Planetary Science Letters 255, 70–84.

Claesson, S., Bogdanova, S.V., Bibikova, E.V., Gorbatschev, R., 2001. Isotopic evidence for Palaeoproterozoic accretion in the basement of the East European Craton. Tectonophysics 339, 1–18.

Collins, A.S., Pisarevsky, S.A., 2005. Amalgamating eastern Gondwana: the evolution of the Circum–Indian Orogens. Earth-Science Reviews 71, 229–270.

Compston, W., Williams, I.S., Meyer, C., 1984. U–Pb geochronology of zircons from lunar breccia 73217 using a sensitive high mass-resolution ion microprobe. Journal of Geophysical Research 89, 525–534.

Cox, R., Coleman, D.S., Chokel, C.B., DeOreo, S.B., Wooden, J.L., Collins, A.S., De Waele, B., Kroner, A., 2004. Proterozoic tectonostratigraphy and paleogeography of central Madagascar derived from detrital zircon U–Pb age populations. Journal of Geology 112, 379–399.

Davoudzadeh, M., 1997. Iran. In: Moores, E.M., Fairbridge, R.W. (Eds.), Encyclopedia of European and Asian Regional Geology. Chapman and Hall, London, pp. 384–405.

DeCelles, P.G., Gehrels, G.E., Quade, J., LaReau, B., Spurlin, M., 2000. Tectonic implications of U–Pb zircon ages of the Himalayan orogenic belt in Nepal. Science 288 (5465), 497–499.

DeCelles, P.G., Carrapa, B., Gehrels, G.E., 2007. Detrital zircon U–Pb ages provide provenance and chronostratigraphic information from Eocene synorogenic deposits in northwestern Argentina. Geology 35, 323–326.

DeGraaff-Surpless, K., Mahoney, J.B., Wooden, J.L., McWilliams, M.O., 2003. Lithofacies control in detrital zircon provenance studies: insights from the Cretaceous Methow basin, southern Canadian Cordillera. Geological Society of America Bulletin 115, 899–915.

Delaloye, M., Jenny, J., Stampfli, G., 1981. K–Ar dating in the eastern Elburz (Iran). Tectonophysics 79, T27–T36.

Dercourt, J., Zonenshain, L.P., Ricou, L.E., Kazmin, V.G., Le Pichon, X., Knipper, A.L., Grandjacquet, C., Sbortschikov, I.M., Geyssant, J., Lepvreir, C., Perchersky, D.H., Boulin, J., Sibuet, J.C., Savostin, L.A., Sorokhtin, O., Westphal, M., Bazhenov, M.L., Lauer, J.P., Biju-Duval, B., 1986. Geological evolution of the Tethys belt from the Atlantic to the Pamirs since the Lias. Tectonophysics 123, 241–315.

Dewey, J.F., Pitman III, W.C., Ryan, W.B.F., Bonnin, J., 1973. Plate tectonics and evolution of the Alpine system. Geological Society of America Bulletin 84, 3137–3180.

Dodson, M.H., Compston, W., Williams, I.S., Wilson, J.F., 1988. A search for ancient detrital zircons in Zimbabwean sediments. Journal of the Geological Society of London 145, 977–983.

Fakhari, M.D., Axen, G.J., Horton, B.K., Hassanzadeh, J., Amini, A., 2008. Revised age of proximal deposits in the Zagros foreland basin and implications for Cenozoic evolution of the High Zagros. Tectonophysics 451, 170–185 (this volume). doi:10.1016/j.tecto.2007.11.064.

Falcon, N.L., 1974. Southern Iran: Zagros Mountains. In: Spencer, A.M. (Ed.), Mesozoic–Cenozoic orogenic belts, Data for orogenic studies, vol. 4. Geological Society of London Special Publication, pp. 199–211.

Fedo, C.M., Sircombe, K.N., Rainbird, R.H., 2003. Detrital zircon analysis of the sedimentary record. Reviews in Mineralogy and Geochemistry 53, 277–303.

Fildani, A., Cope, T.D., Graham, S.A., Wooden, J.L., 2003. Initiation of the Magallanes foreland basin: timing of the southernmost Patagonian Andes orogeny revised by detrital zircon provenance analysis. Geology 31, 1081–1084.

Fitzsimons, I.C.W., Hulscher, B., 2005. Out of Africa: Detrital zircon provenance of central Madagascar and Neoproterozoic terrane transfer across the Mozambique Ocean. Terra Nova 17, 224–235.

Gansser, A., 1955. New aspects of the geology in central Iran. 4th World Petroleum Congress Proceedings, Rome, Section I/A/5, paper 2, pp. 279–300.

Garzanti, E., Gaetani, M., 2002. Unroofing history of Late Paleozoic magmatic arcs within the "Turan Plate" (Tuarkyr, Turkmenistan). Sedimentary Geology 151, 67–87.

Gehrels, G.E., McClelland, W.C., Samson, S.D., Patchett, P.J., Jackson, J.L., 1990. Ancient continental margin assemblage in the northern Coast Mountains, southeast Alaska and northwest Canada. Geology 18, 208–211.

Gehrels, G.E., DeCelles, P.G., Martin, A., Ojha, T.P., Pinhassi, G., Upreti, B.N., 2003. Initiation of the Himalayan orogen as an early Paleozoic thin-skinned thrust belt. GSA Today 13, 4–9. doi:10.1130/1052-5173.

Gehrels, G.E., DeCelles, P.G., Ojha, T.P., Upreti, B.N., 2006a. Geologic and U–Pb geochronologic evidence for early Paleozoic tectonism in the Dadeldhura thrust sheet, far-west Nepal Himalaya. Journal of Asian Earth Sciences 28, 385–408.

Gehrels, G.E., DeCelles, P.G., Ojha, T.P., Upreti, B.N., 2006b. Geologic and U–Th–Pb geochronologic evidence for early Paleozoic tectonism in the Kathmandu thrust sheet, central Nepal Himalaya. Geological Society of America Bulletin 118, 185–198.

Ghasemi, A., Talbot, C.J., 2006. A new tectonic scenario for the Sanandaj–Sirjan Zone (Iran). Journal of Asian Earth Sciences 26, 683–693.

Ghavidel-Syooki, M., 1995. Palynostratigraphy and paleogeography of a Paleozoic sequence in the Hassanakdar area, central Alborz range, northern Iran. Review of Palaeobotany and Palynology 86, 91–109.

Ghavidel-Syooki, M., 2003. Palynostratigraphy of Devonian sediments in the Zagros Basin, southern Iran. Review of Palaeobotany and Palynology 127, 241–268.

Ghavidel-Syooki, M., 2006. Palynostratigraphy and palaeogeography of the Cambro–Ordovician strata in southwest of Shahrud City (Kuh-e-Kharbash, near Deh-Molla), Central Alborz Range, northern Iran. Review of Palaeobotany and Palynology 139, 81–95.

Glennie, K.W., Boeuf, M.G.A., Hughescl, M.W., Moodystu, M., Pilaar, W.F.H., Reinhard, B.M., 1973. Late Cretaceous nappes in Oman mountains and their geologic evolution. American Association of Petroleum Geologists Bulletin 57, 5–27.

Golonka, J., 2004. Plate tectonic evolution of the southern margin of Eurasia in the Mesozoic and Cenozoic. Tectonophysics 381, 235–273.

Gradstein, F.M., Ogg, J.G., Smith, A.G., 2004. A Geologic Time Scale 2004. Cambridge University Press, Cambridge. 384 p.

Guest, B., Axen, G.J., Lam, P.S., Hassanzadeh, J., 2006a. Late Cenozoic shortening in the west-central Alborz Mountains, northern Iran, by combined conjugate strike-slip and thin-skinned deformation. Geosphere 2. doi:10.1130/GES00019.1, 35–52.

Guest, B., Stockli, D.F., Grove, M., Axen, G.J., Lam, P.S., Hassanzadeh, J., 2006b. Thermal histories from the central Alborz Mountains, northern Iran: implications for the spatial and temporal distribution of deformation in northern Iran. Geological Society of America Bulletin 118, 1507–1521.

Guest, B., Horton, B.K., Axen, G.J., Hassanzadeh, J., McIntosh, W.C., 2007. Middle to late Cenozoic basin evolution in the western Alborz Mountains: implications for the onset of collisional deformation in northern Iran. Tectonics 26, 6011. doi:10.1029/2006TC002091.

Guiraud, R., Bosworth, W., Thierry, J., Delplanque, A., 2005. Phanerozoic geological evolution of Northern and Central Africa: an overview. Journal of African Earth Sciences 43, 83–143.

Hamdi, B., Brasier, M.D., Jiang, Z., 1989. Earliest skeletal fossils from Precambrian–Cambrian boundary strata, Elburz Mountains, Iran. Geolological Magazine 126, 283–289.

Haq, B.U., Al-Qahtani, A.M., 2005. Phanerozoic cycles of sea-level change on the Arabian Platform. GeoArabia 10 (2), 127–160.

Hargrove, U.S., Stern, R.J., Kimura, J.I., Manton, W.I., Johnson, P.R., 2006. How juvenile is the Arabian–Nubian Shield? Evidence from Nd isotopes and pre-Neoproterozoic inherited zircon in the Bi'r Umq suture zone, Saudi Arabia. Earth and Planetary Science Letters 252, 308–326.

Hassanzadeh, J., Ghazi, A.M., Axen, G., Guest, B., Stockli, D.F., Tucker, P., 2002. Oligocene mafic-alkaline magmatism in north and northwest of Iran: evidence for the separation of the Alborz from the Urumieh–Dokhtar magmatic arc. Geological Society of America Abstracts with Programs 34 (6), 331.

Hassanzadeh, J., Axen, G., Guest, B., Stockli, D.F., Ghazi, A.M., 2004. The Alborz and NW Urumieh–Dokhtar magmatic belts, Iran: rifted parts of a single ancestral arc. Geological Society of America Abstracts with Programs 36 (5), 434.

Hassanzadeh, J., Stockli, D.F., Horton, B.K., Axen, G.J., Stockli, L.D., Grove, M., Schmitt, A., Walker, J.D., 2008. U–Pb zircon geochronology of upper Neoproterozoic–Early Cambrian granitoids in Iran: Implications for paleogeography, metallogeny, and exhumation history of Iranian basement. Tectonophysics 451, 71–96 (this volume). doi:10.1016/j.tecto.2007.11.062.

Haynes, S.J., McQuillan, H., 1974. Evolution of the Zagros suture zone, southern Iran. Geological Society of America Bulletin 85, 739–744.

Hempton, M.R., 1987. Constraints on Arabian plate motion and extensional history of the Red Sea. Tectonics 6, 687–705.

Hessami, K., Koyi, H.A., Talbot, C.J., Tabasi, H., Shabanian, E., 2001. Progressive unconformities within an evolving foreland fold-thrust belt, Zagros Mountains. Journal of the Geological Society of London 158, 969–981.

Homke, S., Verges, J., Graces, M., Emami, H., Karpuz, R., 2004. Magnetostratigraphy of Miocene–Pliocene Zagros foreland deposits in the front of the Push-e Kush Arc, (Lurestan Province, Iran). Earth and Planetary Science Letters 225, 397–410.

Husseini, M.I., 1989. Tectonic and deposition model of Late Precambrian–Cambrian Arabian and adjoining plates. American Association of Petroleum Geologists Bulletin 73, 1117–1131.

James, G.A., Wynd, J.G., 1965. Stratigraphic nomenclature of Iranian oil consortium agreement area. American Association of Petroleum Geologists Bulletin 49, 2182–2245.

Jacobs, J., Thomas, R.J., 2004. Himalayan-type indenter-escape tectonics model for the southern part of the late Neoproterozoic–early Paleozoic East African–Antarctic orogen. Geology 32, 721–724.

Jenny, J.G., 1977. Geologie et stratigraphie de l'Elbourz oriental entre Aliabad et Shahrud, Iran. Ph.D. thesis, Université de Genève, 238 pp.

Johnson, P.R., Woldehaimanot, B., 2003. Development of the Arabian–Nubian shield: perspectives on accretion and deformation in the northern East African orogen and the assembly of Gondwana. In: Yoshida, M., Windley, B.F., Dasgupta, S. (Eds.), Proterozoic East Gondwana: Supercontinent Assembly and Breakup, vol. 206. Geological Society of London Special Publication, pp. 289–325.

Keppie, J.D., Nance, R.D., Murphy, J.B., Dostal, J., 2003. Tethyan, Mediterranean, and Pacific analogues for the Neoproterozoic–Paleozoic birth and development of peri-Gondwanan terranes and their transfer to Laurentia and Laurussia. Tectonophysics 365, 195–219.

Khain, V.E., Koronousky, N.V., 1997. Caucasus. In: Moores, E.M., Fairbridge, R.W. (Eds.), Encyclopedia of European and Asian Regional Geology. Chapman and Hall, London, pp. 127–136.

Kimura, H., Matsumoto, R., Kakuwa, Y., Hamdi, B., Zibaseresht, H., 1997. The Vendian–Cambrian δ13C record, north Iran: evidence for overturning of the ocean before the Cambrian Explosion. Earth and Planetary Science Letters 147, E1–E7.

Kolodner, K., Avigad, D., McWilliams, M., Wooden, J.L., Weissbrod, T., Feinstein, S., 2006. Provenance of north Gondwana Cambrian–Ordovician sandstone: U–Pb SHRIMP dating of detrital zircons from Israel and Jordan. Geological Magazine 143, 367–391.

Koop, W., Stoneley, R., 1982. Subsidence history of the Middle East Zagros basin, Permian to Recent. Philosophical Transactions of the Royal Society of London A305, 149–168.

Kostyuchenko, S.L., Morozov, A.F., Stephenson, R.A., Solodilov, L.N., Vedrentsev, A.G., Popolitov, K.E., Aleshina, A.F., Vishnevskaya, V.S., Yegorov, T.P., 2004. The evolution of the southern margin of the East European Craton based on seismic and potential field data. Tectonophysics 381, 101–118.

Kröner, A., Eyal, M., Eyal, Y., 1990. Early Pan-African evolution of the basement around Elat, Israel, and the Sinai peninsula revealed by single-zircon evaporation dating, and implications for crustal accretion rates. Geology 18, 545–548.

Kröner, A., Pallister, J.S., Fleck, R.J., 1992. Age of initial oceanic magmatism in the Late Proterozoic Arabian shield. Geology 20, 803–806.

Lam, P.J., 2002. Geology, geochronology, and thermochronology of the Alam Kuh area, central Alborz Mountains, northern Iran. M.S. thesis, University of California, Los Angeles, 135 pp.

Leather, J., Allen, P.A., Brasier, M.D., Cozzi, A., 2002. Neoproterozoic snowball Earth under scrutiny: evidence from the Fiq glaciation of Oman. Geology 30, 891–894.

Lemaire, M.M., Westphal, M., Gurevitch, E.L., Nazarov, K., Feinberg, H., Pozzi, J.P., 1997. How far between Iran and Eurasia was the Turan plate during Triassic–Jurassic times? Geologie en Mijnbouw 76, 73–82.

Lyberis, N., Manby, G., Poli, J.T., Kalougin, V., Yousouphocaev, H., Ashirov, T., 1998. Post-Triassic evolution of the southern margin of the Turan plate. Comptes Rendus Académie des Sciences, série II 326, 137–143.

Mapes, R.W., Coleman, D., Cox, R., Nogueira, A.C.R., 2005. Significant changes in the detrital zircon age signature along a transect of the modern Amazon River. Geological Society of America Abstracts with Programs 37 (7), 481.

McQuarrie, N., 2004. Crustal scale geometry of the Zagros fold-thrust belt, Iran. Journal of Structural Geology 26, 519–535.

McQuarrie, N., Stock, J.M., Verdel, C., Wernicke, B.P., 2003. Cenozoic evolution of Neotethys and implications for the causes of plate motions. Geophysical Research Letters 30, 2036. doi:10.1029/2003GL 017992.

Metcalfe, I., 1996. Gondwanaland dispersion, Asian accretion and evolution of eastern Tethys. Australian Journal of Earth Sciences 43, 605–623.

Mohajjel, M., Fergusson, C.L., Sahandi, M.R., 2003. Cretaceous–Tertiary convergence and continental collision, Sanandaj–Sirjan Zone, western Iran. Journal of Asian Earth Sciences 4, 397–412.

Mouthereau, F., Lacombe, O., Meyer, B., 2006. The Zagros folded belt (Fars, Iran): constraints from topography and critical wedge modeling. Geophysical Journal International 165, 336–356.

Murphy, J.B., Fernandez-Suarez, J., Keppie, J.D., Jeffries, T.E., 2004. Contiguous rather than discrete Paleozoic histories for the Avalon and Meguma terranes based on detrital zircon data. Geology 32, 585–588.

Natal'in, B.A., Sengör, A.M.C., 2005. Late Palaeozoic to Triassic evolution of the Turan and Scythian platforms: the pre-history of the Palaeo-Tethyan closure. Tectonophysics 404, 175–202.

Nikishin, A.M., Ziegler, P.A., Stephenson, R.A., Cloetingh, S.A.P.L., Furne, A.V., Fokin, P.A., Ershov, A.V., Bolotov, S.N., Korotaev, M.V., Alekseev, A.S., Gorbachev, V.I., Shipilov, E.V., Lankreijer, A., Bembinova, E.Y., Shalimov, I.V., 1996. Late Precambrian to Triassic history of the East European Craton: dynamics of sedimentary basin evolution. Tectonophysics 268, 23–63.

Paces, J.B., Miller, J.D., 1993. Precise U–Pb age of Duluth Complex and related mafic intrusions, northeastern Minnesota: geochronological insights into physical, petrogenic, paleomagnetic, and tectonomagnetic processes associated with the 1.1 Ga midcontinent rift system. Journal of Geophysical Research 98, 13,997–14,013.

Quidelleur, X., Grove, M., Lovera, O.M., Harrison, T.M., Yin, A., Ryerson, F.J., 1997. Thermal evolution and slip history of the Renbu Zedong thrust, southeastern Tibet. Journal of Geophysical Research 102, 2659–2679.

Ramezani, J., Tucker, R.D., 2003. The Saghand Region, Central Iran: U–Pb geochronology, petrogenesis and implications for Gondwana tectonics. American Journal of Science 303, 622–665.

Rastsvetaev, L.M., 1997. Turkmenistan. In: Moores, E.M., Fairbridge, R.W. (Eds.), Encyclopedia of European and Asian Regional Geology. Chapman and Hall, London, pp. 743–759.

Robertson, A.H.F., Ustaömer, T., Parlak, O., Ünlügenç, U.C., Tasli, K., Inan, N., 2006. The Berit transect of the Tauride thrust belt, S Turkey: Late Cretaceous–Early Cenozoic accretionary/collisional processes related to closure of the Southern Neotethys. Journal of Asian Earth Sciences 27, 108–145.

Rowley, D.B., 1996. Age of initiation of collision between India and Asia: a review of stratigraphic data. Earth and Planetary Science Letters 145, 1–13.

Ruttner, A.W., 1993. Southern borderland of Triassic Laurasia in north-east Iran. Geologische Rundschau 82, 110–120.

Sanudo-Wilhelmy, S.A., Flegal, A.R., 1994. Temporal variations in lead concentrations and isotopic composition in the Southern California Bight. Geochimica et Cosmochimica Acta 58, 3315–3320.

Samani, B.A., Zhuyi, G., Xuetao, G., Chuan, T., 1994. Geology of Precambrian in central Iran; on the context of stratigraphy, magmatism and metamorphism. Geosciences Quarterly Journal of Geological Survey of Iran 3 (10), 40–63.

Schmitt, A.K., Grove, M., Harrison, T.M., Lovera, O.M., Hulen, J., Waters, M., 2003a. The Geysers–Cobb Mountain Magma System, California (Part 1): U–Pb zircon ages of volcanic rocks, conditions of zircon crystallization and magma residence times. Geochimica et Cosmochimica Acta 67, 3423–3442.

Schmitt, A.K., Grove, M., Harrison, T.M., Lovera, O.M., Hulen, J., Waters, M., 2003b. The Geysers–Cobb Mountain Magma System, California (Part 2): timescales of pluton emplacement and implications for its thermal history. Geochimica et Cosmochimica Acta 67, 3443–3458.

Seber, D., Vallve, M., Sandvol, E., Steer, D., Barazangi, M., 1997. Middle East tectonics: applications of geographical information systems (GIS). GSA Today 7, 1–6.

Sengör, A.M.C., 1987. Tectonics of the Tethysides: orogenic collage development in a collisional setting. Annual Review of Earth and Planetary Sciences 15, 213–244.

Sengör, A.M.C., 1990. A new model for the late Palaeozoic–Mesozoic tectonic evolution of Iran and implications for Oman. In: Robertson, A.H.F., Searle, M.P., Ries, A.C. (Eds.), The Geology and Tectonics of the Oman Region, vol. 49. Geological Society of London Special Publication, pp. 797–831.

Sepehr, M., Cosgrove, J.W., 2004. Structural framework of the Zagros Fold-Thrust Belt, Iran. Marine and Petroleum Geology 21, 829–843.

Seyed-Emami, K., Fursich, F.T., Wilmsen, M., Cecca, F., Majidifard, M.R., Schairer, G., Shekarifard, A., 2006. Stratigraphy and ammonite fauna of the upper Shemshak Formation (Toarcian–Aalenian) at Tazareh, eastern Alborz, Iran. Journal of Asian Earth Sciences 28, 259–275.

Shalaby, A., Stüwe, K., Fritz, H., Makroum, F., 2006. The El Mayah molasse basin in the Eastern Desert of Egypt. Journal of African Earth Sciences 45, 1–15.

Stacey, J.S., Kramers, J.D., 1975. Approximation of terrestrial lead isoptope evolution by a two-stage model. Earth and Planetary Science Letters 26, 207–221.

Stampfli, G.M., 1978. Etude géologique générale de l'Elbourz oriental au sud de Gonbad-e-Qabus (Iran NE). Ph.D. thesis, Université de Genève, 329 pp.

Stampfli, G., Marcoux, J., Baud, A., 1991. Tethyan margins in space and time. Palaeogeography, Palaeoclimatology, Palaeoecology 87, 373–409.

Stampfli, G.M., Borel, G.D., 2002. A plate tectonic model for the Paleozoic and Mesozoic constrained by dynamic plate boundaries and restored synthetic oceanic isochrons. Earth and Planetary Science Letters 196, 17–33.

Stern, R.J., 1985. The Najd fault system, Saudi Arabia and Egypt; a late Precambrian rift-related transform system? Tectonics 4, 497–511.

Stern, R.J., 1994. Arc assembly and continental collision in the Neoproterozoic East African orogen: implications for the consolidation of Gondwanaland. Annual Review of Earth and Planetary Sciences 22, 319–351.

Stern, R.J., Avigad, D., Miller, N.R., Beyth, M., 2006. Evidence for the snowball Earth hypothesis in the Arabian–Nubian shield and the East African orogen. Journal of African Earth Sciences 44, 1–20.

Stöcklin, J., 1968. Structural history and tectonics of Iran: a review. American Association of Petroleum Geologists Bulletin 52, 1229–1258.

Stöcklin, J., 1974. Northern Iran: Alborz Mountains. In: Spencer, A.M. (Ed.), Mesozoic–Cenozoic orogenic belts, Data for orogenic studies, vol. 4. Geological Society of London Special Publication, pp. 213–234.

Stöcklin, J., 1980. Geology of Nepal and its regional frame. Journal of the Geological Society of London 137, 1–34.

Stoeser, D.B., Frost, C.D., 2006. Nd, Pb, Sr, and O isotopic characterization of Saudi Arabian shield terranes. Chemical Geology 226, 163–188.

Stoneley, R., 1990. The Arabian continental margin in Iran during the Late Cretaceous. In: Robertson, A.H.F., Searle, M.P., Ries, A.C. (Eds.), The Geology and Tectonics of the Oman Region, vol. 49. Geological Society of London Special Publication, pp. 787–795.

Talbot, C.J., Alavi, M., 1996. The past of a future syntaxis across the Zagros. In: Alsop, G.I., Blundell, D.J., Davison, I. (Eds.), Salt Tectonics, vol. 100. Geological Society of London Special Publication, pp. 89–109.

Thomas, J.C., Cobbold, P.R., Shein, V.S., Le Douaran, S., 1999. Sedimentary record of late Paleozoic to Recent tectonism in central Asia—analysis of subsurface data from the Turan and south Kazak domains. Tectonophysics 313, 243–263.

Thomas, W.A., Astini, R.A., Mueller, P.A., Gehrels, G.E., Wooden, J.L., 2004. Transfer of the Argentine Precordillera terrane from Laurentia: constraints from detrital-zircon geochronology. Geology 32, 965–968.

Tillman, J.E., Poosti, A., Rossello, S., Eckert, A., 1981. Structural evolution of Sanandaj–Sirjan ranges near Esfahan, Iran. American Association of Petroleum Geologists Bulletin 65, 674–687.

Veevers, J.J., 2004. Gondwanaland from 650–500 Ma assembly through 320 Ma merger in Pangea to 185–100 Ma breakup: supercontinental tectonics via stratigraphy and radiometric dating. Earth-Science Reviews 68, 1–132.

von Raumer, J.F., Stampfli, G.A., Bussy, F., 2003. Gondwana-derived microcontinents—the constituents of the Variscan and Alpine collisional orogens. Tectonophysics 365, 7–22.

Weislogel, A.L., Graham, S.A., Chang, E.Z., Wooden, J.L., Gehrels, G.E., Yang, H., 2006. Detrital zircon provenance of the Late Triassic Songpan–Ganzi complex: sedimentary record of collision of the North and South China blocks. Geology 34, 97–100.

Wendt, J., Kaufmann, B., Belka, Z., Farsan, N., Karimi Bavandpur, A., 2005. Devonian/Lower Carboniferous stratigraphy, facies patterns and palaeogeography of Iran; Part II. Northern and central Iran 1. Acta Geologica Polonica 55, 31–97.

Wensink, H., Zijderveld, J.D.A., Varekamp, J.C., 1978. Paleomagnetism and ore mineralogy of some basalts of Geirud Formation of Late Devonian–Early Carboniferous age from southern Alborz, Iran. Earth and Planetary Science Letters 41, 441–450.

Wilde, S.A., Youssef, K., 2002. A re-evaluation of the origin and setting of the Late Precambrian Hammamat Group based on SHRIMP U–Pb dating of detrital zircons from Gebel Umm Tawat, North Eastern Desert, Egypt. Journal of the Geological Society of London 159, 595–604.

Windley, B.F., Whitehouse, M.J., Ba-Bttat, M.A.O., 1996. Early Precambrian gneiss terranes and Panafrican island arcs in Yemen: crustal accretion of the eastern Arabian Shield. Geology 24, 131–134.

Yilmaz, Y., 1993. New evidence and model on the evolution of the southeast Anatolian orogen. Geological Society of America Bulletin 105, 251–271.

Zonenshain, L.P., Kuzmin, M.I., Natapov, L.M., 1990. Geology of the USSR: a plate-tectonic synthesis. Geodynamics Series, vol. 21. American Geophysical Union, Washington, D.C. 242 pp.